



Scuola Universitaria Superiore IUSS Pavia

**Integrated Performance-Based Seismic Design: Traversing
Affordances for Practical Implementation**

A Thesis Submitted in Partial Fulfilment of the Requirements
for the Degree of Doctor of Philosophy in

**EARTHQUAKE ENGINEERING AND
ENGINEERING SEISMOLOGY**

Obtained in the framework of the Doctoral Programme in
Understanding and Managing Extremes

by

Davit Shahnazaryan

November, 2021



Scuola Universitaria Superiore IUSS Pavia

**Integrated Performance-Based Seismic Design: Traversing
Affordances for Practical Implementation**

A Thesis Submitted in Partial Fulfilment of the Requirements
for the Degree of Doctor of Philosophy in

**EARTHQUAKE ENGINEERING AND
ENGINEERING SEISMOLOGY**

Obtained in the framework of the Doctoral Programme in
Understanding and Managing Extremes

by

Davit Shahnazaryan

Supervisors: Dr. Gerard J. O'Reilly, Scuola Universitaria Superiore IUSS Pavia, Italy

Prof. Ricardo Monteiro, Scuola Universitaria Superiore IUSS Pavia, Italy

November, 2021

ABSTRACT

Performance-based earthquake engineering (PBEE) has become an important framework for quantifying seismic losses in buildings and infrastructure. However, due to its computationally expensive implementation through a detailed component-based approach, it has primarily been used for assessing existing structures within academic research and specific studies in practice. Building upon PBEE, expected annual loss (EAL) and collapse safety expressed in terms of mean annual frequency of collapse (MAFC) are explored here. To this end, a novel integrated performance-based seismic design (IPBSD) framework is proposed, utilising the two aforementioned parameters as its principal design objectives. The framework uses storey loss functions (SLFs) to limit economic losses by restricting demands at the serviceability limit state (SLS) via a permissible secant to yield period range, within which the building's principal periods of vibration must lie. By satisfying this condition, it is ensured that the building is neither too stiff, resulting in excessive floor acceleration-sensitive losses, nor too flexible, resulting in excessive drift-sensitive losses, at SLS, therefore ensuring a satisfactory EAL limit. The collapse fragility function of the building is then estimated based on expected backbone parameters, which along with the considered site's seismic hazard curve, is used to target a satisfactory MAFC. The output of those calculations are the demands on the structural elements of the building for subsequent design and detailing.

Furthermore, to aid practitioners in utilising IPBSD with easily accessible SLFs, a simplified tool developed in Python that builds, customises and uses SLFs to estimate a building's expected loss per storey due to seismic demands is proposed. These SLFs reduce the data required compared to a detailed study, which is particularly handy at a design stage when component information is likely missing, thus aiding the flow of the proposed IPBSD framework significantly. A comparative demonstration of its application to a real case-study school building is outlined and illustrates how independency and correlation of damage states can be considered. A comparison of SLF-based and FEMA P-58 type component-based loss estimation approaches shows good agreement and demonstrates the quality and ease of an SLF-based approach in achieving accurate results for a more expedite assessment of building performance.

Finally, several case study buildings with reinforced concrete frames as their lateral load-resisting system are evaluated using the proposed IPBSD framework and the results appraised via non-linear time history verification analysis. The performance is evaluated using both incremental dynamic analysis and a storey-based loss assessment procedure to estimate MAFC and EAL of risk-targeted designs, respectively. The agreement and consistency of design solutions and intended performance objectives are then checked to demonstrate the validity of the IPBSD framework, with MAFC being effectively targeted and the EAL limited as initially foreseen by the method. Further scrutiny of the results highlights the validity of the assumptions made in the IPBSD framework and sheds further light on the pertinent sources of economic losses when designing structures. This is seen as part of the next-generation risk-targeted and loss-driven design approaches in line with modern PBEE requirements.

Keywords: PBEE; expected annual loss; mean annual frequency of collapse; risk-targeted design; reinforced concrete.



ACKNOWLEDGEMENTS

The work presented in this thesis has been developed within the framework of the project “Dipartimenti di Eccellenza”, funded by the Italian Ministry of Education, University and Research at IUSS Pavia, which is gratefully acknowledged. I would also like to thank my two advisors, Ricardo Monteiro and Gerard John O'Reilly for their valuable and insightful comments on this research. This research could not have been completed without their elaborate contributions to this work.



TABLE OF CONTENTS

ABSTRACT.....	v
ACKNOWLEDGEMENTS	viii
TABLE OF CONTENTS.....	x
LIST OF FIGURES	xv
LIST OF TABLES	xx
LIST OF ABBREVIATIONS	xxiii
1. INTRODUCTION	1
1.1 MOTIVATION	1
1.2 OBJECTIVES AND SCOPE	4
1.3 THESIS OUTLINE.....	4
2. SEISMIC DESIGN AND ASSESSMENT OF STRUCTURES	8
2.1 CHAPTER OVERVIEW	8
2.2 EXISTING DESIGN CODE APPROACHES.....	8
2.3 PERFORMANCE-BASED SEISMIC DESIGN METHODS.....	9
2.4 LOSS ASSESSMENT APPROACHES.....	14
2.4.1 FEMA P-58 component-based approach.....	14
2.4.2 Storey-loss function-based approach.....	16
2.5 SUMMARY	17
3. REVIEW AND APPLICATION OF CONCEPTUAL SEISMIC DESIGN METHOD	20
3.1 CHAPTER OVERVIEW	20
3.2 INTEGRATED COLLAPSE RISK AND ECONOMIC LOSS-BASED SEISMIC DESIGN FRAMEWORK OVERVIEW.....	20
3.3 CASE STUDY APPLICATION.....	23
3.3.1 Identification of Site Hazard	23
3.3.2 Definition of Building Performance Objectives.....	24

3.3.3	Identification of Structural Design Parameters	27
3.3.4	Compute Spectral Values	29
3.3.5	Quantification of Feasible Initial Secant to Yield Period Range for SLS	30
3.3.6	Establishment of Required System Strength and Ductility	31
3.3.7	Computation of Structure's Backbone Behaviour	33
3.3.8	Identification of Structural Layout	35
3.4	SENSITIVITY STUDIES	36
3.4.1	Influence of SLS Parameters	36
3.4.2	Sensitivity Study on SLFs	37
3.4.3	Validation of the Plastic Hinge Yield Rotation Assumption	39
3.4.4	Consideration of Collapse Performance in Design	39
3.5	SUMMARY	40
4.	STOREY LOSS FUNCTIONS FOR SEISMIC DESIGN AND ASSESSMENT: DEVELOPMENT OF TOOLS AND APPLICATION.....	43
4.1	CHAPTER OVERVIEW	43
4.2	DEVELOPMENT OF A SLF ESTIMATION TOOLBOX	43
4.2.1	Step 1: Building characterisation	45
4.2.2	Step 2: Component inventory	46
4.2.3	Step 3: Component grouping	48
4.2.4	Step 4: Consideration of correlations between components	49
4.2.5	Step 5: Monte Carlo simulation of damage states and repair costs	50
4.2.6	Step 6: Repair cost computation	52
4.2.7	Step 7: Storey loss function fitting	53
4.2.8	Summary	54
4.3	CASE STUDY APPLICATION	56
4.3.1	Characterisation of case-study building	56
4.3.2	Building components and cost distributions	57
4.3.3	Component fragility and consequence functions	58
4.3.4	Correlated components	62
4.4	DERIVATION OF SLFs USING THE TOOLBOX	63
4.4.1	Estimating SLFs assuming uncorrelated components	63

4.4.2	Estimating SLFs assuming correlated components	65
4.5	COMPARISON BETWEEN FEMA P-58 COMPONENT-BASED AND SLF-BASED LOSS ASSESSMENT	66
4.5.1	Assessment results.....	67
4.6	SUMMARY AND CONCLUSIONS.....	69
5.	INTEGRATING EXPECTED LOSS AND COLLAPSE RISK IN PERFORMANCE-BASED SEISMIC DESIGN OF STRUCTURES	72
5.1	CHAPTER OVERVIEW	72
5.2	PROPOSED INTEGRATED PERFORMANCE-BASED SEISMIC DESIGN (IPBSD)	72
5.2.1	Overview.....	72
5.2.2	Step-by-step implementation of the proposed IPBSD framework.....	73
5.3	CASE STUDY APPLICATION	81
5.3.1	Definition of case study buildings	81
5.3.2	Numerical modelling.....	83
5.3.3	Site hazard and ground motions	84
5.4	DESIGN OF CASE STUDY STRUCTURES	85
5.4.1	FBD according to EC8	86
5.4.2	DDBD	86
5.4.3	RTSA method	88
5.4.4	Proposed IPBSD formulation.....	90
5.4.5	RTS approach.....	95
5.4.6	Summary	96
5.5	ANALYSIS RESULTS.....	97
5.5.1	FBD according to EC8	98
5.5.2	RTSA method	100
5.5.3	Proposed IPBSD formulation.....	102
5.5.4	Refined estimate of collapse risk	104
5.6	SUMMARY AND CONCLUSIONS.....	105
6.	ON THE SEISMIC LOSS ESTIMATION OF INTEGRATED PERFORMANCE-BASED DESIGNED BUILDINGS	109
6.1	CHAPTER OVERVIEW	109
6.2	INTEGRATED PERFORMANCE-BASED SEISMIC DESIGN (IPBSD)	109

6.2.1	Performance objectives.....	109
6.2.2	IPBSD implementation.....	111
6.2.3	Python-based iterative framework.....	116
6.3	CASE STUDY APPLICATION	117
6.3.1	Definition of case study buildings and numerical modelling.....	117
6.3.2	Site hazard and ground motions	120
6.3.3	Eurocode 8.....	121
6.3.4	IPBSD formulation	122
6.4	STOREY LOSS FUNCTIONS	125
6.5	STRUCTURAL PERFORMANCE AND LOSS ASSESSMENT RESULTS.....	129
6.5.1	Buildings designed according to EC8	130
6.5.2	Buildings designed using IPBSD.....	131
6.6	DETAILED ANALYSIS OF LOSS ESTIMATES	135
6.6.1	Secant-to-yield (T_1) period range considerations	135
6.6.2	Influence of the EDP profiles	138
6.7	SUMMARY AND CONCLUSIONS.....	140
7.	SUMMARY AND CONCLUSIONS.....	143
7.1	SUMMARY.....	143
7.2	KEY FINDINGS AND RESEARCH OUTCOMES.....	144
7.2.1	Storey loss functions for seismic design and assessment: development of tools and application.....	144
7.2.2	Integrating expected loss and collapse risk in performance-based seismic design of structures.....	145
7.2.3	On the seismic loss estimation of integrated performance-based designed buildings	
	147	
7.3	LIMITATIONS AND FUTURE DEVELOPMENTS.....	148
REFERENCES.....		149



LIST OF FIGURES

Figure 1.1. PEER-PBEE framework [Porter 2003].....	2
Figure 2.1. Comparison of key similarities and differences of available seismic design methods.	11
Figure 3.1. Overview of the framework for RC frames ([O'Reilly and Calvi 2019])	22
Figure 3.2. Elevation view of the case study structure.	23
Figure 3.3. Second-order fit of a hazard curve for PGA at L'Aquila	25
Figure 3.4. Approximate and refined loss curves, used to establish the design EAL shaded in red.	26
Figure 3.5. Design spectra at SLS and ULS.....	27
Figure 3.6. SLFs adopted from Ramirez and Miranda [2009].....	28
Figure 3.7. Illustration of the SLFs, and the identification of the design parameters for the SLS (red) and ULS (blue)	28
Figure 3.8. Identification of permissible initial secant to yield period range based on PFA and PSD limits for the SLS.....	31
Figure 3.9. Identification of design solution space shaded in grey considering the permissible period range and the trialled value of lateral strength capacity (adopted from O'Reilly and Calvi [2019]).....	32
Figure 3.10. Required backbone response for the case study building design solution, where the period limits show how the design conditions have been respected.	34
Figure 3.11. Impact of varying γ_{SLS} and $T_{R,SLS}$ on the design EAL.....	37
Figure 3.12. Sensitivity study on the modification of SLFs for the framework by the variation of PSD until EAL error, ε_{EAL} , is beyond 0.2%.	38
Figure 3.13. Potential development of the framework to incorporate MAFC as a design variable.	40
Figure 4.1. Flowchart of storey loss function generation framework.....	44
Figure 4.2. Component group and storey loss function identification.....	47
Figure 4.3. Relationship between causation and dependent components.	49
Figure 4.4. A sampling of damage states using Monte Carlo simulation.	51
Figure 4.5. Damage states and fragility functions of a sample: (a) causation component and (b) dependent component.....	51

Figure 4.6. Assignment of component repair costs based on sampled damage states.....	52
Figure 4.7. Consequence function describing the relationship of repair cost as a function of quantity	53
Figure 4.8. Programming structure of the SLF generation toolbox.	55
Figure 4.9. Overview of the storey loss function generator interface.	56
Figure 4.10. Main geometrical and structural properties of the case study building adapted from O'Reilly <i>et al.</i> [2019].	57
Figure 4.11. Storey loss functions for the case-study school building intermediate (2 nd) storey level and 2 nd floor (Equation 4 and Equation 5). (a) PSD-sensitive structural components, (b) PSD-sensitive non-structural components, (c) PFA-sensitive non-structural components.....	64
Figure 4.12. (a) SLFs for the case-study school building intermediate storey level: PSD-sensitive structural and non-structural components; (b) fragility functions of interdependent components.....	65
Figure 4.13. Hazard curve for the site considered in Ancona, Italy.	67
Figure 4.14. (left) Vulnerability curves and (right) Expected annual loss ratio showing the breakdown between different contributors in a comparative assessment between an SLF-based and component-based approach.	68
Figure 4.15. Relative contribution to expected loss with respect to increasing return period for a (left) SLF-based approach and (right) Component-based approach. As reference points, the 100, 475 and 2475-year return periods have been annotated on each plot.	69
Figure 5.1. Phase 1 of the proposed framework, where the loss curve is constructed and SLS performance objectives established to limit EAL	74
Figure 5.2. Phase 2 of the proposed framework, where design spectrum and acceptable design limits at SLS are identified, leading towards the establishment of the feasible initial period range.	75
Figure 5.3. Illustration of the SPO backbone response parameters and the various approaches to identify the design value.....	78
Figure 5.4. Phase 3 of the proposed framework, where the collapse capacity and backbone curve of the solution is identified.....	79
Figure 5.5. Phase 4 of the proposed framework, where the demands on the structural elements are identified and detailing of sections is carried out.....	80
Figure 5.6. Illustration of plan layout and elevation of archetypical RC frames in a discussion (tributary area of gravity loads on seismic frames shaded grey).	82
Figure 5.7.Illustration of the numerical modelling approach, where (left) shows the layout of elements and beam-column connection modelling and (right) denotes the hysteretic model adopted for each hinge location.	84

Figure 5.8. Seismic hazard with 1 st and 2 nd order fits corresponding to a spectral acceleration at a period of 0.7s, 1.0s and PGA	85
Figure 5.9. (a) Loss curve and (b) design spectrum at SLS of design case 4	91
Figure 5.10. Utilisation of the SLFs adopted from Ramirez and Miranda [2009]	92
Figure 5.11. SPO and IDA curves attained via the SPO2IDA tool.....	94
Figure 5.12. Illustration of the λ_c values for each case study structure and design approach considered, where for each group of designs the target value is denoted by the vertical text at the top of the plot	98
Figure 5.13. Interaction of curvature ductility capacity, μ_ϕ , with respect to cross-section effective area, A_{eff} , and tensile reinforcement ratio, ρ , as per EC2 for square columns with symmetric B500C reinforcement, C25/30 concrete, with μ_ϕ computed as the ratio of curvatures at peak and yield moment	100
Figure 5.14. Comparison of the Dolšek <i>et al.</i> model values for (a) γ_{ls} and (b) β_{RTR} as a function of T_1 provided by [Dolšek <i>et al.</i> 2017] with the actual values computed from IDA upon designing and detailing.....	101
Figure 5.15. Comparison of the assumed values for (a) r_s and (b) μ_{NC} ratios, with the actual values computed from SPO upon designing and detailing, where the notation A refers to D-TA and I-A cases, and A/B refers to I-TA/D-TB cases.....	102
Figure 5.16. Comparison of computed and assumed values of (a) β_{RTR} and (b) η at CLS.....	103
Figure 5.17. Comparison of computed and design values of q_s	104
Figure 5.18. Illustration of collapse risks using $Sa(T_1)$ or $ArgSa$ as the IM	105
Figure 6.1. Flowchart of the IPBSD framework	111
Figure 6.2. Identification of the loss curve and SLS performance objectives to limit the EAL	112
Figure 6.3. Storey loss functions and computation of design limits (S and NS stand for structural and non-structural component groups, respectively). (a) Computation of θ_{cr} and identification of θ for non-structural (NS) and structural (S) components; (b) Reapplication of Equation 6.3 and estimation of $\gamma_{NS,PSD}$ and $\gamma_{S,PSD}$; (c) Computation of design loss curve.....	113
Figure 6.4. Establishment of a feasible initial period range. (a) Design spectrum at SLS, (b) SLF and estimation of design limits, (c) identification of period limits	115
Figure 6.5. (left) Expected backbone behaviour, (right) identification of collapse capacity and computation of λ_c	116
Figure 6.6. Illustration of plan layout and elevation of the case study buildings.....	119
Figure 6.7. Seismic hazard for medium and high seismicity corresponding to a spectral acceleration at a period of $T_1=1.0$ s.....	120
Figure 6.8. SPO and IDA curves obtained via the SPO2IDA tool	124

Figure 6.9. SLFs for the case study building's (left) 2nd storey level for PSD-sensitive elements and (right) 2nd floor for the PFA-sensitive elements.....	129
Figure 6.10. Illustration of λ_c and λ_y values for each case study building and design approach considered.....	130
Figure 6.11. Comparison of computed and assumed values of (left) β_{RTR} and (right) η at CLS..	132
Figure 6.12. Comparison of computed and design values of q_s	132
Figure 6.13. (left) Period limits in X direction and (right) Variation of design solutions through the modification of performance objectives, where three distinct lines corresponding to three separate axes are superposed for graphical correspondence.....	134
Figure 6.14. Loss curves for case 1-IPBSD.	135
Figure 6.15. Loss contributions of different performance groups to the total repair cost at SLS.	136
Figure 6.16. PSD and PFA profiles along with the height of the structure at SLS.....	138
Figure 6.17. Comparison of loss curves for the 2D frames with the initial and updated loss curves.	139
Figure 7.1. Proposed IPBSD framework.	144

LIST OF TABLES

Table 3.1. Design performance objectives defined by an ELR at each limit state, necessary to compute their respective MAFE and the design intensities.....	25
Table 3.2. Summary of structural design parameters for both limit states	29
Table 3.3. Conversion of θ_{\max} and a_{\max} to spectral values at the SLS	30
Table 3.4. Identification of structural system parameters to respect the design constraints, which fall within the design solution space.....	34
Table 3.5. Suitable building geometry	35
Table 3.6. Yield deformation verification.....	39
Table 4.1. Mean quantities for the damageable structural components of the case-study school building in the longitudinal direction (quantities for the transverse direction listed in parenthesis).	58
Table 4.2. Mean quantities for the damageable non-structural components of the case-study school building in the longitudinal direction (quantities for the transverse direction listed in parenthesis).	59
Table 4.3. Fragility function parameters and repair costs for structural components of the 2nd storey.....	60
Table 4.4. Fragility function parameters and repair costs for non-structural components of the 2nd storey.....	61
Table 4.5. Example correlation between components of the case-study school building examined.....	63
Table 4.6. Regression parameters for both equations fitted for the intermediate storey SLF of the case-study school building.....	64
Table 4.7. Accuracy metrics of regression analysis.....	65
Table 5.1. Archetypical RC frame structures	81
Table 5.2. Summary of the design solutions obtained using FBD according to EC8, where G indicates cases where the gravity load combination was included.	87
Table 5.3. Summary of the design solutions obtained using DDBD according to Priestley <i>et al.</i> [2007].....	88

Table 5.4. Summary of the RTSA design solutions using the direct and indirect formulations for cases A ($r_s = 1, \mu_{NC} = 3$) and B ($r_s = 2, \mu_{NC} = 6$), where T indicates period updating.....	89
Table 5.5. Summary of the design solutions from the proposed IPBSD	94
Table 5.6. Variation of $S\alpha^{c,x}$ with X and $\lambda_{c,target}$ for a $\beta = 0.5$ (with the exception of ASCE 7-16, where $\beta = 0.6$), $T_1 = 0.7s$ and $q = 3.9$ (with the exception of ASCE 7-16, where $q = 4.5$).....	95
Table 5.7. Comparison of the design spectral acceleration, Sa_d , obtained for different frameworks.	97
Table 5.8. Summary of the λ_c for each case study structure and design approach considered.	98
Table 6.1. Case study building configurations.	117
Table 6.2. Summary of design solutions obtained using EC8.....	121
Table 6.3. Performance group contributions to γ_{SLS} in % and associated EDPs.	122
Table 6.4. Summary of design solutions from the IPBSD.	124
Table 6.5. Mean quantities for the damageable PSD-sensitive structural components in the X(Y) direction.	126
Table 6.6. Mean quantities for the damageable PSD-sensitive non-structural components in the X(Y) direction.	126
Table 6.7. Mean quantities for the damageable PFA-sensitive non-structural components.	127
Table 6.8. Summary of actual λ_c and λ_y for each case study building and design approach considered.....	130
Table 6.9. Summary of case study buildings located in medium seismicity region.	133
Table 6.10. Summary of IPBSD results for a single seismic frame.....	134
Table 6.11. Loss contributions of different performance groups to the total repair cost at SLS.	137
Table 6.12. Updated EDP profiles and corresponding γ values.	139



LIST OF ABBREVIATIONS

2D	= two dimensional
3D	= three dimensional
ATC	= Applied Technology Council
CLS	= collapse limit state
CMR	= collapse margin ratio
CPBD	= conceptual performance-based design
CSD	= conceptual seismic design
DBD	= displacement-based design
DCM	= ductility class medium
DDBD	= direct displacement-based design
DMF	= displacement modification factor
DS	= damage state
DV	= decision variable
EAL	= expected annual loss
EC0	= Eurocode 0
EC2	= Eurocode 2
EC8	= Eurocode 8
EDP	= engineering demand parameter
ELF	= equivalent lateral force
ELR	= expected loss ratio
FBD	= force-based design

HVAC	= heating, ventilation and air-conditioning
IDA	= incremental dynamic analysis
IM	= intensity measure
IPBSD	= integrated performance-based seismic design
MAFC	= mean annual frequency of collapse
MAFE	= mean annual frequency of exceedance
MCE	= maximum considered earthquake
MDOF	= multi-degree of freedom
MRF	= moment resisting frame
NC	= non-collapse
NLRHA	= non-linear response history analysis
NTC	= Italian national code
OLS	= operational limit state
PACT	= Performance Assessment Calculation Tool
PBEE	= performance-based earthquake engineering
PEER	= Pacific Earthquake Engineering Research
PFA	= peak floor acceleration
PFV	= peak floor velocity
PGA	= peak ground acceleration
PSD	= peak storey drift
PSHA	= probabilistic seismic hazard assessment
RC	= reinforced concrete
RPSD	= residual peak storey drift
RSMA	= response spectrum method of analysis
RTBF	= risk-targeted behaviour factors
RTR	= record-to-record

RTS	= risk-targeted spectra
RTSA	= risk-targeted seismic action
SDOF	= single degree-of-freedom
SLF	= storey loss function
SLS	= serviceability limit state
SPO	= static pushover
SRSS	= square-root-sum-of-the-squares
UHS	= uniform hazard spectrum
ULS	= ultimate limit state
YFS	= yield frequency spectra



1. INTRODUCTION

1.1 MOTIVATION

Over the years, the earthquake engineering community has worked towards preventing damage of structural and non-structural elements in frequent low-intensity earthquakes and preventing collapse in rare high-intensity earthquakes. After the economic impact of the 1994 Northridge earthquake in the US, due to extensive damage and overall disruption, an immediate shift was necessary for building performance definition. Traditional objectives of seismic codes or assessment frameworks, focusing on life safety and collapse prevention of buildings, were not sufficient for complete satisfactory building performance. The change happened with the introduction of performance-based earthquake engineering (PBEE) during the latter half of the 1990s with the Vision 2000 framework [SEAOC 1995]. It related desired building performance to various seismic hazard levels via the definition of limit states or performance levels. These were termed fully operational, operational, life-safe, and near-collapse, corresponding to hazard levels of frequent, occasional, rare, and very rare events, respectively. In the early 2000s, FEMA-356 [2000] emerged and established element deformation and force-based acceptability criteria for different performance levels of structural and non-structural elements.

Following the initial interpretations of PBEE, a more robust and powerful probabilistic framework was developed and set the basis for what is known as the Pacific Earthquake Engineering Research (PEER) Center PBEE methodology [Cornell and Krawinkler 2000] (Figure 1.1). It centres around the idea of probabilistically quantifying the mean annual frequency of exceedance (MAFE), or failure, of a limit state, λ_f , by integrating the probability of failure for a chosen intensity measure (IM), $P[f | IM=im]$, with the site hazard curve, $H(im)$, as shown in Equation 1.1 [Cornell *et al.* 2002].

$$\lambda_f = \int_0^{+\infty} P[f | IM = im] dH(im) \quad (1.1)$$

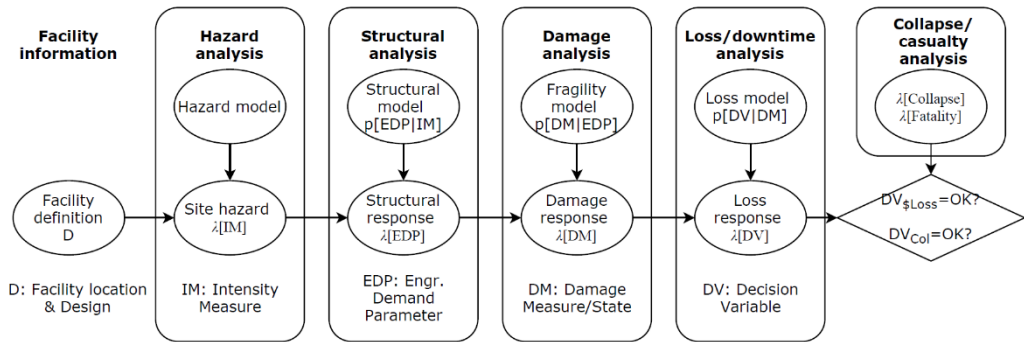


Figure 1.1. PEER-PBEE framework [Porter 2003].

This modernised approach quantifies the building performance in an overall risk sense and is flexible in its definition of failure, allowing consistent consideration across all pertinent limit states (*e.g.*, onset of structural/non-structural damage or collapse). It is widely recognised as a fundamental framework for characterising seismic risk, using terms that are more meaningful to stakeholders and practitioners. These performance measures can be subdivided into three categories: losses, downtime, and casualties/fatalities. Instead of describing performance at discrete hazard levels, as is typically prescribed in design codes (*e.g.* [ASCE 7-16 2016; CEN 2004a; NZS 1170.5:2004 2004]), it acts as a fully probabilistic framework with the inclusion of uncertainties for hazard, structural response, damage and monetary loss.

The goal of this thesis is to propose a risk-targeting and loss-driven seismic design framework that incorporates heavy computations in a software code level (*e.g.*, in object-oriented Python) without compromising the integrity of the probabilistic methods and featuring a user interface and tools to be applied easily by practitioners. To achieve this, the framework should be suitable for both academic and practising communities. Affordances were first observed by Gibson [1979], establishing a theory of affordances and signifying the quality or property of an object that defines its possible uses or makes clear how it can or should be used. The important aspect of the theory of affordances is the perception that the environment is taking place through its affordances, in a way there is an action possibility [Bucher and Helmond 2017]. Depending on who is using the tool within the context of this study, the affordances will vary, *i.e.*, they are relative to the user's native capabilities. Affordances are both physical and psychological, meaning that practitioners in contrast to academics, will be more reluctant to use probabilistic frameworks primarily because of their perception of them being complex and unapproachable. Consequently, what the framework allows or affords the user to do may be considered as separate and independent from the needs of the user in a way that the user cannot even perceive them, but affordances of the tools are inherent as such, as they are there to be perceived. Essentially, they can be a constraint for activities since they do not trigger certain behaviour,

while being there for any activity. To avoid such constraints, methods should be implemented to ease into the use of such activities. Within this thesis, the goal is to traverse these affordances in PBEE for design applications. In other words, make them accessible to those who may not be specifically trained or inclined to use probabilistic or next-generation approaches.

As mentioned previously, the PBEE framework has become popular within academic research or specialised reports, such as FEMA P-58 [2012a], rather than a widespread code-based implementation for practitioners. This is primarily due to the probabilistic nature and its computationally expensive implementation; therefore, practitioners would rather use the deterministic approaches recommended by design codes rather than spend time on developing non-linear models of buildings and carrying out detailed non-linear time history analyses and loss assessment. For instance, for the seismic assessment of existing buildings, a full inventory of all building components may be known, but for new designs, this information is yet to be identified. To simplify the codification of these approaches, where lack of initial data is inevitable, alternatives are sought. There is a recent trend in developing risk-targeting and/or loss-driven design frameworks, which tackle the issues related with both types of methods (probabilistic and deterministic). Many researchers have developed risk-targeted design methods over the years [Aschheim and Black 2000; Cornell 1996; Kennedy and Short 1994; Krawinkler *et al.* 2006; Luco *et al.* 2007; O'Reilly and Calvi 2019; Vamvatsikos and Aschheim 2016; Žižmond and Dolšek 2019], among others. Risk-targeted approaches use collapse risk as the primary design objective, while others [Krawinkler *et al.* 2006; O'Reilly and Calvi 2019] explore the possibility of utilising economic losses as a metric. In other words, less time consumption and simpler tools affordable to the practitioners as well as scientists are sought. Accordingly, the aim within this thesis is to establish a framework, which, while implementable from a mathematical and conceptual point of view, does not compromise the rigour of probabilistic seismic design frameworks. In other words, a framework is developed to be well versed and adopt the strengths of both types of the aforementioned methods (*i.e.*, comprehensiveness and simplicity).

Figure 1.1 demonstrates the complex nature of probabilistic frameworks, which is the case of the PEER-PBEE framework. It acts as a fully probabilistic framework with the inclusion of uncertainties for hazard, structural response, damage and loss analysis to gain information for final decision making for performance in terms of metrics, such as expected loss and collapse safety. Therefore, a framework more suited for quick calculations based on targeting collapse safety and limitation of economic losses due to seismic events is developed and proposed within this thesis. Furthermore, the framework should be probabilistic in nature and stay in line with the modern PBEE objectives. However, it is by no means supposed to be a replacement of a component-based approach of FEMA P-58 (PACT), but rather to make it a more affordable framework for practical design implementation.

1.2 OBJECTIVES AND SCOPE

The goals of this thesis are to demonstrate the applicability and implement risk-targeted loss-driven design methods, in line with the objectives of performance-based earthquake engineering. Specifically, the objectives are as follows:

- Develop a framework to obtain seismic design solutions with limited economic losses and targeted collapse safety. In particular, expected annual loss (EAL) acts as the metric to limit direct losses due to damaged components following a seismic event, and mean annual frequency of collapse (MAFC) acts as a proxy for targeting the collapse safety of the building. This framework is termed integrated performance-based seismic design (IPBSD) and uses the aforementioned two metrics as inputs for attainment of valid design solutions;
- Proposal of a simplified methodology that uses simplified computations to achieve seismic design solutions that meet the primary objectives of IPBSD. Such a methodology is supported by a Python-based object-oriented programming tool, which is developed to aid practitioners in carrying out quick, but optimised, designs following the proposed IPBSD procedure;
- Development and implementation of a Python-based toolbox to integrate the aforementioned framework with the generation of generic storey-loss functions, a key ingredient to the IPBSD approach, depending on the needs of the user. This will allow the framework to account for expected economic loss of a building's entire inventory, both in terms of structural and non-structural components, in addition to drift- and floor acceleration-sensitive components.

1.3 THESIS OUTLINE

In line with the main objectives previously outlined, this thesis is structured in chapters corresponding to the different steps leading to the development and refinement of the IPBSD framework. Many of the chapters have already been published, in part or almost entirely, as peer-reviewed articles and others have been presented at international conferences, as indicated in the beginning of each chapter.

Chapter 2 addresses the existing seismic design code approaches, specifically, the force-based design approach within the context of Eurocode 8 and the displacement-based approach by Priestley *et al.* [2007]. Furthermore, it provides extensive discussions of recent developments in risk-targeting seismic design approaches and, finally, the discussion of the FEMA P-58 component-based and storey-loss function-based loss assessment approaches.

Chapter 3 outlines the early stages of IPBSD development. Detailed calculations with regards to meeting the primary objectives of the framework are documented and, by means of application to a case-study reinforced concrete moment-resisting frame, the framework

capabilities are demonstrated. The goal is to draw directions of improvement and refinement of the framework through sensitivity studies, summarising the scope and limitations of previous studies (*e.g.*, conceptual seismic design by O'Reilly and Calvi [2019]) which lay the foundation for the development of IPBSD. In addition, it identifies gaps in modern design methods and addresses these, providing further motivation for the goals of this thesis.

Chapter 4 supplements the IPBSD framework, by proposing a toolbox for production of storey loss functions (SLFs) as a simplified alternative to typically detailed component-based approaches. The goal of this chapter was not only the production of generic loss functions for specific building occupancies but also the development of a flexible tool for practitioners to create their own functions depending on their own specific needs. The framework is demonstrated in a step-by-step application to an existing school building in Italy and is validated via comparison with a component-based loss assessment of the same building.

Chapter 5 outlines the developments of IPBSD to use expected annual loss (EAL) and mean annual frequency of collapse (MAFC) as design parameters and utilises the SLF toolbox developed in Chapter 4. Through simple steps, it directly identifies feasible structural solutions without the need for detailed calculations and numerical analysis. It demonstrates the implementation of the framework as well as applications of modern risk-targeted and code-based approaches outlined in Chapter 2. Multiple case study reinforced concrete frame structures are evaluated using these approaches and the results are appraised through validation analysis. The proposed framework is viewed as a steppingstone for seismic design with advanced performance objectives in line with modern performance-based earthquake engineering requirements.

Chapter 6 builds on the IPBSD framework to explore the impacts of design decisions on the effective limitation of losses. The framework uses collapse risk and economic loss as main design inputs and is briefly recalled with further developments for three-dimensional buildings. Following the parametric investigations conducted, this chapter makes use of a refined version of the IPBSD framework and demonstrates its capabilities to target a certain MAFC and limit EAL through its application to several reinforced concrete case-study buildings. Furthermore, the efficiency of the framework in satisfying the pre-established performance objectives is also investigated. A detailed disaggregation of the main sources of losses within the building is examined to shed further light and provide justification needed for the simplified assumptions necessary for the implementation of the framework in an efficient manner. Finally, the solutions of IPBSD are compared with the solutions of similar buildings designed according to Eurocode 8. The investigations within this chapter illustrate the applicability of the framework through potential developments to account for

various building typologies as well as demonstrating the need for developing risk-consistent design methods within modern design codes.

Chapter 7 summarises the results and contributions from this thesis. Conclusions are drawn from the results and extended to recognise potential refinements for performance-based seismic design methods. Moreover, areas of research are identified to lay groundwork for future developments accounting for other building typologies.



2. SEISMIC DESIGN AND ASSESSMENT OF STRUCTURES

2.1 CHAPTER OVERVIEW

This chapter includes a discussion of existing seismic design code approaches in Section 2.2, specifically, the force-based design (FBD) approach within the context of Eurocode 8 (EC8) [CEN 2004a] and the displacement-based approach by Priestley *et al.* [2007]. Then, the development of performance-based risk-targeting seismic design methods is presented in Section 2.3 and, finally, the chapter is concluded with the discussion of FEMA P-58 component based [FEMA 2012a] and storey-loss function-based loss assessment approaches in Section 2.4.

2.2 EXISTING DESIGN CODE APPROACHES

Current seismic design codes primarily focus on ensuring the life safety of building occupants by avoiding structural collapse. Additionally, performance at frequent levels of ground shaking is to be checked and verified. These are termed the *no-collapse requirement* and *damage limitation requirement* in the current version of EC8 [CEN 2004a] and are implemented at ground shaking return periods of 475 and 95 years, respectively, with possible modifications to account for building importance class. New Zealand's NZS1170 [NZS 1170.5:2004 2004] defines two limits states, termed as *serviceability* and *ultimate* with design return periods of 25 and 500 years, respectively, with the possibility of modification for different importance classes similar to EC8. A slightly modified approach is outlined in the recently revised design code in the US, ASCE 7-16 [2016], where the building is designed using a fraction of the maximum considered event (MCE) as input, which is determined from a series of risk-targeted hazard maps developed for a target collapse risk of 1% in 50 years (\sim 5,000-year return period). It uses a generic structural fragility curve along with some other adjustments following an approach outlined by Luco *et al.* [2007] but has recently been noted by Vamvatsikos [2017] to perhaps not be the most ideal approach.

The design method employed in seismic design codes follows what may be referred to as FBD. It calculates a design base shear force from a reduced elastic spectrum using either the equivalent lateral force (ELF) method or response spectrum method of analysis (RSMA). Despite seismic codes having the option to use non-linear numerical models for static pushover (SPO) analysis or non-linear response history analysis (NLRHA) with a set

of suitable ground motion records, these approaches may be deemed too computationally expensive at times and not always implemented given the simpler linear-static options available.

While FBD boasts an attractive simplicity, Priestley [2003] and others pointed out several shortcomings. The use of displacement-based design (DBD) was thus advocated, where deformation demands in the individual elements drive the design process, culminating in the development of the direct displacement-based design (DDBD) method [Priestley *et al.* 2007] and other similar methods [Sullivan *et al.* 2003]. One of the principal arguments by Priestley *et al.* [2007] was that it was not reasonable to quantify the expected ductility and spectral demand reduction for different structural configurations via unique behaviour factors and proposed employing a ductility- and typology-dependant spectral reduction approach.

Both FBD and DBD methods can be good approximations for the initial seismic design of structures. However, neither explicitly quantify the structural performance in a manner that may be considered as having fully satisfied the goals of modern performance-based earthquake engineering, PBEE (*i.e.*, the Pacific Earthquake Engineering Research, PEER, PBEE) methodology. This means that the actual performance of structures designed using these methods is not expected to be risk-consistent (*i.e.*, the annual probability of it exceeding a certain performance threshold is not accurately known or consistent among different structures), and building performance parameters like collapse risk, expected economic losses and downtime do not feature in the design process. A recent initiative in Italy [Iervolino *et al.* 2018] has shown that buildings designed according to the Italian national code (NTC) [2018], which is similar to EC8, do not exhibit the same level of collapse safety when evaluated extensively, with large variations observed between different structural typologies and configurations. These FBD and DBD methods' design solutions may be refined and modified to become more in-line with risk-based objectives, as discussed in O'Reilly and Calvi [2020], or the behaviour factors adopted for different structural typologies may be adjusted and refined [Vamvatsikos *et al.* 2020], for example. Nevertheless, the fundamental issue of modern PBEE not being at the core of these classical methods remains.

2.3 PERFORMANCE-BASED SEISMIC DESIGN METHODS

Over the years, different design methods aimed at risk-targeted have been developed and are widely accepted to eventually be prescribed and recommended in future design codes [Fajfar 2018; Vamvatsikos *et al.* 2016]. The US has already implemented criteria in the seismic design code ASCE 7-16 [2016] and FEMA P-750 [FEMA 2009], and the new draft version of EC8 [CEN 2018] will include an informative annex on the probabilistic

verification of structures. Any risk-targeted approach aims to control the risk of exceeding a limit state related to the performance of the building.

The concept of risk-targeted behaviour factors (RTBF) was developed based on the works of Kennedy and Short [1994] and Cornell [1996], whereby behaviour factors are adjusted and revamped using more risk-consistent approaches. Procedures like FEMA P695 [ATC 2009] and recently by Vamvatsikos *et al.* [2020] outlined such approaches. Luco *et al.* [2007] introduced the concept of a risk-targeted design spectra to ensure uniform collapse risk for structures in the US. Douglas *et al.* [2013] and Silva *et al.* [2016] explored the extension of such an approach to Europe. Vamvatsikos and Aschheim [2016] further developed the yield point spectrum method by Aschheim and Black [2000] and introduced the yield frequency spectra (YFS) as a design aid to link the mean annual frequency of exceedance (MAFE) of any displacement or ductility-based parameter with the system design strength. Additionally, Žižmond and Dolšek [2019] introduced the risk-targeted seismic action method to be integrated with the current FBD procedures in EC8. Krawinkler *et al.* [2006] also introduced an iterative approach, where effective structural systems are selected and sized and the performance of structural, non-structural, and content systems is evaluated for each. This approach utilises acceptable loss and collapse risk for decision-making to intuitively aid designers when implementing the PEER PBEE framework in design. These aforementioned studies are not intended to be an exhaustive list of available methods, but rather some of the noteworthy proposals to integrate modern PBEE in seismic design codes.

With the brief overview of existing seismic design methods, a critical discussion is provided here. Figure 2.1 shows several design methods with the following abbreviations: integrated performance-based seismic design (IPBSD) proposed within this thesis and Shahnazaryan and O'Reilly [2021]; FBD present in many seismic design codes [ASCE 7-16 2016; CEN 2004a; NTC 2018; NZS 1170.5:2004 2004]; DDBD outlined by Priestley *et al.* [2007]; RTBF described by Cornell [1996], amongst others; conceptual performance-based design (CPBD) proposed by Krawinkler *et al.* [2006; Zareian and Krawinkler 2012]; risk-targeted spectra (RTS) proposed by Luco *et al.* [2007]; YFS proposed by Vamvatsikos and Aschheim [2016]; and the risk-targeted seismic action (RTSA) method comprising both the direct (D) and indirect (I) approaches by Žižmond and Dolšek [2019].

The rows of Figure 2.1 list several categories common to each seismic design method. These are abbreviated and described as follows: performance objective(s) (PO), which describe the primary quantity that each design method targets, limits or bases itself upon; seismic hazard (H) definition, meaning how seismicity is characterised in the design process; non-linearity (NL) meaning how ductile structural behaviour is accounted for to adequately determine a suitable set of reduced design forces; relative difficulty and directness (DD) meaning how difficult (*i.e.* is the method feasible with just a spreadsheet

or is extensive NLRHA required?) and direct (*i.e.* are multiple iterations required to obtain the final solution?) the method is; (PBEE) whether or not the method is risk-consistent; and the flexibility (FLX) of the method meaning how easy is it to tailor the design targets beyond what it has been developed for so far.

	IPBSD	FBD	DDBD	RTBF	CPBD	RTS	YFS	RTSA-D	RTSA-I
PO	λ_c λ_v	$E[D T_R]$ $E[R T_R]$	$E[D T_R]$	CMR λ_c	$E[L T_R]$ $P[C T_R]$	λ_c	λ_0 λ_u	λ_c	λ_c
H	$H(Sa(T))$	UHS	UHS	UHS $H(AvgSa)$	$H(Sa(T_1))$	UHS	$H(Sa(T_1))$	$H(Sa(T_1))$	$H(Sa(T_1))$ & UHS
NL	Assume μ and q_s and get q_u from SPO2IDA	Traditional q factors	Equivalent viscous damping	Calibrated q factors	NLRHA	Traditional q factors	SPO2IDA	Assume r_s and μ_{NC} and calculate C_1 from IDA	Assume r_s and μ_{NC} and calculate C_1 from IDA (Equivalent q factor)
DD	Moderate	Easy	Easy	Easy	Very Extensive	Easy	Moderate	Extensive	Extensive
FLX	Flexible	Limited	Flexible	Limited	Flexible	Limited	Flexible	Flexible	Flexible
PBEE	Yes	No	No	Yes	Yes	No	Yes	Yes	Yes

Figure 2.1. Comparison of key similarities and differences of available seismic design methods.

The first comparative point concerns the POs. Beginning with FBD, the PO is related to the expected (or average) values of displacement, D , and lateral resistance, R , at specified return period, T_R , intensities. This requires a designer to ensure sufficient lateral strength at very rare T_R events, whilst limiting the expected displacement at frequent T_R events. DDBD follows a similar approach whereby the expected level of displacement demand at multiple T_R levels is used. This is quite typical of design codes, whereby a series of intensity-based checks with corresponding limit states are stipulated for practitioners to follow and verify. This essentially stemmed from the early interpretation of PBEE in Vision 2000 [SEAOC 1995].

As research grew on probabilistic-related aspects, it became clear that such an intensity-based approach may not be entirely appropriate for modern PBEE [Günay and Mosalam 2013] and structures designed this way did not provide the consistent level of safety they were perceived to have [Iervolino *et al.* 2018]. This led to developments on how these approaches may be improved but maintaining the same intensity-based approach familiar to practitioners. RTS, RTBF and RTSA-I are examples of such developments, where some *behind the scenes* adjustments are made to maintain the familiar intensity-based approach via a uniform hazard spectrum (UHS) while seeking to maintain risk-consistency among designs. They typically have collapse safety as their PO but differ slightly in their definitions of it. For example, to identify suitable behaviour factors to reduce the UHS in design, FEMA P-695 [ATC 2009] employs a collapse margin ratio (CMR, see Figure 5.3), whereas a recent proposal by Vamvatsikos *et al.* [2020] for Europe employed λ_c .

YFS provides a way to identify structures that can limit the MAPE of deformation-based quantities like storey drift, θ , or ductility, μ . CPBD was a proposal that was in some ways ahead of its time as many of the tools needed to feasibly implement it were either not available, or yet to be developed. It discussed using an array of POs in its formulation and made an effort to illustrate these quantities for designers to understand. Further development of this approach by Zareian and Krawinkler [2012] utilised a storey-based approach with POs being defined as expected losses and collapse probabilities at specified intensities. This is one of the few methods that has attempted to directly incorporate economic losses into its formulation, although the manner in which it was framed appeared rather tough to practically implement at the time. The last is the proposed IPBSD approach where the POs are the λ_c and the λ_y to target a certain collapse risk but also to limit the expected economic losses over all intensities, as initially proposed by O'Reilly and Calvi [2019]. It is seen that the collapse risk objective is in line with other methods but the relatively simple integration of expected annual loss (EAL) as a design variable makes it an attractive option. This was a key point highlighted by Krawinkler *et al.* [2006], stating that performance-based designs are not readily condensable to a single design parameter but multiple parameters that affect different facets of response; for example, should the building possess insufficient strength and ductility, its collapse safety may be inadequate, whereas should it be too flexible, it may accumulate excessive drift-sensitive loss at low T_R events, but at the same time potentially accumulate too much acceleration-sensitive if too stiff. It was for this reason that O'Reilly and Calvi [2019] introduced the restriction of the initial secant to yield period range and the subsequent identification of sufficient lateral strength and ductility.

The next broad comparison is the manner in which they define seismic hazard. Traditional methods like FBD and DDBD rely on the use of a UHS at specified T_R levels. These UHS are anchored to some level of ground shaking computed using probabilistic seismic hazard assessment (PSHA). In the case of EC8, peak ground acceleration (PGA) on rock is used and a predefined shape for all other periods at that T_R is fitted. It should be noted that while the use of specific T_R levels may not be ideal, neither is anchoring the shape of the entire design spectrum to a single parameter like PGA, as recently discussed by Calvi *et al.* [2018]. The main problem with using a UHS is that in order to make the resulting design solutions risk-consistent, they need to either have some modifications made in how they are utilised or how they are defined. For example, RTS attempts to define the anchoring value of a UHS whereas RTSA-I instead modifies how the force reduction is introduced. Alternatively, there is the use of seismic hazard curves determined from suitable PSHA, and are generically defined as $H(IM)$, noting that different intensity measures (IMs) may be used. The most common hazard curve definition is at the first mode period of vibration of the structure, $H(Sa(T_1))$, which is employed by YFS, RTSA-D, RTSA-I and also IPBSD. The proposed method utilises several hazard curves defined within a range of feasible periods of vibration and not one specific value giving a degree of flexibility of final

structural configuration when identified and sized. Other methods focus on the identification of a singular T_1 assumption for design which needs to be then iterated should the actual value not match. It is also noted how the RTBF quantification approach described by Vamvatsikos *et al.* [2020] for Europe utilises a more advanced IM definition of average spectral acceleration [Eads *et al.* 2015], $H(\text{AvgSa})$, to characterise suitable behaviour factors.

In terms of how each method deals with non-linearity, FBD uses the traditional approach of behaviour factors for each structural system whereas other methods like RTBF have attempted to correct the definition of these to be more risk-consistent. However, the underlying assumption of a single force reduction factor for certain typologies remains. RTS as defined in ASCE 7-16 [2016] also utilises force reduction factors but as pointed out by Gkimprixis *et al.* [2019], this use of traditional behaviour factors means that the risk-consistency breaks down in this implementation of RTS. The RTBF approach attempts to rectify this inconsistency through appropriate behaviour factor calibration. DDBD utilises the concept of equivalent viscous damping, which is somewhat similar to behaviour factors but different because the spectral reduction is a function of the expected ductility demand rather than a fixed value. CPBD utilised a rather strenuous approach of multiple NLRHA for identification of suitable designs. The RTSA methods proposed by Žižmond and Dolšek [2019] account for non-linearity by assuming a set of values for the expected ductility capacity at the near-collapse limit state, μ_{NC} , and overstrength of the structure, r_s , which are later verified for the subsequent design and iterated if needed. An additional C_1 parameter is also computed via an incremental dynamic analysis (IDA) on an equivalent single degree-of-freedom (SDOF) oscillator. It is worth noting that for the RTSA-I method, Žižmond and Dolšek [2019] describe how an equivalent risk-consistent behaviour factor may be identified, highlighting the link between it and other methods discussed here. To circumvent the use of assumed values for force reduction and subsequent verification, YFS and the proposed IPBSD method both utilise the SPO2IDA tool [Vamvatsikos and Cornell 2006] to compute the force reduction distribution directly. This tool relates the distribution of dynamic behaviour to the expected backbone shape of the structure using an extensive library of empirical coefficients calibrated using NLRHA. This has the advantage of allowing the dynamic behaviour to be estimated with a high degree of accuracy prior to designing the structure without any numerical analysis.

Regarding the relative difficulty and directness of each method, a generic ranking has been provided based on the authors' subjective opinion. Due to their direct nature and no essential requirement to iterate design solutions or conduct extensive dynamic verifications, the FBD, DDBD, RTBF and RTS methods are ranked as easy methods to implement. The CPBD method is ranked as very extensive due to the sheer amount of analysis required to implement it. The YFS and IPBSD methods are ranked as moderate as they do not require any dynamic analysis to implement. If the designer is confident in SPO2IDA tool's ability

to characterise the dynamic behaviour of the structure, then no great difficulty is encountered. Small iterations may be needed to refine the solution, with some cases being refined to a spreadsheet whereas others require pushover analysis of numerical models. The RTSA methods are denoted as extensive by requiring an IDA on an SDOF oscillator to determine one of the design parameters. Designs may take a few iterations, with full numerical models being required. The authors of this approach have, to their credit, provided ample parametric studies and practical guidance for designers [Sinković *et al.* 2016] on how to tackle this aspect and good initial assumptions can easily be made, still making it an attractive option.

In terms of flexibility of tailoring the design targets, the methods using behaviour factors (FBD and RTBF) are relatively limited since their performance is inherently linked to the assumption made in the derivation of the behaviour factor and no end-control is left to the designer. DDBD's use of equivalent viscous damping makes it somewhat more flexible as it allows designers to tailor their intensity-based drift limitations. The assumptions needed to derive RTS have been discussed by Gkimprixis *et al.* [2019] to not be without their difficulties as to how the general method ought to be employed and the spectra derived with different studies advocating different anchoring values of the parameter X [Douglas *et al.* 2013; Silva *et al.* 2016]. All other methods are deemed as flexible as they let designers choose and tailor their specific design targets, thus increasing their appeal.

Lastly, Figure 2.1 categorises the different methods as being PBEE-compliant or not. While this is not a new discussion (*e.g.* [Vamvatsikos *et al.* 2016]), it is included here for completeness. Unsurprisingly, neither FBD nor DDBD meet modern PBEE goals, at least without some additional verifications (*e.g.* [O'Reilly and Calvi 2020]). Again, RTS fails this categorisation not because of a conceptual flaw but rather in how it has come to be implemented, as discussed by Gkimprixis *et al.* [2019]. The other methods, including the proposed IPBSD, are all seen to be PBEE-compliant as their formulations directly incorporate the use of risk-oriented metrics and are implemented consistently.

2.4 LOSS ASSESSMENT APPROACHES

2.4.1 FEMA P-58 component-based approach

The Applied Technology Council (ATC) finalized the FEMA P-58 [2012a] document in the context of developing next-generation performance-based seismic design procedures. Performance within the methodology may be measured in terms of probability of casualties, direct loss and repair time. It may be applied to both new or existing building with the goal to assess building's probable performance, to design new buildings capable of achieving desired performance and to assess possible improvements for existing buildings. The methodology employs a rigorous procedure requiring a full building inventory along with fragility and consequence functions at component level. Here, the

damage information from damageable structural and non-structural components is converted to decision variables. Those are more commonly known as deaths, dollars, and downtime as established within the PEER framework [Cornell and Krawinkler 2000]. The FEMA P-58 methodology includes the following:

- Probabilistic procedures, where uncertainties are explicitly considered and the performance is expressed in terms of human losses (deaths and injuries), direct economic losses incurring due to building repair or replacement costs following a seismic event, and indirect losses due to unsafe placarding, environmental impacts where downtime is expected;
- For its practical implementation, fragility and consequence data for most common structural systems and building occupancies, non-structural components are included via the electronic Performance Assessment Calculation Tool (PACT) for carrying out probabilistic calculations and assessment of losses. The goal is to provide stakeholders or practitioners performance-based design solutions to aid in seismic design decision making.
- In addition to assessment of seismic performance, the performance-based design process within the framework is capable of including considerations of additional consequences, such as other environmental impacts.
- Basic inventory management on structural and non-structural component vulnerability is required for the implementation of the methodology.

Performance-based design process initiates with the identification of performance objectives at the onset of design by decision makers, *i.e.*, stakeholders and/or practitioners. One or more performance objectives may be considered, where each objective is characterised through an acceptable risk of damage or loss given the specific earthquake hazard. Preliminary design is carried out to assess the performance capability of the building. Structural analyses are carried out along with damage and component-based loss assessment for decision making. During loss assessment, the probability of exceeding losses for all damageable components at different loss functions is computed. Once performance assessment is carried out, the estimated performance capability is compared with the performance objectives initially set out. If the assessed performance is satisfactory, *i.e.*, better or equal to the objectives, the design is completed. Otherwise, the design or performance objectives are modified until concurrence through an iterative process. However, the component-based approach due to its complexity could prove to be discouraging for many practitioners. Therefore, simpler alternatives for loss assessment are often sought while retaining the principal goals of performance-based design.

2.4.2 Storey-loss function-based approach

A simplification to the component level loss assessment approach is the utilisation of storey loss functions (SLFs) to carry out storey-based loss assessment. The approach proposed by Ramirez and Miranda [2012] was used within this thesis to perform SLF-based loss assessment for the selected case study buildings. The approach takes residual deformations into account to compute the probability of the building to be demolished after a seismic event. The economic loss condition on the ground motion intensity is computed as the summation of the following terms: losses due to the building collapse; repair costs due to the building's components being damaged; and losses resulting from the demolition of the building if it has experienced excessive residual drifts. The expected total economic loss is the sum of three mutually exclusive, collectively exhaustive events, conditioned on a ground motion IM, and is given by Equation 2.1:

$$\begin{aligned} E[L_T | IM] = & E[L_T | NC \cap R, IM] P(NC \cap R | IM) \\ & + E[L_T | NC \cap D] P(NC \cap D | IM) + E[L_T | C] P(C | IM) \end{aligned} \quad (2.1)$$

where $E[L_T | NC \cap R, IM]$ is the expected total loss in the building given no collapse and the components are repaired given the ground motion IM, which is the quantity output from the SLFs; $E[L_T | NC \cap D]$ is the expected loss given no collapse but the building is demolished, and $E[L_T | C]$ is the expected loss when the building has collapsed. The weights in Equation 2.1 are described as follows: $P(NC \cap R, IM)$ is the probability of the building not collapsing but being repaired given the ground motion IM; $P(NC \cap D | IM)$ is the probability of the building not collapsing but being demolished due to excessive residual drifts given the ground motion IM, and $P(C | IM)$ is the probability of the building collapsing given the ground motion IM. Equation 2.1 can be rewritten as Equation 2.2:

$$\begin{aligned} E[L_T | IM] = & E[L_T | NC \cap R, IM] P(R | NC, IM) P(NC | IM) \\ & + E[L_T | NC \cap D] P(D | NC, IM) P(NC | IM) + E[L_T | C] P(C | IM) \end{aligned} \quad (2.2)$$

where $P(R | NC, IM)$ and $P(NC | IM)$ are the probabilities that the building will be repaired given no collapse, and that the building did not collapse, respectively, given the ground motion IM; $P(D | NC, IM)$ is the probability of the building to be demolished, given the ground motion IM. Equation 2.2 can be rewritten as follows:

$$\begin{aligned} E[L_T | IM] = & E[L_T | NC \cap R, IM] \{1 - P(D | NC, IM)\} \{1 - P(C | IM)\} + \\ & + E[L_T | NC \cap D] P(D | NC, IM) \{1 - P(C | IM)\} + E[L_T | C] P(C | IM) \end{aligned} \quad (2.3)$$

The probability of demolishing the building given no collapse at a ground motion IM is computed as a function of residual peak storey drift (RPSD) following the recommendations of FEMA P-58 [2012a] given in Equation 2.4.

$$P(D|NC, IM) = \int_0^{\infty} P(D|RPSD) dP(RPSD|NC, IM) \quad (2.4)$$

where $P(D|RPSD)$ is the probability of having to demolish the building conditioned on RPSD and $P(RPSD|NC, IM)$ is the probability of experiencing a certain level of RPSD in the building given that the building has not collapsed and it was subjected to a ground motion shaking intensity IM . Recognizing how to compute the expected loss at a given intensity level, the EAL may be computed by integrating over all possible intensities, as given in Equation 2.5.

$$E(L_T) = \int_0^{\infty} E(L_T | IM) d\lambda(IM) \quad (2.5)$$

where $\lambda(IM)$ is the mean annual frequency of the ground motion intensity IM .

2.5 SUMMARY

Performance-based design of structures following simplified methodologies has been of interest within the earthquake engineering community for many years. Within this chapter, existing design code approaches as well as performance-based seismic design methods were described and critically reviewed by comparing some common categories, such as performance objectives, seismic hazard definition, non-linear behaviour treatment, risk-consistency and the flexibility of each method. Many of those methods were also tested through their application to case study structures in order to have a broad and thorough comparison between them in Chapters 4, 5 and 6. In addition, loss assessment approaches, in particular the FEMA P-58 component-based and the storey-loss function-based approach, were briefly described. These will form the core of the developments and discussion in later chapters.



3. REVIEW AND APPLICATION OF CONCEPTUAL SEISMIC DESIGN METHOD

This chapter is based on the following reference:

Shahnazaryan, D., O'Reilly, G. J., and Monteiro, R. [2019] "Using direct economic losses and collapse risk for seismic design of RC buildings," COMPDYN Proceedings, Vol. 3, pp. 4968–4983.

3.1 CHAPTER OVERVIEW

This chapter covers primarily the preliminary developments of "Integrated collapse risk and economic loss-based seismic design" framework, previously known as "Conceptual seismic design" [O'Reilly and Calvi 2019], at its early stages of development. Portions of the chapter include the overview of the framework (Section 3.2) demonstrated by a detailed case study application (Section 3.3), sensitivity studies on input parameters, and discussions of the portions of the framework (Section 3.4) that needed improvement and led to their further developments.

3.2 INTEGRATED COLLAPSE RISK AND ECONOMIC LOSS-BASED SEISMIC DESIGN FRAMEWORK OVERVIEW

Current seismic design guidelines have a two-fold performance objective: the protection of human lives and the limitation of earthquake-induced damage. Hence, it is important to limit the likelihood of structural collapse, which is obtained by providing sufficient strength and ductility, in addition to proper detailing and capacity design, ensuring a controlled and stable ductile mechanism during strong seismic shaking. Additionally, damage limitation can be controlled during more frequent events. Neglecting damage control at a design stage can have severe consequences during an earthquake as both structural and non-structural damage, in conjunction with the interruption of building use, may entail disproportionately high economical losses compared to the costs of the structure itself. These aspects partially form what has become known as the PEER PBEE methodology initially outlined by Cornell and Krawinkler [2000]. This PBEE methodology [Porter 2003; SEAOC 1995] is an approach to quantify the performance of a given structural system. It utilises a fully probabilistic framework, employing methodologies with a solid scientific basis to improve seismic risk decision-making and expresses the levels of performance in terms of metrics meaningful to stakeholders and building owners. New guidelines like FEMA P58 [2012a]

were developed, which allow the performance of existing buildings to be quantified in terms of metrics like EAL and MAFC. However, due to its iterative and cumbersome nature, more simplified options to take EAL into account have been sought.

O'Reilly and Calvi [2019] proposed a novel conceptual seismic design (CSD) framework that employs EAL as a design metric and requires very little building information at the design onset. The framework encompasses the idea that designers may start with the definition of a required or limiting value of EAL and arrive at multiple feasible structural solutions without the need for any detailed design calculations or numerical analysis. Initially, the building performance definition is transformed into a design solution space using several simplifying assumptions. Subsequently, with a suitable structural response backbone, several feasible building typologies and associated structural geometries are identified. It is important to note that the methodology forms a steppingstone prior to further member detailing and robust design verifications, such as that outlined in FEMA P58.

This study aims to describe a detailed implementation of the CSD framework [O'Reilly and Calvi 2019] and provide further insight by means of a parametric study, that lay the foundation for the development of the IPBSD framework. Serviceability limit state parameters are initially varied to see their effect on the design EAL and an alteration of the design solution space. A study on the use of SLFs is then carried out for their modification to overcome their incompatibility with the CSD framework at the ultimate limit state (ULS), in view of it not affecting the EAL. Finally, an approach to consider target collapse safety and define prospective structure's dynamic and strength characteristics is discussed, which could potentially solve the issues identified during the sensitivity study on SLFs. The latter became the first variation of IPBSD with respect to the CSD framework.

In order to implement the CSD framework shown in Figure 3.1, some simplifying assumptions are needed initially. First, SLFs are used to convert expected loss ratios (ELRs) to design peak storey drift (PSD) and peak floor acceleration (PFA). Three limit states were utilised: fully operational limit state (OLS); serviceability limit state (SLS); and ULS. Two limit state intensities, SLS and ULS, are considered to characterise the structure's elastic and ductile non-linear behaviour, respectively. The OLS performance point describes the point when direct monetary losses begin to accumulate due to building damage, which can be thought of as an initial threshold akin to the excess amount on an insurance policy. The ULS performance point describes the point of building's full monetary replacement cost (Figure 3.4).

In this chapter, the general recommendations provided in Section 2.2 for the definition of limit state return period will be followed for the case study application in Section 3.3 and parametric studies in Section 3.4.

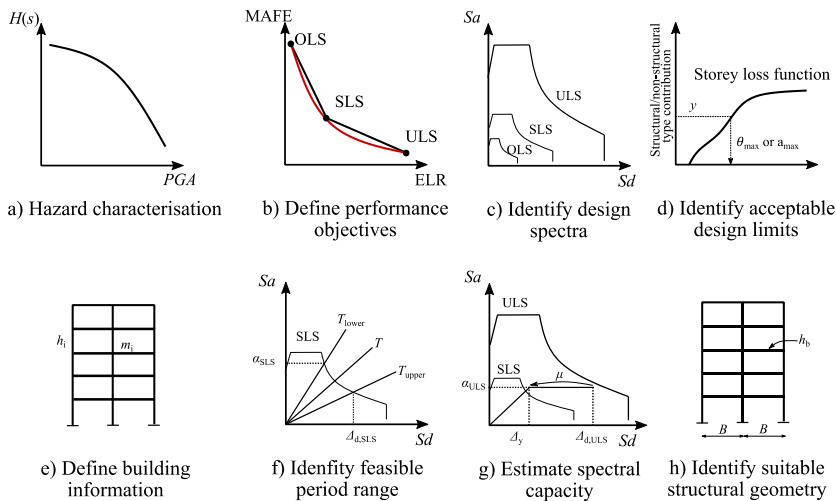


Figure 3.1. Overview of the framework for RC frames ([O'Reilly and Calvi 2019])

The CSD framework [O'Reilly and Calvi 2019] is separated into two distinct parts: the identification of performance requirements, and the identification of feasible structural solutions. An overview of the framework for a reinforced concrete (RC) frame is described in Figure 3.1. The first part includes: a) the site hazard initially identified with a UHS for different return periods; b) performance objectives are set to establish the design loss curve characterised by an ELR (y), and corresponding MAFE (λ), for each limit state. The loss curve is then integrated for the definition of design EAL, which has to be met by the subsequent obtainment of design solutions (Figure 3.4); c) using the MAFE for each limit state and the return periods of the UHS to be designed for, design spectra are identified; d) with the identification of design spectra, SLFs are used to relate expected monetary losses to design parameters like the maximum PSD, θ_{\max} , and maximum PFA, a_{\max} , along the height of the building. The vertical axis in Figure 3.1(d) represents the y contribution from PSD or PFA sensitive structural or non-structural elements.

The second part includes the following steps: e) minimal building information is needed, such as the number of storeys, n , seismic mass, m_i , and storey heights, h_i ; f) at SLS, θ_{\max} and a_{\max} are converted to spectral displacement and acceleration limits, $\Delta_{d,SLS}$ and $a_{d,SLS}$, respectively. These are then used to identify the feasible initial secant to yield period range, where the initial period, T_i , of the sought structure must lie; g) knowing the design

displacement at ULS, $\Delta_{d,ULS}$, and the required ductility, μ , the bilinear backbone curve is identified; h) and finally a suitable structural geometry from the established yield displacement, Δ_y , knowing that the yield displacement is a function of structural geometry and material properties. In the case of RC frames, the bay width, B , and the beam height, h_b , are computed. Overall, the framework works as an initial screening for suitable design before detailing and verification of the structure.

3.3 CASE STUDY APPLICATION

The CSD framework summarised in the previous section was used for a case study application herein. The goal of the study was to define certain performance objectives and come up with a set of design solutions in terms of bilinear backbone behaviour and required structural dimensions. No detailed verification analysis of these designs was carried out. Reasonable assumptions were made during the design process since some information was not readily available. Minimal building information was necessary to implement the CSD framework. For the case study building depicted in Figure 3.2, a four-storey building with a floor area of 200m^2 , seismic floor loading of 6kN/m^2 and roof loading of 5kN/m^2 was considered. The storey height was taken as 3.5m. The target EAL for the case study RC frame was predefined as 0.3%. With the already identified building performance requirements and minimal global characteristics of the possible building, several feasible design solutions were identified as part of a preliminary investigation of the CSD method.

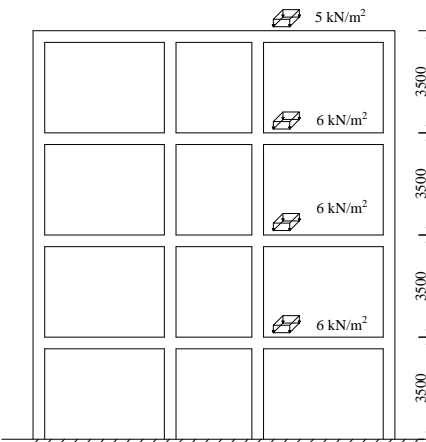


Figure 3.2. Elevation view of the case study structure.

3.3.1 Identification of Site Hazard

For the first step, the site hazard curve, H , was identified. PGA was adopted along with EC8 [CEN 2004a] type 1 design spectrum and soil type C was assumed. A higher fidelity

second-order hazard model [Vamvatsikos 2013] was adopted instead of the first-order model initially utilised by O'Reilly and Calvi [2019] to give a more accurate representation of the hazard, as described by Equation 3.1.

$$H(s) = k_0 \exp(-k_2 \ln^2 s - k_1 \ln s) \quad (3.1)$$

where the coefficients k_0 , k_1 and k_2 were found to be 8.43E-05, 3.252 and 0.403, respectively, via a least-squares regression of the SHARE model [Woessner and Wiemer 2005] for a site in L'Aquila, Italy; and $H(s)$ is the hazard function representing the MAFE of a certain IM value s equal to PGA (Figure 3.3).

3.3.2 Definition of Building Performance Objectives

Design performance objectives for the case study building are identified in Table 3.1. The values of return period, T_R , and ELR are decided. Then $H=1/T_R$ is used to determine the MAFE, λ , from Equation 3.2.

$$\begin{aligned} \lambda &= \sqrt{p} k_0^{1-p} \left[H(\hat{s})^p \right] \exp\left(\frac{1}{2} p k_1^2 \beta_s^2\right) \\ p &= \frac{1}{1 + 2k_2 \beta_s^2} \end{aligned} \quad (3.2)$$

where \hat{s} is the median value of s for a given limit state exceedance. Through the integration of the refined loss curve of Figure 3.4 and Equation 3.3, the EAL is computed and verified against the target one. And the PGA is computed by using Equation 3.3.

$$PGA = \exp\left[\left(-k_1 + \sqrt{k_1^2 - 4k_2 \ln \frac{\lambda}{k_0}}\right) / (2k_2)\right] \quad (3.3)$$

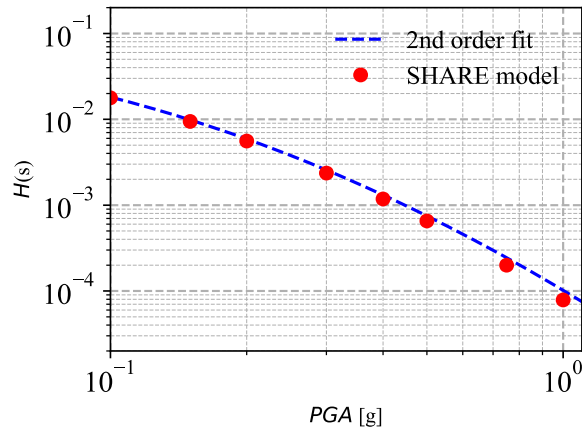


Figure 3.3. Second-order fit of a hazard curve for PGA at L'Aquila

Table 3.1. Design performance objectives defined by an ELR at each limit state, necessary to compute their respective MAFE and the design intensities.

	OLS	SLS	ULS	Source
γ	1%	4%	100%	User choice
T_R [years]	10	150	1600	User choice
H	1.00e-1	6.66e-3	0.625e-3	$=1/T_R$
β	0.1	0.2	0.3	Eurocode 8
λ	1.00e-1	7.03e-3	0.821e-3	Equation 3.2
EAL		0.29%		Equation 3.4
PGA [g]	-	0.177	0.461	Equation 3.3

Dispersions, β_s , were assumed based on those recommended in Appendix F of the recent draft of the revised EC8 [CEN 2018] and are therefore deemed to be suitable for the present scope of illustration. In Figure 3.4, the EAL may be computed as the area beneath the approximate loss curve and is shaded in red. It is important to pay careful consideration since while the difference in area between the approximate and refined loss curve may appear insignificant, this is a result of the log scale of the vertical axis in Figure 3.4. However, it is possible to have an area between the two curves resulting in an EAL overestimation of up to 50% when compared to the refined curve. This can be overcome by using a closed-form expression with the same functional form of the refined loss curve as suggested by O'Reilly and Calvi [2019]:

$$\lambda = c_0 \exp[-c_1 \ln y - c_2 \ln^2 y] \quad (3.4)$$

where the coefficients c_0 , c_1 and c_2 can be fitted to pass through the three limit state points shown in Figure 3.4. The EAL was then evaluated as the area beneath this closed-form expression and is expected to be more representative of the actual EAL using more refined analysis. The ELR's were taken as $y_{OLS}=1\%$, $y_{SLS}=4\%$ and $y_{ULS}=100\%$, for the case study building. The values for the OLS and ULS limit states were based on the same consideration by O'Reilly and Calvi [2019] whereby the OLS point is intended to represent the point at which the losses begin to accumulate and ULS when the losses reach the value of the building. The SLS point was chosen here and the sensitivity of the EAL to this value will be discussed in Chapter 3.4.1. The design EAL was established as the area under the refined curve, which was obtained as 0.29%, slightly lower than the target EAL (0.3%). Based on the calculated PGA, design spectra may be identified, as illustrated in Figure 3.5.

From each of these design limit state return periods, the design PGA was identified by inverting the hazard model in Equation 3.1 in terms of PGA. In the revised EC8, the 1600-year return period for the ULS corresponds to the significant damage limit state, so it was assumed to represent the complete replacement of the structure. In case of different design codes being used with differing minimum design requirements, such as NZS1170 or ASCE 7-16, the design return period of 2500 years is required at ULS, which may need to be accommodated as well.

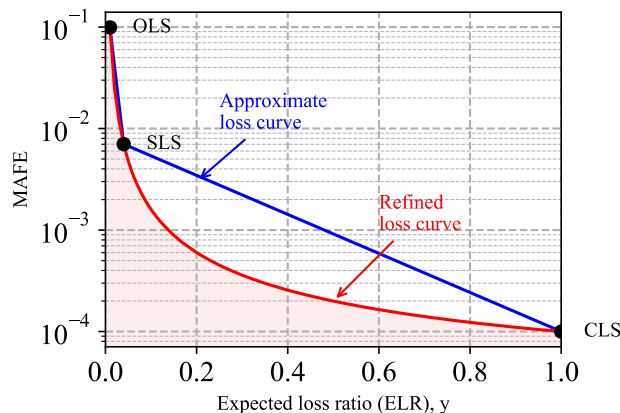


Figure 3.4. Approximate and refined loss curves, used to establish the design EAL shaded in red.

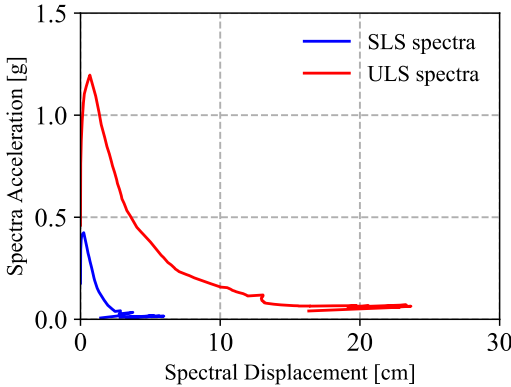


Figure 3.5. Design spectra at SLS and ULS.

3.3.3 Identification of Structural Design Parameters

In order to convert the design loss ratios at both SLS and ULS into structural design parameters, SLFs were utilised and adopted from the literature [Ramirez and Miranda 2009]. Office occupancy was assumed and, for simplicity, only the typical SLFs were adopted (Figure 3.6). Considering the SLFs, the current formulation of CSD, as initially proposed by O'Reilly and Calvi [2019], is not entirely compatible with their use when ELR is equal to 100% at ULS, since these functions' formulations tend to asymptotically increase towards large structural demand values of 15% storey drift (Figure 3.6), which are not realistic in design. To address this, two options will be adopted here, namely by a limiting value of 2% for PSD and then reducing the limit to 1%. Initially, we carry on with the 2% limit, then the change in the value will take place to showcase the difference of the design solutions and the type of complications. Furthermore, some future developments to address this aspect relating to ULS performance are also envisaged in Chapter 3.4.4.

To link the ELR at each limit state to a structural demand parameter via the SLFs, as illustrated in Figure 3.6, the relative weights or contributions of the different component groups to expected loss, γ , were required. The ELR at each limit state is described by Equation 3.5.

$$\gamma_{S,PSD} + \gamma_{NS,PSD} + \gamma_{NS,PEA} = \gamma \quad (3.5)$$

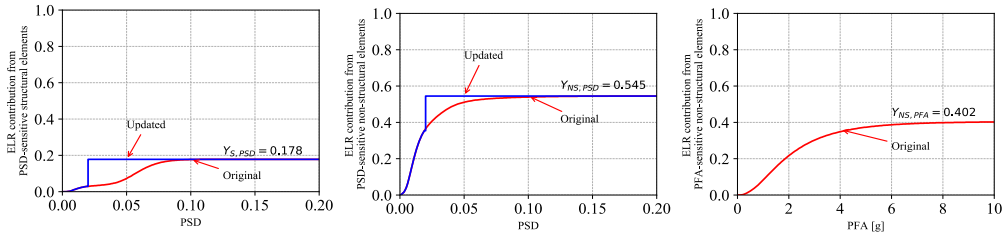


Figure 3.6. SLFs adopted from Ramirez and Miranda [2009]

Equation 3.5 is the sum of all sources of loss resulting from PSD-sensitive structural ($\gamma_{S,PSD}$) and non-structural ($\gamma_{NS,PSD}$) elements and PFA-sensitive non-structural ($\gamma_{NS,PFA}$) loss contributions given in Figure 3.6. From Equation 3.5, the following expressions in Equation 3.6 can be written:

$$\begin{aligned}\gamma_{S,PSD} &= \gamma Y_{S,PSD} \\ \gamma_{NS,PSD} &= \gamma Y_{NS,PSD} \\ \gamma_{NS,PFA} &= \gamma Y_{NS,PFA}\end{aligned}\quad (3.6)$$

Meaning that the individual values of the damageable element group loss was computed as a product of the target ELR, γ , and its relative weighting, Y , shown in Figure 3.6. By entering the vertical axis in Figure 3.6, these two values of θ_{max} and one value of a_{max} returned are not to be exceeded in order to maintain that level of expected loss for that limit state. Taking the more critical of the two θ_{max} values at SLS, which will almost always be the non-structural-based value, the design demand parameters were established and are illustrated in Figure 3.7 and listed in Table 3.2.

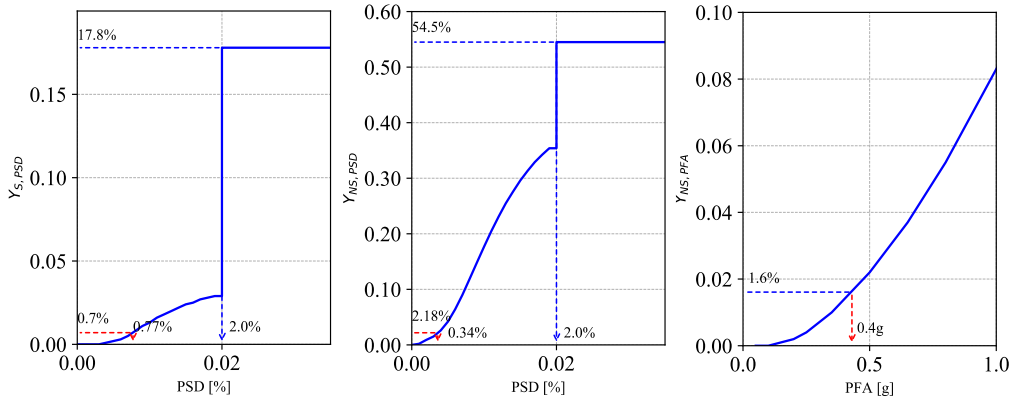


Figure 3.7. Illustration of the SLFs, and the identification of the design parameters for the SLS (red) and ULS (blue)

Table 3.2. Summary of structural design parameters for both limit states

Structural demand parameter	SLS	ULS
PSD	0.86%	2.00%
PFA	1.12g	-

3.3.4 Compute Spectral Values

The identified values of θ_{\max} and a_{\max} at the SLS then needed to be converted to design spectral accelerations and displacements, $\Delta_{d,SLS}$ and a_{SLS} , respectively, as per Figure 3.1(d). An equivalent SDOF system is then employed in CSD to characterise a first mode dominated multi-degree of freedom (MDOF) system. This is similar to the approach adopted in DBD [Priestley *et al.* 2007] where the displacement of the equivalent SDOF system is given by Equations 3.7 and 3.8:

$$\Delta_d = \frac{\sum_{i=1}^n m_i \Delta_i^2}{\sum_{i=1}^n m_i} \quad (3.7)$$

$$\Delta_i = \omega_0 \theta_{\max} H_i \left(\frac{4H_n - H_i}{4H_n - H_1} \right) \quad (3.8)$$

where n is the number of storeys, m_i is the mass, Δ_i is the displaced shape at storey level i , ω_0 is the higher mode reduction factor and H_i is the i -th storey's elevation above the base. Unlike the PSD profile, PFA cannot be assumed to be first mode dominated, however, since the process of identifying a spectral acceleration, Sa for various building solutions assumes that the structure remains in the elastic range of response, some simplifications can be made. The contribution to the PFA at j^{th} mode and at the i^{th} floor for an elastically responding structure may be computed following Equation 3.9.

$$a_{i,j} = \varphi_{i,j} \Gamma_j Sa(T_j) \quad (3.9)$$

Where $Sa(T_j)$ is the spectral acceleration at the j^{th} mode, $\varphi_{i,j}$ is the j^{th} mode shape value at i^{th} floor and Γ_j is the j^{th} mode's participation factor, given by Equation 3.10.

$$\Gamma_j = \frac{\sum_i m_i \varphi_{i,j}}{\sum_i m_i \varphi_{i,j}^2} \quad (3.10)$$

Combining the first few modes using square-root-sum-of-the-squares (SRSS) gives the PFA profile along the height, a_i , with a maximum value of a_{\max} . For the case study building of RC frame with 4 storeys, the PFA may be approximated by a single coefficient γ defined as in Equation 3.11.

$$\alpha_{SLS} \approx \gamma a_{\max} = 0.6 a_{\max} \quad (3.11)$$

Initial parametric studies on the elastic modal properties of structures suggested that values of γ for low rise structures of 4 storeys of RC frame typology be around 0.6. For the purposes of CSD discussed here, they were deemed reasonable. Table 3.3 lists the spectral acceleration and displacement for the case study building.

Table 3.3. Conversion of θ_{\max} and a_{\max} to spectral values at the SLS

θ_{\max}	$\Delta_{d,SLS}$	a_{\max}	γ	α_{SLS}
0.34%	0.033m	0.4g	0.60	0.24g

3.3.5 Quantification of Feasible Initial Secant to Yield Period Range for SLS

The range of feasible initial secant to yield periods was identified using the equivalent SDOF spectral limits as presented in Table 3.3, which are illustrated in Figure 3.8, and the upper period bound, T_{upper} , for the RC frame in discussion was found to be 2.1 seconds, and the lower period bound, T_{lower} , was found to be 0.4 seconds. These bounds basically imply that the structure's stiffness will be limited so that it does not undergo excessive PFAs, while its flexibility will be limited so that it does not undergo excessive PSDs. For this particular scenario, the period range is quite large, meaning that many potential design solutions could be accommodated. The damping was assumed as 5% for the case study RC frame.

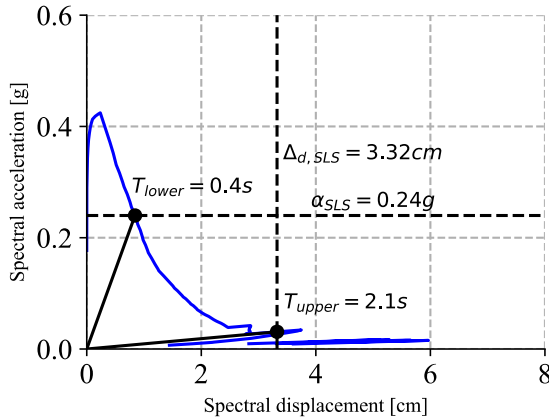


Figure 3.8. Identification of permissible initial secant to yield period range based on PFA and PSD limits for the SLS.

3.3.6 Establishment of Required System Strength and Ductility

At the ULS, where the goal is to limit excessive PSD and provide a margin of safety against collapse during strong shaking, the effects of system non-linearity need to be accounted for. Figure 3.9 presents the permissible period range identified within the points 1 and 2, the trialled value of lateral strength capacity and the design solution space shaded in grey.

For the given ULS spectrum and target design displacement, $\Delta_{d,ULS}$, a suitable SDOF system behaviour needed to be established. As noted by O'Reilly and Calvi [2019], one way of doing this for the ULS, whilst still maintaining control over the initial period, is to simply trial a value of lateral strength. Then, by computing how much spectral reduction capacity would be required via non-linear behaviour, the structure's required ductility demand could be computed. This approach simply reworks the general DDDBD approach, as the design displacement and ULS spectrum are known, but differs since the lateral strength is trialled and a compatible structural geometry is found (via the required yield displacement). DDDBD, on the other hand, operates by commencing with a fixed structural geometry (meaning the yield displacement is known) and for the required ductility with respect to the design displacement and ULS spectrum, the lateral strength is found.

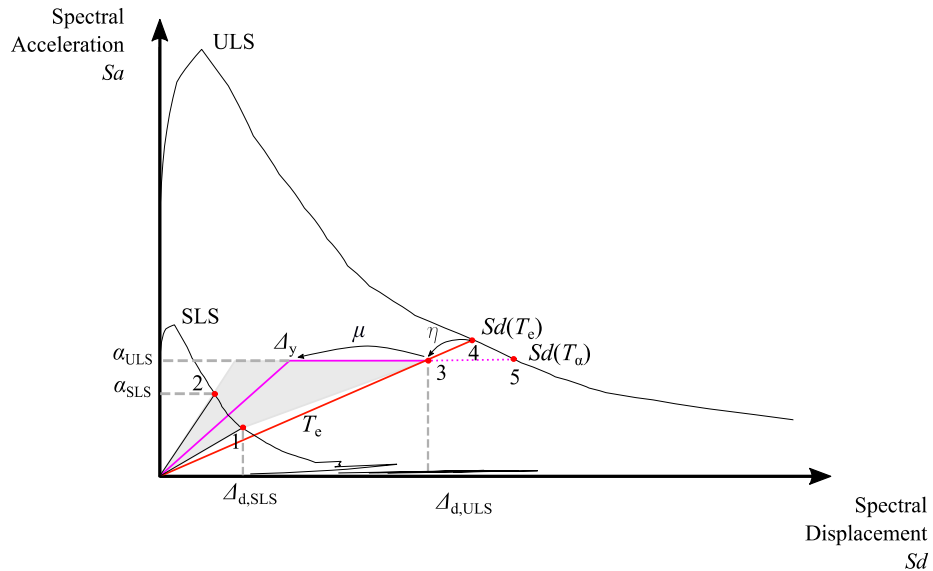


Figure 3.9. Identification of design solution space shaded in grey considering the permissible period range and the trialled value of lateral strength capacity (adopted from O'Reilly and Calvi [2019]).

In this example, the approach described in O'Reilly and Calvi [2019] is followed but potential developments are described in Chapter 3.4.4. To account for the amplification in the structure's spectral capacity via non-linear behaviour of the structure, the effective period, T_e , passing from the origin through point 3 to point 4 was considered. In other words, the relation between linear and non-linear behaviour was found via a displacement modification factor (DMF) to the elastic design spectrum. As stated earlier, the design maximum PSD at ULS was 2.0% which gave a design displacement at ULS, $\Delta_{d,ULS}$, of 0.195m. Given $\Delta_{d,ULS}$ and the spectral displacement of the elastic response spectrum at T_e , $Sd(T_e)$, the required DMF, η , was determined from Equation 3.12.

$$\eta = \frac{A_{d,\text{ULS}}}{Sd(T_e)} \quad (3.12)$$

Priestley *et al.* [2007] outlined various expressions for different structural systems characterised by different hysteretic models, representative of several structural systems and the one for RC frames was utilised here. From this relation, the required ductility, μ , was found by knowing the required spectral modification factor, η .

3.3.7 Computation of Structure's Backbone Behaviour

With the knowledge of permissible period range, the design displacement, the lateral strength and the required structural ductility, the structure's backbone behaviour that respects these conditions was defined. The minimum required ductility previously identified was then used to back calculate to find the yield displacement of the system, Δ_y , as per Equation 3.13.

$$\Delta_y = \frac{A_{d,ULS}}{\mu} \quad (3.13)$$

The final bilinear backbone of the structural system was identified and is illustrated in Figure 3.10, where it was assumed that the second-order geometry effects, or P-Delta effects, were balanced out by the post-yield hardening of the structure to result in an elastic-perfectly plastic system.

The detailed results of the above demonstrations are given in Table 3.4. The designs are essentially governed by a 2% limit imposed on the PSD at ULS, therefore mean annual frequency of collapse (MAFC) targeting approach is preferred in further developments of IPBSD in Chapters 5 and 6. The first case will result in a structure that is too stiff and remains elastic at the ULS. In other words, we may have situations, where in a given location, with a certain return period at ULS, our structure does not need to have a ductile response. Cases 2 and 3 are very flexible and need a certain level of ductility to satisfy the design requirements. However, this is not always true, as in current situations one of the requirements is always unsatisfied. The case 2 structure satisfies the condition imposed by the DMF, which implies that the structure needs to have a very high fundamental period and low ductility, while the case 3 structure is designed in a manner to have higher ductility and lower fundamental period but fails to satisfy the condition imposed by the DMF requirement. When the PSD limit is relaxed, to obtain a valid design solution is easier, even though the reduction of the limit is arbitrary. One common observation with regards to all the cases is that the value of ductility is difficult to control, and unrealistic values might be obtained. However, we need to bear in mind, that a structure might have higher ductility beyond the level of ULS spectra, meaning that the ductility values presented herein consider the response prior to the ULS spectra.

This reflects the current constraints imposed by the CSD at the ULS, where the advantage of being able to identify structural layouts is hampered by the fact that it tends to result in very flexible systems, as was the case demonstrations in this example. Further consideration of the ULS performance that moves away from a single intensity-based verification of one PSD level (*i.e.*, 2% PSD at 1600 years) should be pursued to arrive at a more risk-consistent

approach to collapse safety. This would bring both CSD approach to a reasonable point whereby the losses via EAL and collapse safety are handled in a comprehensive manner. This was a limitation of CSD noted by O'Reilly and Calvi [2019].

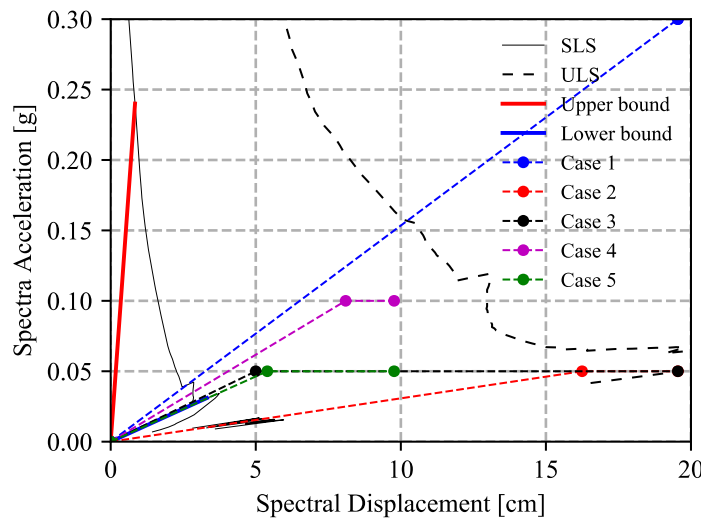


Figure 3.10. Required backbone response for the case study building design solution, where the period limits show how the design conditions have been respected.

Table 3.4. Identification of structural system parameters to respect the design constraints, which fall within the design solution space.

Case	a_{ULS} [g]	$\Delta_{d,ULS}$ [cm]	T_e [s]	$Sd(T_e)$ [cm]	$[\eta_{req} - \eta_{prov}]$	$\mu_{provided}$	Δ_y [cm]	T_1 [s]	C	
$PSD_{limit} = 2\%$	1	0.30	19.6	1.62	10.0	0.00	1.0	19.55	1.62	0.273
	2	0.05	19.6	3.97	23.4	0.00	1.2	16.25	3.61	0.045
	3	0.05	19.6	3.97	23.4	0.25	3.9	5.00	2.00	0.045
	4	0.10	9.8	1.98	11.7	0.00	1.2	8.10	1.81	0.091
	5	0.05	9.8	2.80	14.3	0.00	1.8	5.40	2.08	0.045

3.3.8 Identification of Structural Layout

The final step of the design process was the identification of required geometry for the RC frame. In order to make use of the identified backbone leading to an acceptable building performance, defined in terms of expected loss, two parameters were required: the lateral strength and the yield displacement. As the lateral strength is a function of the member strengths, it can be easily adjusted by modifying the dissipative zone capacities. Structural geometry and material properties were required to establish the yield displacement. As the yield displacement was already known, the final dimensions and material properties of the structural system were identified as they are independent of the lateral strength [Priestley 2003]. For an RC frame with a ductile beam-sway mechanism, the yield drift, θ_y , has been shown by Priestley *et al.* [2007] to be:

$$\theta_y = \frac{0.5\epsilon_y B}{b_b} \quad (3.14)$$

where B is the bay width of the frame and b_b is the beam section height. Assuming a reinforcement of yield strength 350MPa and 200GPa of Young's modulus required dimensions are obtained and shown in Table 3.5. Knowing the lateral load resisting system, structural geometry and the design base shear for the system, the structure can be detailed by providing enough capacity to ensure a ductile and stable mechanism. The resulting structural system would be representative of the backbone identified in Figure 3.10 and should satisfy the performance goals initially defined in terms of EAL described in Section 3.3.2.

Table 3.5. Suitable building geometry

Case		Δ_y [cm]	b_b [m]	B [m]
$\text{PSD}_{\text{limit}} = 2\%$	1	19.55	0.5	10.0
			0.3	6.0
	2	16.25	0.5	8.5
$\text{PSD}_{\text{limit}} = 1\%$	3	5.00	0.5	2.5
	4	8.10	0.5	4.5
	5	5.40	0.5	3.0

As observed, at ULS, a situation may occur where $\Delta_{d,ULS}$ is equal, or very close, to $Sd(T_c)$, meaning that the required DMF and consequently the ductility, μ , will be limited or equal to 1. This will essentially result in designs with very long periods and limited ductility demand. Consequently, a high bay width will be required to provide a yield displacement equal to the required one. An alternative would be to neglect the condition of DMF equality, as also briefly discussed in O'Reilly and Calvi [2019], and provide the structure with ductility higher than 1, which would then result in a lower bay width.

3.4 SENSITIVITY STUDIES

Using the design framework summarised in Section 3.2 and implemented in a case study application in Section 3.3, additional studies on essential characteristics of the framework were conducted. Those lay the foundation for the improvements to be discussed in Chapters 5 and 6. The goal was to understand whether the methodology could be improved in relation to the definition of the ULS performance and the sensitivity of the EAL to the SLFs. As before, the RC bare frame with office occupancy described in Section 3.3 was the reference design used for comparison throughout the discussion.

3.4.1 Influence of SLS Parameters

One of the first studies regarding the definition of the performance objectives listed in Table 3.1 was on the sensitivity of the design EAL to the choices made regarding the return period of ground shaking, T_R , and the level of ELR at the SLS. The same values of y and T_R assumed for the OLS and ULS in Table 3.1 were maintained and the EAL was computed for numerous combinations of y_{SLS} and $T_{R,SLS}$. A summary of these design scenarios is presented in Figure 3.11. In essence, the hazard curve relates PGA (right axis) to T_R (left axis), and the SLF relates θ_{max} (top axis) to ELR (bottom axis). By increasing the y_{SLS} and $T_{R,SLS}$, the EAL, represented in green shades, will essentially stay constant. While, if the y_{SLS} is increased only or $T_{R,SLS}$ is decreased only, then the EAL will increase. Figure 3.11 then shows the design solutions depending on $T_{R,SLS}$ and y_{SLS} . Only the upper bound results are shown, since the resulting designs indicated no required lower period bound. The empty solution space represents an area where the solutions are beyond practicality, *e.g.*, having an excessively high base shear coefficient, C , or an impractically high required bay width, B .

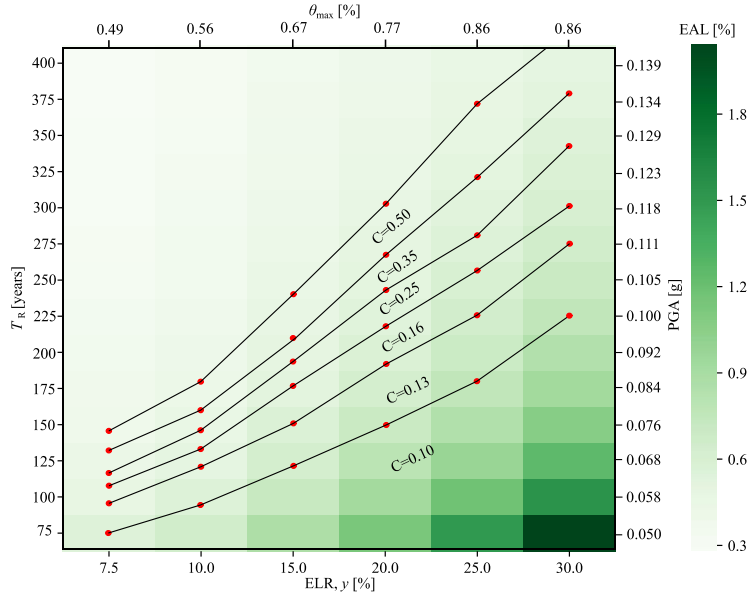


Figure 3.11. Impact of varying y_{SLS} and $T_{R,SLS}$ on the design EAL.

The study carried out on the variation of SLS parameters, showed high sensitivity of EAL to the SLS parameters. Additionally, the lower period range limit will be highly dependent on the PGA (and subsequently $T_{R,SLS}$) while the upper period range limit will be highly dependent on the θ_{max} (and subsequently y_{SLS}). The curves defining C represent structures with an initial period equal to the upper period range limit and conditions imposed by each pair of $T_{R,SLS}$ and y_{SLS} below the curves can be satisfied by a structure with C equal to the curve value. Hence, the curves depend on an upper period range limit. Higher y_{SLS} and lower $T_{R,SLS}$ imply higher upper period range limit. For the study, the y_{SLS} was kept constant, while the $T_{R,SLS}$ was increased gradually, leading to a decreasing upper period range limit further constraining the design solution space, which resulted in the curves defining C boundaries.

3.4.2 Sensitivity Study on SLFs

When using the SLFs as per Figure 3.6, the PSD at ULS for ELR=100% will be in the order of $\theta_{max}=10$ to 20%. This value of θ_{max} may make sense purely from a monetary loss accumulation point of view but is clearly unfeasible from a collapse performance perspective. To implement the CSD with these SLFs, a decision was made to limit θ_{max} to a limit similar to what ASCE 7-16 [2016] prescribes to provide a level of life safety against collapse in their designs. This approach of utilising SLFs for the definition of the SLS

design parameters but simply limiting the PSD to 2% at the ULS was adopted in the case study described in Section 3.3. The goal of the sensitivity study described here is to understand what impact this decision has on the design EAL. The SLF for PFA sensitive non-structural elements was not modified as the CSD methodology does not utilise the PFA at ULS.

Figure 3.12 shows the steps of the sensitivity study for the modification of SLFs for the CSD methodology. Initially, an original EAL was calculated through the employment of the SLF curves of the PSD-sensitive structural and non-structural elements adopted from Ramirez and Miranda [2009]. Then a cut-off vertical line (in blue) representing a PSD value was gradually lowered, where the cut-off line describes a value of the PSD above which the ELR is assumed 100% times the respective weight of the element, Y_{PSD} . With each version of SLF, a corresponding EAL value was computed and then compared to the original one. The procedure was repeated until the error, ε_{EAL} , increased beyond 0.2% and the final updated SLF with the corresponding PSD cut-off line was used in the CSD presented herein.

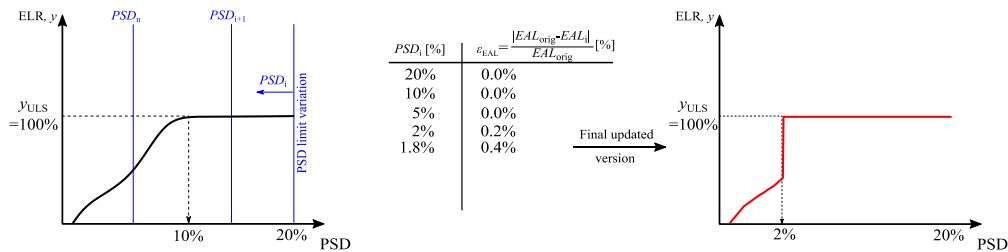


Figure 3.12. Sensitivity study on the modification of SLFs for the framework by the variation of PSD until EAL error, ε_{EAL} , is beyond 0.2%.

The preliminary limit value obtained through the sensitivity study was 2% for PSD. By using the original and updated curves shown in Figure 3.6, the EAL variation error was found to be below 0.2%. Hence, the inclusion of such a limitation of PSD when utilising SLFs at ULS does not significantly impact the design EAL. Therefore, it can be concluded that the limitation of the PSD to 2% at ULS similar to what is done in the US with ASCE 7-16 [2016], does not have any major impact on the design EAL that has been focused on up until now in CSD. Should the nature of determining the performance goals in CSD change from utilising EAL solely for the definition of the SLS limits and establishing an initial period range and then other possible criteria related to strength or ductility be utilised to protect against collapse, these two performance definitions will not have any major interaction with each other and can be treated separately.

3.4.3 Validation of the Plastic Hinge Yield Rotation Assumption

A test was carried out to check the validity of the plastic hinge yield rotation assumption by using Equation 3.14. For case 4 obtained in Section 3.3, a model was created, and a non-linear SPO analysis was carried out to compute the yield displacement corresponding to the base shear. Ideally, the yield displacement identified earlier should match the one obtained via the model with the same base shear and fundamental period characteristics. The results are presented in Table 3.6, and demonstrate that in certain occasions the equation might not be a good estimator based on purely beam cross-section height and bay width. The frame has 4 storeys, 2 bays, and has the already identified 4.5 m widths and a beam cross-section height of 0.5m.

Table 3.6. Yield deformation verification.

Case	Type	Sa_y [g]	Δ_y [cm]	T_1 [s]
1	Equation 3.13	0.10	8.10	1.80
2	Model	0.093	10.10	1.78

3.4.4 Consideration of Collapse Performance in Design

As shown in the previous section, SLS and ULS performance can be handled with separate criteria without any major interference between them. With regards to collapse safety, MAFC, λ_c , may be used and a potential procedure to incorporate this in the CSD framework is described in Figure 3.13. The reasons for this are also illustrated in Figure 3.13(a) and are as follows. At ULS, a situation may occur where $\Delta_{d,ULS}$ is equal, or very close, to $S_d(T_c)$, meaning that the required DMF and consequently the ductility, μ , will be limited or equal to 1 (red point in Figure 3.13(a)). This will essentially result in designs with very long periods and limited ductility demand. Consequently, a high bay width will be required to provide a yield displacement equal to the required one. An alternative would be to neglect the condition of DMF equality, as also briefly discussed in O'Reilly and Calvi [2019], and provide the structure with ductility higher than 1 (in blue in Figure 3.13(a)), which would then result in a lower bay width.

Alternatively, this could also be achieved by using MAFC to design for collapse safety in a more risk-consistent manner, as described as follows. An SDOF with period T that falls within the already identified period range $[T_{lower}, T_{upper}]$ and an anticipated ductility capacity μ is considered. Knowing the yield lateral spectral acceleration, Sa_y , the dynamic performance of a trialled SDOF up to complete collapse can be quantified via the SPO2IDA tool [Vamvatsikos and Cornell 2005], as shown in Figure 3.13(b). Knowing the

collapse fragility and the hazard curve, these may be integrated to get the MAFC, λ_c , where the collapse fragility defined in terms of R (Figure 3.13(b)) is transformed to spectral acceleration Sa by using a transformation factor, Γ , to a collapse fragility of the actual MDOF system (Figure 3.13(c)). By setting a target collapse safety to be respected by the resulting design, the base shear coefficient can be found for a given ductility, μ , and initial period, T_1 . By varying T_1 , a satisfactory base shear coefficient curve can be plotted in Sa versus Sd and the feasible structural solutions may be found (Figure 3.13(d)). It is noted that this approach is not too dissimilar to the YFS method of Vamvatsikos and Aschheim [2016] but here just the collapse behaviour is focused on, in addition to maintaining a degree of control on the EAL via the initial period range.

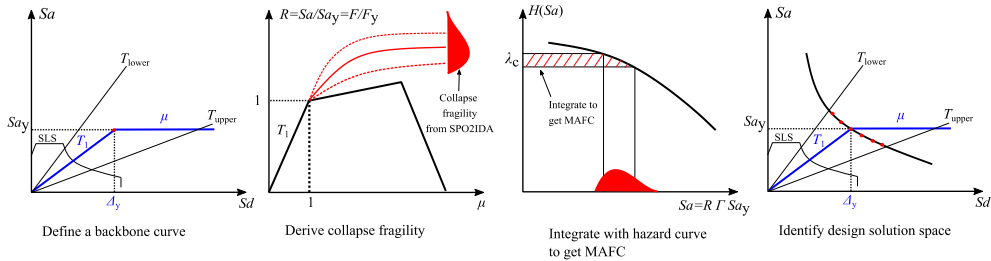


Figure 3.13. Potential development of the framework to incorporate MAFC as a design variable.

The red dots in Figure 3.13(d) represent several of the numerous feasible design solutions within the period range that satisfy the collapse safety criterion. This approach would help to avoid the issue of SLFs identified in the previous section and overcome the difficulties explained in Section 3.3.6.

3.5 SUMMARY

A novel CSD framework utilising EAL was used to identify feasible structural solutions aligning with the conceptual objectives of performance-based design. The general procedure with a case study application for a RC moment resisting frame was presented herein for its illustration. Several assumptions were made: first, SLFs were used to convert ELRs to design PSD and PFA. At ULS, where a collapse prevention requirement has to be met, the PSD was cut-off at 2%, corresponding to the requirement brought forth by ASCE 7-16 [2016]. Two limit state intensities, SLS and ULS, were utilised to characterise the structure's initial elastic and ductile non-linear behaviour. At SLS, design PSD and PFA were used to define a permissible initial secant to yield period range. Subsequently, with the choice of lateral strength and the knowledge of required system ductility, the yield displacement of the system was computed. Finally, the design solution space was established, and a potential bilinear backbone determined. Based on the characteristics

identified, the required dimensions of the structure were calculated as part of the first phase of design.

Moreover, some sensitivity studies were carried out to further investigate some particular aspects of the CSD framework. Several notes could be made based on these studies:

- High sensitivity of EAL and period range limits to the SLS parameters, as: 1) increasing ELR or decreasing T_R results in an increase of the EAL; and 2) decreasing T_R and increasing ELR will lead to an increase of the upper period range limit, meaning that care must be taken when establishing these points in design;
- Limiting PSD to 2% (similar to what is done in ASCE 7-16 with the aim to design for collapse safety) and modifying SLFs corresponded to an error in EAL of only 0.2%, demonstrating that it does not have any major impact on the design EAL;
- To avoid observed difficulties of implementing the CSD framework at ULS, an alternative approach was pondered. This does away with the issue where the required DMF and ductility could potentially lead to large bay widths to satisfy the yield displacement requirement. The alternative approach foresees that the ULS is no longer considered, but rather a target MAFC, which is satisfied by a system with base shear coefficient, C , for a given ductility, μ , and an initial period, T , which must lie with the period range identified for SLS.

In the following chapters, the CSD framework will be improved to include the current approach for SLS, where the elastic properties of the structure are chosen to satisfy the target EAL, while a simplified collapse analysis is used to satisfy a target MAFC, in addition to the development of software tools that may permit their application.



4. STOREY LOSS FUNCTIONS FOR SEISMIC DESIGN AND ASSESSMENT: DEVELOPMENT OF TOOLS AND APPLICATION

This chapter is based on the following reference:

Shahnazaryan, D., O'Reilly, G. J., Monteiro, R. [2021] "Story loss functions for seismic design and assessment: development of tools and application," Earthquake Spectra. DOI: 10.1177/87552930211023523.

4.1 CHAPTER OVERVIEW

As presented in Chapter 2 and 3, SLFs are required for the application of the proposed performance-based seismic design framework. To aid the designers, this chapter proposes a toolbox for the creation of SLF as a simplified alternative to the typically detailed component-based approach (*i.e.*, FEMA P-58, described in Section 2.4.1). These SLFs are used to estimate a building's expected monetary loss per storey due to seismic demand and reduce the data required compared to a detailed study, which is especially true at a design stage, where detailed component information is likely yet to be defined. This chapter proposes a Python-based toolbox for the development of user-specific and customisable SLFs for use within seismic design and assessment of buildings. It outlines the implementation procedure alongside a comparative demonstration of its application where dependency and correlation of damage states between different components are considered. Finally, a comparison of SLF-based and component-based loss estimation approaches is carried out through the application to a real case-study school building. The agreement and consistency of the attained loss metrics demonstrate the quality and ease of the SLF-based approach in achieving accurate results for a more expedite assessment of building performance.

4.2 DEVELOPMENT OF A SLF ESTIMATION TOOLBOX

The framework utilised herein defines SLFs as based on component inventories and their classification into different component groups. For the proper estimation of repair costs associated with each component, consistent integration of component fragilities with repair

costs at the storey level is carried out. The framework consists of the following steps (Figure 4.1):

1. Building characterisation;
2. Component inventory definition;
3. Component grouping;
4. Consideration of correlations between components;
5. Monte Carlo Simulation of damage states;
6. Repair cost computation;
7. SLF fitting.

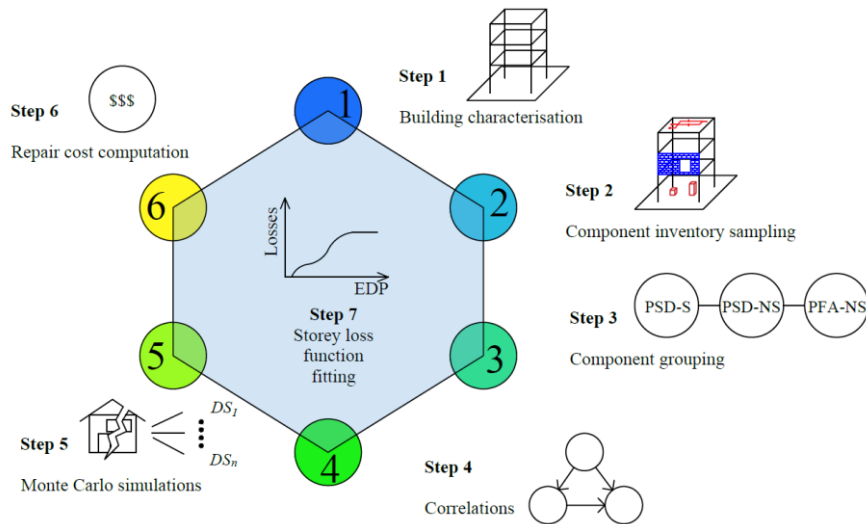


Figure 4.1. Flowchart of storey loss function generation framework.

The approach utilised in this study is based on the storey loss estimation framework by Ramirez and Miranda [2009], which is used to develop a toolbox for creating generic user-based SLFs. Component quantities, fragility and consequence functions are used as input components to generate FEMA P-58 compatible SLFs [FEMA 2012a]. The method proposed by Ramirez and Miranda [2009] uses the 2007 RS Means Square Foot Costs [Balboni 2007], applicable to the US only, to estimate the building cost distributions for different RC building occupancies in California. The main difference of the more recent proposal by Papadopoulos *et al.* [2019] was the use of the FEMA P-58 database [FEMA 2012a], where the functions were customisable with respect to replacement cost and to reflect building's floor area. The functions developed by Papadopoulos *et al.* [2019] were developed for steel buildings in Greece; however, no damage or spatial correlation was considered among the different components, as opposed to the former approach. To aid the generation of engineering demand parameter – decision variable (EDP-DV) functions or loss assessment in general, significant research has been carried out with the goal of

developing fragility and consequence functions for various structural and non-structural components. For example, fragility and consequence functions were developed for unreinforced masonry buildings by Ottonelli *et al.* [2020], many others have focused on masonry infill walls [Cardone and Perrone 2015; Chiozzi and Miranda 2017; Del Gaudio *et al.* 2019; Ruiz-García and Negrete 2009; Sassun *et al.* 2016], while some concentrated on developing functions for RC structural components [Aslani and Miranda 2005; Cardone 2016]. Furthermore, recent studies on loss estimation [Perrone *et al.* 2019; Sullivan 2016] highlighted the need for developing SLFs to cover a wide range of building characteristics (*i.e.* storey-wise functionality, typology of structure, occupancy). Sullivan [2016] presented a simplified loss assessment approach to calculate the EAL which could act as a quick estimation tool for identifying necessary design or retrofit choices early in a project and effectively reduce the monetary costs. However, a limitation was highlighted, whereby the knowledge of quantity, distribution, and characteristics of all damageable components within the building inventory might not always necessarily be readily available and, to address it, SLFs could be used. On the other hand, Perrone *et al.* [2019] proposed a method for estimating EAL of Italian RC buildings, which also utilises suitable SLFs, further demonstrating the need to develop simplified alternatives.

The goal of this chapter is to present a toolbox that allows the automated production of SLFs through regression analysis using the results of random sampling of component damage states and costs, including damage correlation among components. The goal is not the development of generic loss functions for specific building occupancies but the development of a tool for practitioners to create their own functions, based on their needs using an existing database of components, such as FEMA P-58 or any other means (*e.g.*, expert judgment), without being limited to existing SLF libraries.

4.2.1 Step 1: Building characterisation

The first step of the framework foresees examining the characteristics of the building of interest. The user should have relevant information on the structure's height, namely number of storeys, global dimensions, occupancy type and usage. In many situations, the building's components will vary on a storey-by-storey basis (*i.e.*, the components will not necessarily be identical in type and quantity at the ground floor, roof level and intermediate storeys). For example, the contents of the ground storey of a residential building may vary significantly in terms of structural and non-structural components compared to upper storeys, since this may comprise commercial space or car parking. In contrast, the roof level generally includes components, such as heating, ventilation and air-conditioning (HVAC) equipment or necessary equipment for geared elevators, which are not located at other storeys. All such considerations need to be made to arrive at a comprehensive

description of the building's characteristics and where the damageable components are distributed.

4.2.2 Step 2: Component inventory

Once the occupancy type, structural typology, and other specific building characteristics have been established, the damageable component inventory can be created. There are several methods to aid the user to gain insight into the possible distribution of components if it is not preliminary known, as is the case for new designs. The distributions, which assume knowledge of mean and uncertainty of a given component quantity, may be obtained from empirical and statistical data, collected from existing buildings and surveys, or based on expert opinion or personal judgment when such information is unavailable. The inventory consists of structural, non-structural components, and storey contents likely to be damaged, which contribute to the economic losses associated with required repair costs.

In general, the component data inventory should have information on item types, quantity of each component, EDP sensitivity and typology (structural or non-structural) of each component. Three performance groups are to be identified unless otherwise specified, and fragility and consequence functions for the components should be available. To define the component database, damage states with corresponding fragility and consequence functions accounting for best fitting function suggestions (*e.g.*, normal, lognormal, etc.) may be adapted from the FEMA P-58 database or other similar sources.

Another consideration to account for is to distinguish whether certain components will be affected by the PFA of the floor slab above the current storey or by the supporting floor slab (Figure 4.2). For instance, the water distribution piping system connected to the ceiling in a storey will be sensitive to the PFA of the above floor, while contents (*e.g.*, electronic equipment or contents) will be sensitive to the PFA of the supporting floor. To account for this, a simplifying assumption is made in the tool. The component losses in the storey i , but affected by the upper floor, are computed as part of, or moved to, storey $i+1$. This essentially means that the estimation of total costs in the building is theoretically correct, but the physical location of the costs is not (*i.e.*, a storey i component loss sensitive to PFA of the floor above will see its cost be logged as storey $i+1$ losses). This assumption was deemed suitable when considering the alternative simplifying assumption of utilising the incorrect PFA demand at storey i , and subsequently an incorrect loss, to maintain the correct storey location.

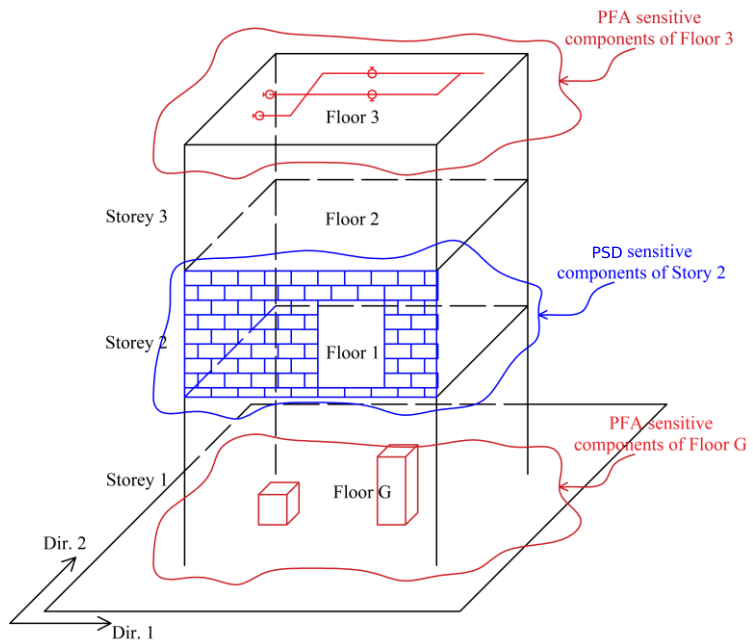


Figure 4.2. Component group and storey loss function identification.

Finally, to generate a component inventory in a meaningful manner, it is important to be aware that, during assessment, even if component information is known, it might not be possible to count the entire physical inventory precisely. A distinction could be made concerning the reference area used for the component inventory. For that purpose, as in FEMA P-58, an approach assuming quantities per m^2 may be applied, which are then scaled to a unit area (*e.g.*, 100 m^2). Then, by counting only the stock of individual components, the quantities are extrapolated to arrive at an estimated amount of a component type within a storey. However, this is only applicable to components whose inventory is large enough and when the counted components are representative. For example, elevator or HVAC systems are specific to certain locations of the building (*i.e.*, neither distributed along with the height nor the area of the building). Hence, in this case, scaling per m^2 will not be applicable and unitary estimates based on floor area thresholds should be considered instead.

The framework adopted in this study assumes two-dimensional (2D) structural modelling, where the damageable components are oriented in the same direction. However, should one apply the framework to three-dimensional (3D) buildings, the SLFs could be calculated by making assumptions on how the building components of different orientations are distributed. In specific, functions for both directions of a storey for that specific

component could be developed. Essentially, the framework could be applied in each direction separately with appropriate care and consideration. In specific, the analyst would need to identify, for each damageable component considered at each storey level, in which principal direction of the building it is sensitive to damage. This way, the components can be grouped and analysed separately using the structural demands in the two orthogonal directions. Furthermore, in the case of non-directional components, such as the acceleration-sensitive non-structural components analysed in the case study building, where both directions of the seismic action are of importance, the maximum value of the two demand parameters in both directions may be multiplied by a non-directional conversion factor, as suggested in FEMA P-58, and used for a single SLF in the analysis. However, similar to components located on different storeys and within different performance groups, interactions of seismic effects in the two directions on a given component are not accounted for and in cases where such interaction is expected to be significant, more advanced methods of loss assessment should be adopted.

4.2.3 Step 3: Component grouping

Once the component inventory has been identified, depending on the type of components (*i.e.*, structural, or non-structural) and their sensitivity to a specific EDP (*i.e.*, to PSD or PFA), the components are classified into performance groups. Three performance groups are established: PSD-sensitive structural, PSD-sensitive non-structural, and PFA-sensitive non-structural components. Components within a performance group will be assessed together for a mutual demand and subsequent losses will be summed up to estimate the group's SLF. In other words, losses from all components within a performance group will be tied to the same EDP.

As in the case of similar past studies [Papadopoulos *et al.* 2019; Ramirez and Miranda 2009], the effects of other EDPs, such as vertical acceleration or building torsion, are not accounted for herein. Additionally, torsion could be better dealt with adopting a component-based approach, as discussed in O'Reilly *et al.* [2017]. However, it is important to keep in mind that if one is to provide the toolbox with fragility and consequence functions associated with components other than PSD or PFA sensitive (*e.g.*, peak floor velocity, PFV), the toolbox will still be capable of producing the corresponding desired SLFs.

In addition to having a separation between different component typologies, the classification into performance groups allows the disaggregation of losses at the later stages to identify the main contributors to the direct economic losses accumulated throughout a building. This is especially important for visualisation purposes, as the loss contribution from collapsing and non-collapsing cases may be easily established along with loss

contributions of individual storeys and performance groups (*e.g.*, structural, and non-structural components).

4.2.4 Step 4: Consideration of correlations between components

Structural and non-structural components that are sensitive to the same EDP may be grouped to allow the consideration of possible correlations between different performance groups. For example, even though a specific intensity level might not entail damage to a specific non-structural component alone, a structural component connected to it might be damaged. This means that to repair the structural component, access should be first granted, which foresees the removal of the portion or the entirety of the undamaged non-structural component. When dependencies are considered, it was shown [Ramirez and Miranda 2009] that there may be an error if the repair cost of the dependent component is counted twice. For example, the columns in a moment-frame building and internal partitions may be damaged, but the repair cost of a dependent component may be counted twice (the so-called double-counting). Hence, care should be taken to provide proper repair costs and to establish correct relationships between components that best align with their actual physical relationship. Essentially, for any component i , if it is not dependent on any other component, then all its damage states (DSs) are assumed to have an independent sequential occurrence unless otherwise specified and each DS is assumed to be mutually exclusive (*i.e.*, the occurrence of one damage state means that the other ones will not happen). A probability of occurrence is assigned (see Step 5) to mutually exclusive DSs, which sums up to 100%. Otherwise, if DS j of component i is also dependent on the occurrence of a DS d of a component m , then the DS of component i is assumed independent of component m unless component m is in DS d or higher (*i.e.*, DS d in component m triggers DS j in component i). For dependent components, this triggered DS, DS_{trig} , is identified, which is based on the causation DS of another component, as illustrated in Figure 4.3. In the example, for an EDP of edp , once the causation component m is in DS3, even if the fragility parameters of the dependent component i do not indicate any damage, it will still be in DS2, as it depends on the DS of component m (*i.e.*, the dependent component's triggered DS is DS2). Analogously, if component m is in DS2, then the triggered DS of i is DS1.

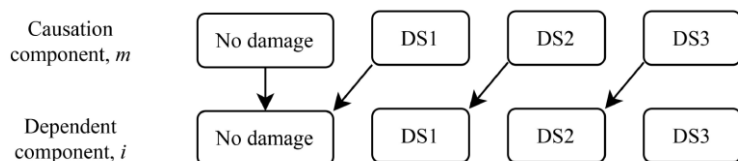


Figure 4.3. Relationship between causation and dependent components.

4.2.5 Step 5: Monte Carlo simulation of damage states and repair costs

With the component inventory identified, along with the fragility and consequence functions and possible correlations among the damage states of different components, Monte Carlo simulations are performed. For each simulation, damage and repair costs are sampled for each component of the performance group and each cost is added to obtain the performance group's total loss for a given EDP. Figure 4.4 presents a flowchart illustrating the algorithm for the estimation of SLFs. For both uncorrelated components, where independence of each component is assumed, and in case of existing correlation among different component types, the algorithm samples damage states for each component at each EDP level and a specified number of simulations. Essentially, a random value is generated between 0 and 1 representing the probability of being in a DS; then, a DS is assigned to a component based on its fragility functions (Figure 4.5). This process, described in Step 4, is repeated for each dependent component for the population of the damage state matrix. For example, to assign a DS to a component from the simulations, if $EDP=0.02$ (point 1 in Figure 4.5) and the sampled probability for the causation component is 0.3, then DS3 is assigned to the component. In the same example, the sampled probability for the dependent component is 0.8 for $EDP=0.02$, meaning that DS1 is assigned. Following the relationship of the components described in Figure 4.3, the DS of the dependent component is modified to DS2. Alternatively, for $EDP=0.03$ (point 2 in Figure 4.5), if through the same process DS2 and DS3 are assigned to the causation and dependent components, respectively, following the relationship in Figure 4.3, no modifications would be required.

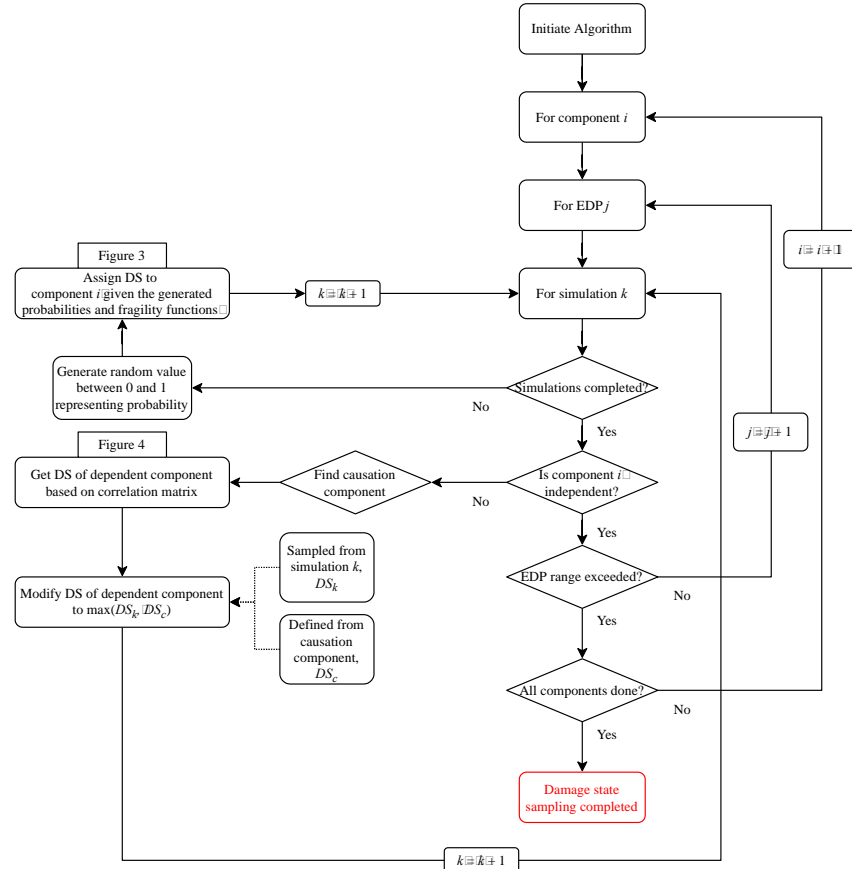


Figure 4.4. A sampling of damage states using Monte Carlo simulation.

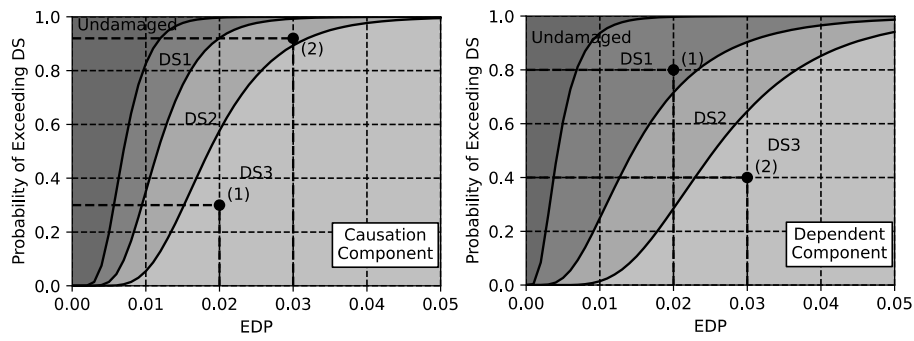


Figure 4.5. Damage states and fragility functions of a sample: (a) causation component and (b) dependent component.

4.2.6 Step 6: Repair cost computation

With the damage states assigned to the components per each Monte Carlo simulation, repair costs may be evaluated (Figure 4.6). For each component at each sampled DS, repair costs are assigned based on the provided consequence functions. In case the consequence function is represented solely through the mean value, then the mean value is assigned. If a distribution of the repair cost is provided (*i.e.*, mean, and standard deviation if normally distributed or median and dispersion for lognormal distributions), then a random value is sampled from the distribution and a corresponding repair cost is assigned to consider the uncertainty in estimating repair costs also.

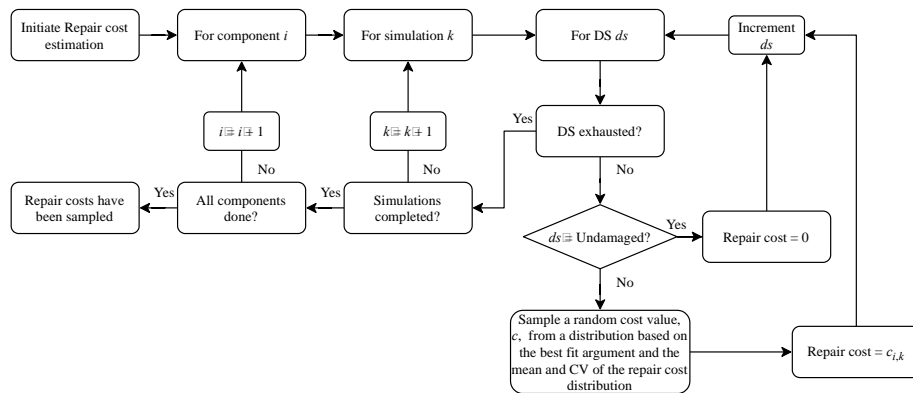


Figure 4.6. Assignment of component repair costs based on sampled damage states.

In order to normalise the repair costs, a replacement cost of the building, $RepCost$, should be provided by the user or else be set equal as unity, meaning that no normalisation is carried out. The previously identified repair cost of component i at simulation k , $c_{i,k}(q_i)$, may then be normalised using Equation 4.1:

$$\hat{C}_{i,k} = \frac{c_{i,k}(q_i)}{ReplCost} \quad (4.1)$$

where $\hat{C}_{i,k}$ is the normalised repair cost of component i at simulation k and q_i is the quantity of component i , of which the repair cost is a function (*i.e.* the repair cost per unit may decrease with increased units). As illustrated in Figure 4.7, based on q_i , the mean repair cost, c_i , is obtained, which is used in conjunction with the coefficient of variation, cor , for generating a normal distribution of repair cost. Finally, a value of $c_{i,k}(q_i)$, is randomly sampled from the distribution.

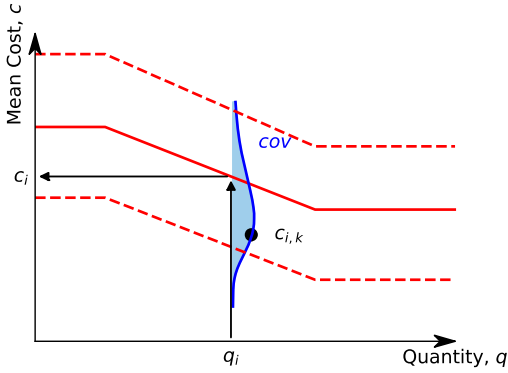


Figure 4.7. Consequence function describing the relationship of repair cost as a function of quantity.

Then, the total normalised repair cost at simulation k , for component i , $\hat{C}_{total,i,k}$, is computed through a summation of the repair costs of all the components according to Equation 4.2:

$$\hat{C}_{total,i,k} = \hat{C}_{i,k} q_i \quad (4.2)$$

The normalised total repair cost of storey st at simulation k , $\hat{C}_{st,k}$, will be the sum of normalised repair costs of all components at that storey, as per Equation 4.3:

$$\hat{C}_{st,k} = \sum_{i=1}^m \hat{C}_{total,i,k} \quad (4.3)$$

where m is the number of component types within the storey inventory.

4.2.7 Step 7: Storey loss function fitting

With the component inventory defined and classified into performance groups, along with the consideration of possible correlations among various components, the SLFs for component groups may be identified through regression analysis on the normalised repair costs sampled. More than one analytical expression may be used within the toolbox, while possible addition of new functions may be considered, as future research identifies better alternatives. The Weibull cumulative distribution function may be used to perform the regression, which is defined in Equation 4.4:

$$y = \alpha \left(1 - \exp \left(- \left(\frac{x}{\beta} \right)^\gamma \right) \right) \quad (4.4)$$

where, α , β and γ are the fitting coefficients, x is the EDP value and y is the fitted loss ratio value. Alternatively, the regression model proposed by Papadopoulos *et al.* [2019], defined in Equation 4.5, may be used:

$$y = \varepsilon \frac{x^\alpha}{\beta^\alpha + x^\alpha} + (1 - \varepsilon) \frac{x^\gamma}{\beta^\gamma + x^\gamma} \quad (4.5)$$

where, α , β , γ , δ and ε are the fitting coefficients of the regression analysis, x is the EDP and y is the fitted loss ratio. The accuracy of the regression is then gauged through the estimation of maximum, $error_{max}$, and cumulative, $error_{cum}$, relative regression errors over the EDP range for each component performance group, according to Equations 4.6 and 4.7:

$$error_{max} = \max \left(\frac{|C_{repair}^{EDP} - \hat{C}_{repair}^{EDP}|}{\max(C_{repair}^{EDP})} \right) \quad (4.6)$$

$$error_{cum} = \int_0^{EDP=\max} \left(\frac{|C_{repair}^{EDP} - \hat{C}_{repair}^{EDP}|}{\max(C_{repair}^{EDP})} \right) dEDP \quad (4.7)$$

where C_{repair}^{EDP} and \hat{C}_{repair}^{EDP} are the original and fitted repair costs, respectively.

4.2.8 Summary

The proposed framework yields, as main outputs, SLFs for each performance group (Figure 4.1). Loss estimation can then be carried out similarly to the FEMA P-58 guidelines, which utilises a probabilistic approach for estimation of damage and corresponding loss. The losses are scaled based on the unit area considered, which could be a small portion of the storey area or the total area of the storey.

While the total loss may be expressed via a monetary measure such as dollars or euros, one may opt to normalise the fitted SLFs with respect to the total storey cost (Equation 4.1), so that they may be scaled or converted to match the common standards of any country. However, attention should be paid to how and where from the component fragility and consequence functions are obtained, given that the data from FEMA P-58, when used

outside the US, even if scaled by a conversion factor, might not be appropriate. In such cases, a rational conversion specific to a country, as proposed by Silva *et al.* [2020], is recommended.

The final stage of estimating SLFs involves a regression on the generated data to obtain the fitted curves, which may be carried out assuming Equation 4.4 or Equation 4.5. The tool itself is implemented in a Python script, which is available at GitHub [Shahnazaryan *et al.* 2021a]. Figure 4.8 illustrates the program structure of the entire SLF generator module and Figure 4.9 presents an overview of the main interface of the toolbox.

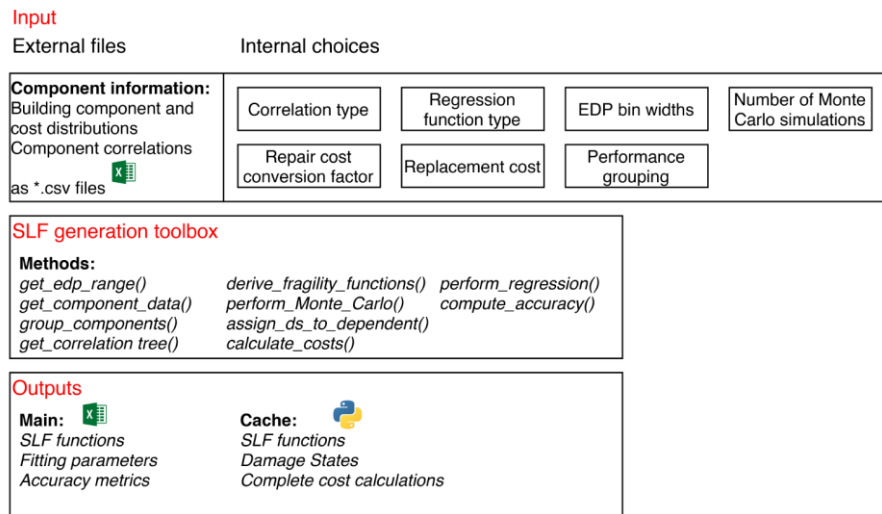


Figure 4.8. Programming structure of the SLF generation toolbox.

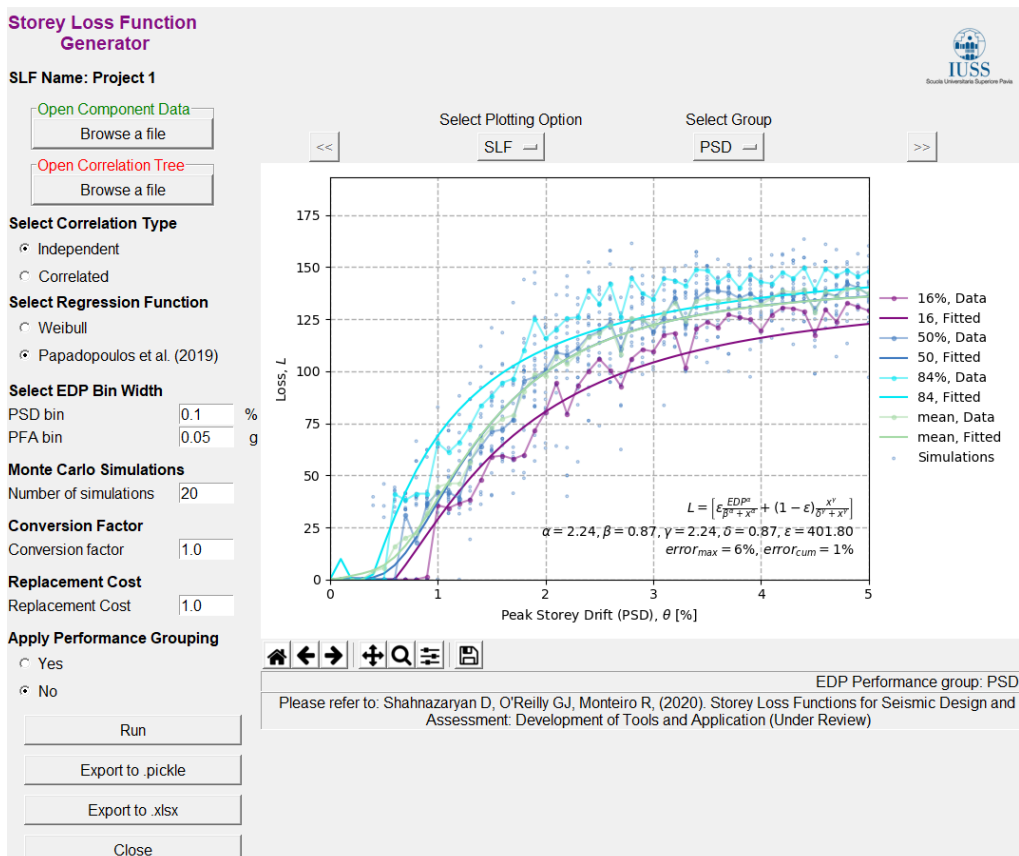


Figure 4.9. Overview of the storey loss function generator interface.

4.3 CASE STUDY APPLICATION

4.3.1 Characterisation of case-study building

For the demonstration of the toolbox and generation of SLFs, a case-study building was adopted from O'Reilly *et al.* [2018] for a testing and validation exercise to be compared with component-based assessment following the FEMA P-58 guidelines. For this, typical cost distributions for the case-study building need identification. The selected school building, constructed in the 1960s, consists of three storeys and has a RC frame with masonry infills as the lateral force-resisting system. The aforementioned study [O'Reilly *et al.* 2018] provides the distribution of the structural and non-structural components, their fragility and consequence functions. Figure 4.10 illustrates the structural configuration of the case study building. The building has RC square columns of 30cm and beams of 30 by 50cm, which were designed for gravity loads only. Infills were identified as double leaf 12 cm hollow clay brick with a 5cm wide internal cavity and the floor systems were identified as

“laterizio” found commonly in Italy at that time of construction. The following subsections address the primary details and assumptions associated with the component data inventory selected and how inputs are created for the toolbox to generate SLFs.

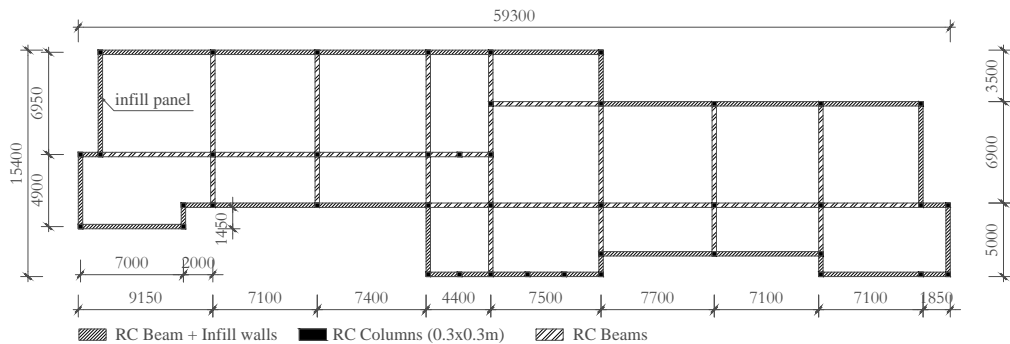


Figure 4.10. Main geometrical and structural properties of the case study building adapted from O'Reilly *et al.* [2019].

4.3.2 Building components and cost distributions

The second storey (intermediate storey) of the case-study building was selected here for the demonstrative analysis comparing SLF generation, assuming both independence and correlation of some components. However, the toolbox was also applied to generate SLFs for the whole structure and loss assessment was carried out to validate the results with respect to a component-based approach. Cost distributions for the structural and non-structural components and detailed component inventory with quantities were adopted from O'Reilly *et al.* [2018]. Table 4.1 and Table 4.2 summarise the mean structural and non-structural component quantities, respectively. The tables identify the type of the component, the demand parameter that the component is sensitive to, the unit for measuring the quantity of the component and the quantities of each type of component. For structural components, PSD is assumed as the EDP, while for non-structural components, the main EDPs are both PSD and PFA.

For the sake of brevity, only PFA and PSD sensitive components were analysed. Only the bookcases were defined as sensitive to the PFV demand parameter in O'Reilly *et al.* [2018] so it was decided to omit it from this study and reimplement the component-based approach without it. Moreover, PFA-sensitive components were grouped depending on the location within a storey and to which EDP they were sensitive. That is, components such as piping systems located in a storey i but sensitive to the EDP of the above storey were tied to the PFA of storey $i+1$, while components such as computers located in the storey i that are not sensitive to the above EDP were tied to the PFA of storey i , as described previously.

Table 4.1. Mean quantities for the damageable structural components of the case-study school building in the longitudinal direction (quantities for the transverse direction listed in parenthesis).

ID	Component	Demand parameter	Unit	Quantity per storey		
				Storey 1	Storey 2	Storey 3
A101	Exterior beam-column joints (end-hooks)	PSD [%]	per unit	20(26)	20(26)	20(26)
A104	Interior beam-column joints (weak columns)			23(15)	23(15)	22(14)
A110	Ductile weak columns (lapped)			44	44	44
A121	Exterior masonry infill (with windows)		per m ²	454.5 (127.77)	454.5 (127.77)	447.4 (125.8)

4.3.3 Component fragility and consequence functions

Creating SLFs requires the definition of fragility and consequence functions for all components considered. Table 4.3 and Table 4.4 provide the damage descriptions, the sources for the function definitions and the fragility function parameters for non-structural and structural components, respectively. For the RC structural components, fragility functions were adopted from the available literature [Cardone 2016; Cardone and Perrone 2015]. For the non-structural components, the fragility functions were adopted from Sassun *et al.* [2016] for the masonry infills, while the remaining component fragility functions were adopted from FEMA P-58 [2012b] and the components were assumed as PFA-sensitive.

For some non-structural components, specific fragility functions were not available, hence O'Reilly *et al.* [2018] assumed that the damage to, for example, doors, windows, desks or chairs, was directly correlated to the collapse damage state of the internal infill walls (*i.e.* DS4).

Table 4.2. Mean quantities for the damageable non-structural components of the case-study school building in the longitudinal direction (quantities for the transverse direction listed in parenthesis).

ID	Component	EDP	Above EDP	Unit	Quantity per storey		
					St 1	St 2	St 3
A123	Internal masonry partition	PSD [%]	No	per m ²	198.9 (65.9)	198.9 (65.9)	195.7 (64.8)
A200	Stairs (C2011.011b)		No	per unit	1	1	1
C100	Internal partition		No	per m ²	317.8 (335)	291.9 (243)	268.1 (231)
C200	Gypsum infill walls with metal studs		No		198.9 (65.9)	198.9 (65.9)	195.7 (64.8)
C300	Doors		No	per unit	18(15)	13(10)	15(10)
C400	Windows		No		23(17)	50(9)	53(9)
C500	Desks		No		110	145	182
C600	Chairs		No		140	182	182
E100	Home entertainment equipment (E2022.020)	PFA [g]	Yes		28	30	30
E100 0	Suspended ceiling systems (C3032.001b)		Yes	per m ²	560	588	566
E110	Switchboards (D3067.011a)		No	per unit	1	3	3
E200	Lights (C3034.001)		Yes		66	48	48
E300	Water distribution piping systems (D2022.011a)		Yes	per 250 m	1.808	1.808	1.808
E400	Heating distribution piping systems (D2022.011a)		Yes		1.904	1.904	1.904
E600	Mobile blackboard (E2022.020)		No	per unit	3	3	4
E700	Electronic blackboard (E2022.020)		No		0	3	3
E800	Personal computer and printer (E2022.023)		No		6	20	0
E900	Independent pendant lighting (C3034.001)		Yes		0	3	3

The assumption was that the dependent components are generally either placed within or adjacent to the causation component (*i.e.*, the internal infill walls in this particular scenario). This sort of indirect fix is also an example of the kind of situations that can be dealt with appropriate correlation models. The last column of Table 4.3 and Table 4.4 defines the mean repair costs as a function of the quantity of components and associated with the DS of each component within the structural and non-structural component inventory, respectively. As per O'Reilly *et al.* [2018], repair costs were defined assuming a normal distribution with coefficient of variation equation to 0.1. A full spatial correlation was assumed among the components of the same type within the same storey.

Table 4.3. Fragility function parameters and repair costs for structural components of the 2nd storey.

ID	Damage states	Source	Fragility function parameters		Mean repair cost €
			Median (%) for PSD, g for PFA)	Dispersion	
A101	DS1 Light cracking DS2 Concrete spalling DS3 Concrete crushing	Cardone [2016]	0.75	0.40	1284
A104			1.25	0.40	2155
A110			2.00	0.40	2895
A104	DS1 Light cracking DS2 Concrete spalling DS3 Concrete crushing	Cardone [2016]	0.65	0.40	1497
A110			1.75	0.35	2574
A110			3.00	0.30	4041
A121	DS1 Light cracking DS2 Extensive cracking DS3 Corner crushing DS4 Collapse	Cardone & Perone [2015]	0.10 0.30 0.75 1.75	0.50 0.50 0.40 0.35	62 117 234 234

In other words, if a given DS of an exterior beam-column joint is recorded, the assumption is that the repair cost is the summation of all exterior beam-column joints. However, in practice, it is unlikely that every single component of the same type will be damaged identically within the storey for the given level of EDP. For a more realistic evaluation, a scaling factor smaller than 1.0 can be applied to reduce the costs through engineering judgment to gauge what fraction of the total will actually be damaged, which may be applied within the toolbox if desired.

Table 4.4. Fragility function parameters and repair costs for non-structural components of the 2nd storey.

ID	Damage states	Source	Fragility function parameters		Mean repair cost €
			Median (% for PSD, g for PFA)	Dispersion	
A123	DS1 Light cracking DS2 Extensive cracking DS3 Corner crushing DS4 Collapse	Cardone & Perone [2015]	0.15 0.40 1.00	0.50 0.50 0.40	62 117 234
A200	DS1 Non-structural damage DS2 Structural damage DS3 Loss of live load capacity	FEMA P-58-3 [2012b]	0.50 1.70 2.80	0.60 0.60 0.45	683 5868 36399
C100	DS1 Operational DS2 Damage limitation DS3 Significant damage DS4 Near collapse limit state	Sassun <i>et al.</i> [2016]	0.18 0.46 1.05 1.88	0.52 0.54 0.40 0.38	35 62 124 124
C200	DS1 Operational DS2 Damage limitation DS3 Significant damage DS4 Near collapse limit state		0.18 0.46 1.05 1.88	0.52 0.54 0.40 0.38	62 117 234 234
C300	DS1 Damaged	O'Reilly <i>et al.</i> [2018]	1.88	0.38	754
C400			1.88	0.38	347
C500			1.88	0.38	191
C600			1.88	0.38	24
E100	DS1 Falls, does not function	FEMA P-58-3 [2012b]	0.80	0.40	1035
E1000	DS1 5% of tiles dislodge and fall		0.55	0.40	49

	DS2 30% of tiles dislodge and fall DS3 Total ceiling collapse		1.00 1.50	0.40 0.40	69 99	
E110	DS1 Damaged, inoperative		0.69	0.40	5569	
E200	DS1 Disassembly of rod system at connections with horizontal light fixture, low cycle fatigue failure of the threaded rod, pull-out of rods from ceiling assembly		1.00	0.40	583	
E300	DS1 Small leakage of joints		0.55 1.10	0.40 0.40	307 2302	
E400	DS2 Large leakage w/ major repair		0.55 1.10	0.40 0.40	307 2302	
E600	DS1 Falls, does not function		0.80	0.40	297	
E700			0.80	0.40	2162	
E800			0.40	0.40	1913	
E900			0.60	0.40	1627	

4.3.4 Correlated components

Consideration was given here for possible correlations among damage states of different components in the considered case-study school building. Doors, windows, desks, and chairs were already tied to the collapse DS of the infill walls. However, for demonstration purposes, logical correlations based on engineering judgment were assigned here among other components within the same EDP-sensitive group. In other words, no correlation was considered between PFA- and PSD-sensitive components, however correlation among PSD-sensitive structural and non-structural components was considered. The description of the damage of the causation component, as well as its effect on the correlated component, is provided in Table 4.5.

Table 4.5. Example correlation between components of the case-study school building examined.

Causation Component ID	Damage description of causation component	Dependant Component ID	Effect on the dependent component	DS of a dependent component	
A101	DS2 Concrete spalling	A121	Demolition of exterior infills, as necessary	DS3	
A104		A123	Demolition of interior partitions, as necessary		
A104		C100			
A104		C200			
A101		A200	Local cracking, localized spalling and yielding	DS1	
A104	DS3 Concrete crushing	C300 C400 C500 C600	Damaged, to be replaced	DS1	

It is important to note that, specifically for the case-study example, the repair action cost of demolition of partitions and their further restorations is included within the consequence function of the causation component (*i.e.*, there might be a possible double counting involved inherently). However, within the context of this study, no action was taken to avoid double counting as the repair cost source data was not available to sufficiently segregate and avoid it. In order to avoid compromising the accuracy of results of future analyses, it is advised to add correlations of components with proper care in the computation of repair costs to avoid double counting.

4.4 DERIVATION OF SLFs USING THE TOOLBOX

The framework was initially applied for a comparative analysis between a scenario where no correlation was assumed among different components' DSs and a scenario where the correlation was assumed. For that purpose, the toolbox was applied at the 2nd storey of the building.

4.4.1 Estimating SLFs assuming uncorrelated components

The toolbox was initially applied to the 2nd storey of the school building assuming no correlation among the damage states of the components. SLFs were estimated using both regression Equations 4.4 and 4.5, the parameters of which are provided in Table 4.6. The curves are quite similar as illustrated in Figure 4.11. In specific, Figure 4.11(a) shows the

loss curves for structural components of the intermediate storey. Regardless of the regression equation being used, the losses start accumulating at low values of PSD, which is particularly due to low capacities of interior and exterior infills (Table 4.3). In turn, losses of PSD-sensitivity non-structural components are given in Figure 4.11(b) and, as is seen, the losses are almost twice as low than the ones associated with the structural components for this particular scenario. Finally, Figure 4.11(c) provides the losses associated with non-structural content elements.

Table 4.6. Regression parameters for both equations fitted for the intermediate storey SLF of the case-study school building.

Performance group	Equation 4.4 - Weibull			Equation 4.5 - Papadopoulos <i>et al.</i> [2019]				
	α	β	γ	α	β	γ	δ	ε
PSD S	1.00	1.26	1.14	1.38	2.15	1.38	2.16	989.71
PSD NS	1.00	1.65	1.43	1.66	2.88	1.66	2.89	606.70
PFA NS	2.47	0.79	1.94	2.47	0.79	2.47	0.79	340.54

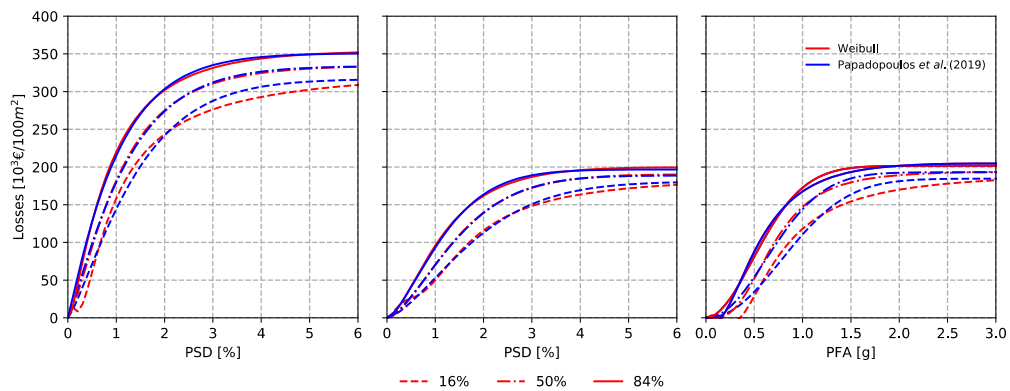


Figure 4.11. Storey loss functions for the case-study school building intermediate (2nd) storey level and 2nd floor (Equation 4 and Equation 5). (a) PSD-sensitive structural components, (b) PSD-sensitive non-structural components, (c) PFA-sensitive non-structural components.

The regression functions were used to fit the fractiles of the distributions and the accuracy of the regression was then gauged through the estimation of maximum, $error_{max}$, and cumulative, $error_{cum}$, relative regression errors, summarised in Table 4.7. The results for Equation 4.4 indicate that, even though a smaller maximum relative error was attained for PFA-sensitive non-structural components, the cumulative relative error is much higher, when compared to the errors of other performance groups, which indicates that, in general, the regression performed worse for the whole data. Nevertheless, Equation 4.5 required higher computational time, due to more coefficients involved in the fitting process.

Table 4.7. Accuracy metrics of regression analysis.

Performance group	Equation 4.4 - Weibull		Equation 4.5 – Papadopoulos <i>et al.</i> [2019]	
	$error_{max}$ [%]	$error_{cum}$ [%]	$error_{max}$ [%]	$error_{cum}$ [%]
PSD S	5.0	0.1	3.0	0.1
PSD NS	4.5	0.1	5.0	0.1
PFA NS	2.9	4.9	0.7	1.5

4.4.2 Estimating SLFs assuming correlated components

The toolbox was also applied assuming component correlations. Figure 4.12(a) depicts the SLFs of PSD-sensitive components at the intermediate storey of the case-study school building following Equation 4.4.

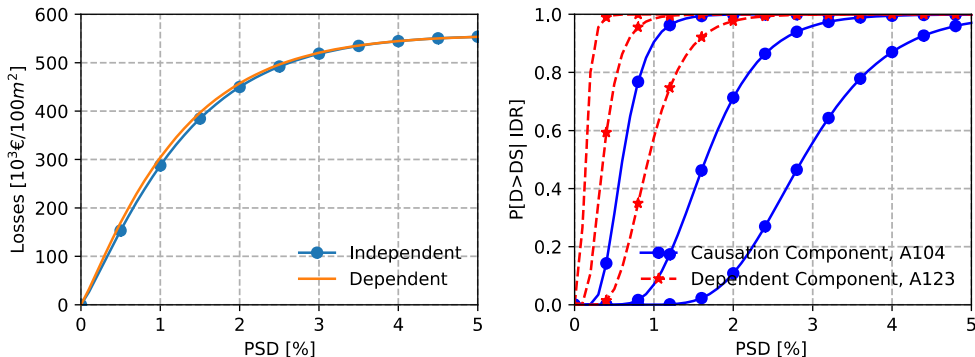


Figure 4.12. (a) SLFs for the case-study school building intermediate storey level: PSD-sensitive structural and non-structural components; (b) fragility functions of interdependent components.

For this particular application, the consideration of correlated components did not impact the loss in a significant manner when compared with the independency assumption, although some increase in vulnerability was noted. This may be attributed to the fragility functions of the components (Figure 4.12(b)), where no notable overlap is observed between the fragility function of the causation and dependent component. Additionally, the dependent component seems to have less capacity when compared to the causation component, meaning that, at a given value of EDP, the dependent component will likely be already damaged, hence, the dependency on the damage state of another component will not be very evident. The greater the overlap, the higher the probability, hence the

expected loss will be, as similarly outlined in Ramirez and Miranda [2009]. The example illustrated here may be modified to further pronounce the influence of the correlation on the SLFs by modifying the fragility parameters, but this was deemed a supplementary exercise that is not critical for the scope of the work presented.

4.5 COMPARISON BETWEEN FEMA P-58 COMPONENT-BASED AND SLF-BASED LOSS ASSESSMENT

Initially, SLFs were derived based on the component data provided in Table 4.1 and Table 4.2. No correlation among component DSs was considered. For the PSD-sensitive components, the complete set of three SLFs were derived, corresponding to each of the three storeys of the building. For PFA-sensitive components, loss functions for four floors were derived, based on whether the component was sensitive to the PFA of the above floor or the floor upon which it is placed. Additionally, PSD-sensitive components were subdivided into separate SLFs based on their orientation (Figure 4.2). The PACT software [FEMA 2012b] was utilised to conduct the component-based loss estimation, where a total of 200 realisations were used per intensity level and the non-directional conversion factor was assumed to be 1.2.

Apart from record-to-record (RTR) variability and in contrast to the original assessment by O'Reilly *et al.* [2018], no epistemic uncertainty related to the numerical modelling parameters was considered for simplicity. Consequently, the component-based loss assessment described herein yielded slightly lower loss values with respect to the original study. Several methods are noted when accounting also for modelling uncertainty. One way is to generate demand results from one single deterministic model (the best representation of the building) using many records and increase the variability to include the effect of modelling uncertainty. Correlations, medians, and dispersions among the distributions of EDPs at each floor are found and resampled, with the same median but an increased dispersion, accounting for modelling uncertainty. For the specific case-study RC frame building, empirical values of modelling uncertainty may be adopted from O'Reilly and Sullivan [2018], for example. Alternatively, different numerical model realisations can be carried out (*e.g.*, different reinforcement values, concrete strength, backbone parameters, etc.), after which NLRHA demands of all models under many records are used to directly account for the modelling uncertainty.

Finally, performance grouping was applied and Equation 4.5 was used to carry out regression to obtain the SLFs. PSHA was performed in O'Reilly *et al.* [2018] and hazard-consistent ground motion record sets were selected for the site location (the city of Ancona). Figure 4.13 illustrates the hazard curve for the selected case-study building location. The IM selected was the spectral acceleration, $Sa(T^*)$, at a conditioning period, T^* . Since, the building possesses principal modes of vibration in two orthogonal directions,

following a suggestion of FEMA P58 [2012a], a T^* of 0.5s equalling the arithmetic mean of the two orthogonal modal periods was selected. NLRHA were conducted and the results were used to conduct loss assessment using the PACT software [2012a] for a component-based approach and using the SLFs generated via the proposed toolbox.

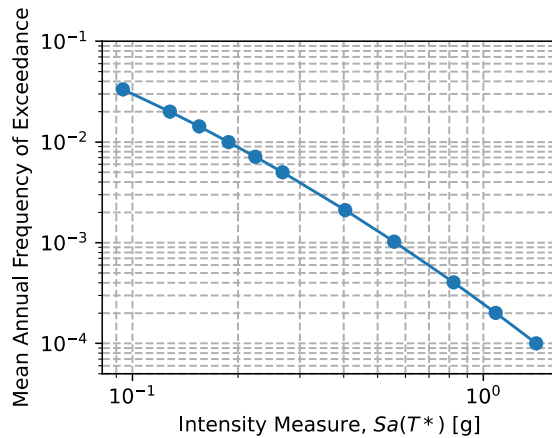


Figure 4.13. Hazard curve for the site considered in Ancona, Italy.

4.5.1 Assessment results

The approach proposed by Ramirez and Miranda [2012] was used herein to perform SLF-based loss assessment. The approach takes residual deformations into account to compute the probability of the building to be demolished after a seismic event. The economic loss condition on the ground motion intensity is computed as the summation of the following terms: losses due to the building collapse; repair costs due to the building's components being damaged; and losses resulting from the demolition of the building if it has experienced excessive residual drifts. The probability of demolishing the building given no collapse at a ground motion IM is computed as a function of RPSD following the recommendations of FEMA P-58 [2012a]. For the case-study building, $P(D|RPSD)$ was assumed to be lognormally distributed with a median of 0.015 and a logarithmic standard deviation of 0.3 [Ramirez and Miranda 2012].

Loss assessment was carried out based on the SLFs developed using the proposed toolbox. Similar to the component-based approach utilised by O'Reilly *et al.* [2018], a 60% threshold was set during the loss assessment, beyond which the total replacement cost of € 3,929,937 was assumed for the building. The EAL was computed for the case-study building by integrating the vulnerability curve, expressed in terms of expected direct economic loss as a function of IM, with the site hazard curve defined according to Equation 4.8:

$$EAL = \int E[L_T | IM] \left| \frac{d\lambda}{dIM} \right| dIM \quad (4.8)$$

where $d\lambda/dIM$ is the mean annual frequency of the ground motion IM. The EAL disaggregated by cost type, along with the vulnerability curve, is presented in Figure 4.14. The EAL computed utilising storey-loss functions was 0.12%, which is slightly higher when compared to the one computed via the FEMA P-58 component-based approach, which was 0.11%. As observed in Figure 4.14(left) the main contribution to the EAL difference comes from the non-structural performance group. Even though the vulnerability curves are quite similar (Figure 4.14(left)), at lower intensity levels, differences can be observed, which are predominantly due to the difficulty in ensuring exact fitting of the regression function (Equation 4.5) in capturing the costs associated with low IM levels regarding non-structural repair cost contributions, resulting in an inevitable EAL difference between the two approaches.

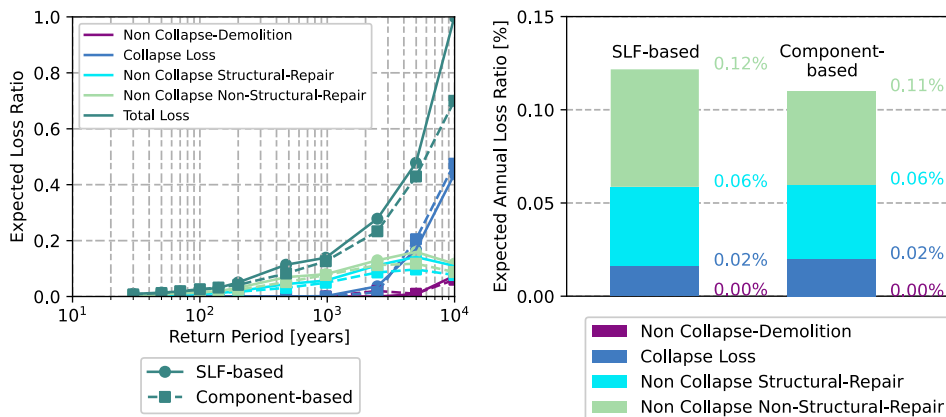


Figure 4.14. (left) Vulnerability curves and (right) Expected annual loss ratio showing the breakdown between different contributors in a comparative assessment between an SLF-based and component-based approach.

Lastly, Figure 4.15 provides the relative contributions to the vulnerability curves as a function of the return period. As observed, the main contributors at low hazard levels (*i.e.*, low return period) are the non-structural and structural repair costs. This reinforces the observation that structural repair cost contributions are lower in the component-based approach in comparison to the SLF-based approach. With increasing return period, the repair cost due to damage to structural components reduces, while the repair cost due to damage to non-structural components remains relatively stable. In contrary, the contribution from collapse and demolition to the ELR starts increasing, however, remains relatively low, compared to repair costs. While it is not possible to compare these losses to real observations for the considered case study building, Del Vecchio *et al.* [2020] presented

actual repair costs of RC residential buildings damaged by the 2009 earthquake in L'Aquila, Italy that can provide some useful comparison. In that study, around 90% of the total replacement cost was attributed to the non-structural components, while structural components averaged around 3-10%. These differ from the respective contributions derived from both component-based and SLF-based assessment methods employed, which are around 38% and 62% at low return periods for structural and non-structural components, respectively. The main reason for this difference could be attributed to exterior masonry infill panels, which contribute notably to the losses, and were classified as structural components within this study while considered a non-structural element by Del Vecchio *et al.* [2020]. This is not deemed a major concern, as it depends on the practitioner's choice for those functions when carrying out loss assessment. The focus of the present study, though, is the comparison of loss outputs between SLF-based and component-based loss assessment frameworks, which indicates how the SLFs produced using the proposed toolbox are capable of providing component-based-quality predictions of loss that would be obtained with more conventional software such as PACT [2012a].

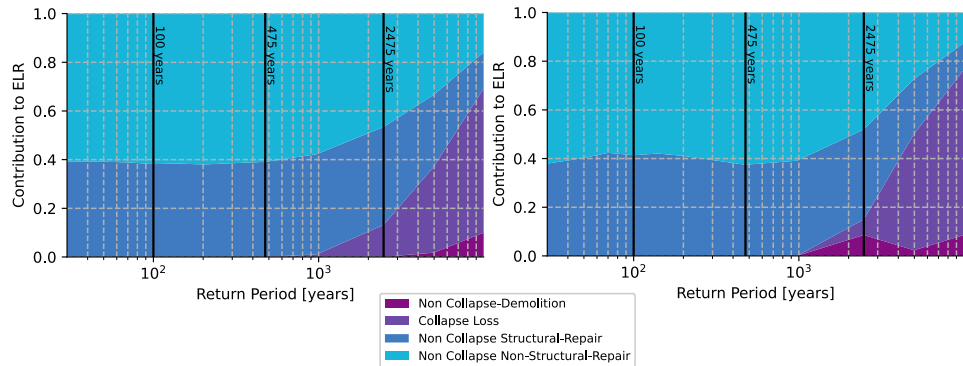


Figure 4.15. Relative contribution to expected loss with respect to increasing return period for a (left) SLF-based approach and (right) Component-based approach. As reference points, the 100, 475 and 2475-year return periods have been annotated on each plot.

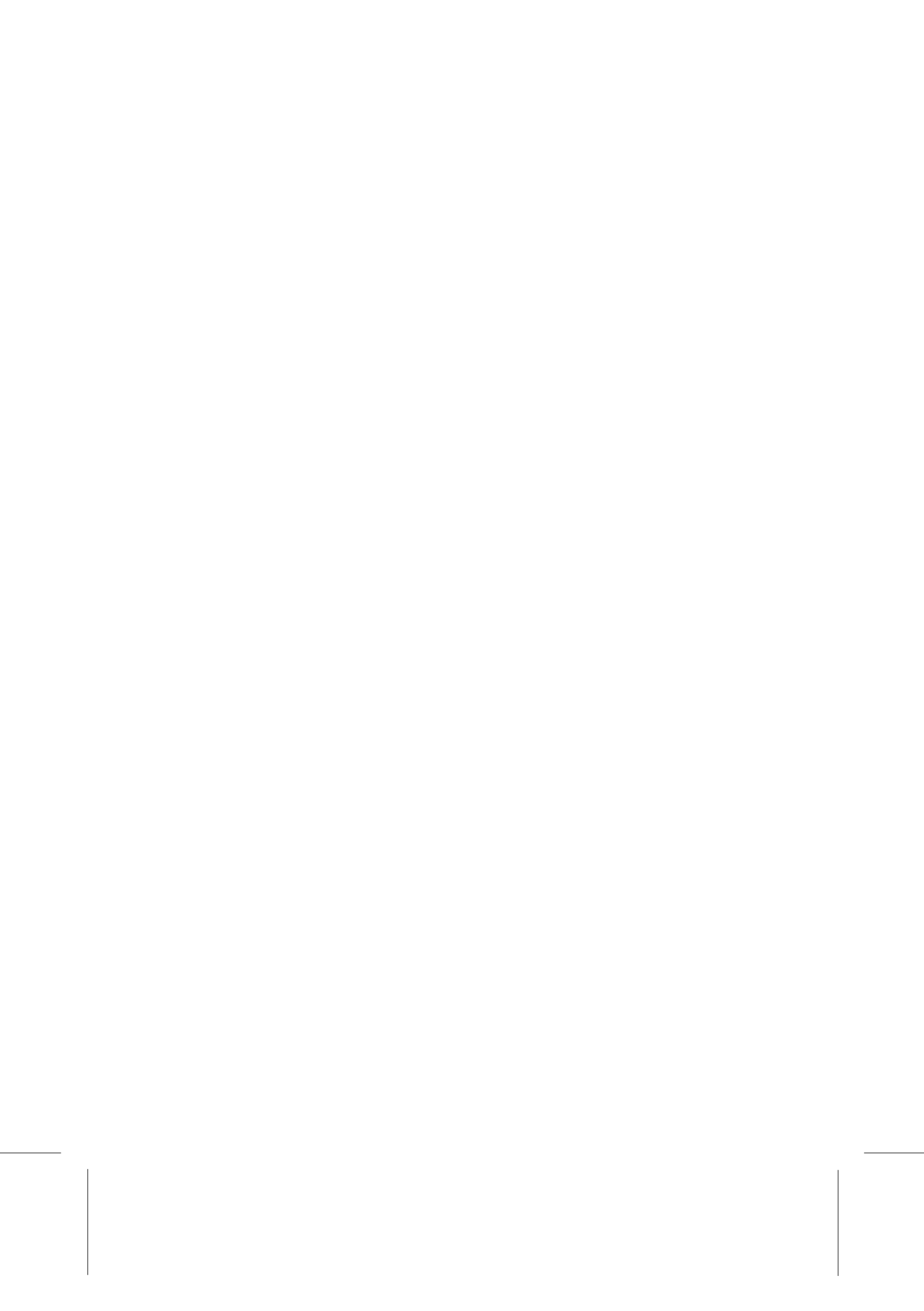
4.6 SUMMARY AND CONCLUSIONS

Given the lack of available tools to develop SLFs to fit any user's own specific needs, this chapter aimed to fill the gap by introducing an SLF generation toolbox for the seismic design and assessment of buildings. This was described with step-by-step implementation and was validated through its application to a case-study school building in a comparative study with the more rigorous component-based loss assessment described in FEMA P-58. Additionally, the toolbox was applied to a single storey, with the goal to compare the effects of assumptions where component damage states were considered independent and where

the dependency of damage states of different components was assumed. The main observations from this study are as follows:

- The toolbox is capable of accounting for component correlation and can avoid the problem of double counting of repair costs that is sometimes encountered in practice. The toolbox was applied to a single storey to investigate how the consideration of component dependency and interaction impacts on the observed vulnerability when compared to the independency assumption;
- SLFs were developed for the entire case-study school building accounting for the response in both directions and a subsequent loss assessment was carried out. Results were compared to a component-based loss assessment approach with a good match in EAL between the two approaches;
- This close matching of the SLF-based loss estimates to the detailed FEMA P-58 component-based loss was also observed in the distribution of the losses among performance groups per intensity. This comparison highlights the validity of the developed tool and its applicability for the intended scopes initially outlined;
- In addition to the typical objective of performing loss assessment on existing buildings, SLFs could act as an important tool for new designs within novel risk-based design approaches. Simplified relationships between expected losses and structural demands (*i.e.*, SLFs) could be integrated and used when designing new structures to limit potential excessive monetary losses due to building damage, as described in O'Reilly and Calvi [2019], for example.

While the developments outlined in this work have shown an ease of SLF development via the proposed toolbox and illustrated its accuracy with respect to more robust approaches to loss estimation, some future extension may be made. These include the consideration of interactions between components physically located at different storeys of a building or associated with different performance groups. A tool for quick manipulation and browsing of component data may also be foreseen to allow the user to add, remove or visualise all existing components. Additionally, the toolbox currently operates on only two types of distributions (*i.e.*, normal, and lognormal). Future extensions could foresee the possibility of including other, such as truncated distributions or multi-modal distributions, that would add flexibility to the toolbox. These additional features would be possible to implement, considering the object-oriented programming used to develop the SLF generation toolbox structured through modular class definitions in Python.



5. INTEGRATING EXPECTED LOSS AND COLLAPSE RISK IN PERFORMANCE-BASED SEISMIC DESIGN OF STRUCTURES

This chapter is based on the following reference:

Shahnazaryan, D., O'Reilly, G. J. [2021] "Integrating expected loss and collapse risk in performance-based seismic design of structures," *Bulletin of Earthquake Engineering* 4(Im). DOI: 10.1007/s10518-020-01003-x.

5.1 CHAPTER OVERVIEW

The preliminary developments of the CSD method were introduced in Chapter 3, and a toolbox for the generation of SLFs was developed in Chapter 4 with the goal of aiding the uninterrupted flow of the method. To further illustrate the necessity of performance-based seismic design methods, this chapter proposes an IPBSD method that uses EAL and MAFC as design parameters. With these, as opposed to conventional intensity-based strength and/or drift requirements, IPBSD limits expected monetary losses and maintains a sufficient and quantifiable level of collapse safety in buildings. Through simple procedures, it directly identifies feasible structural solutions without the need for detailed calculations and numerical analysis. This chapter demonstrates its implementation alongside other contemporary risk-targeted and code-based approaches, discussed in Chapter 2. Multiple case study RC frame structures are evaluated using these approaches and the results appraised via verification analysis. The agreement and consistency of the design solutions and the intended targets are evaluated to demonstrate the suitability of each method. The proposed framework is viewed as a steppingstone for seismic design with advanced performance objectives in line with modern PBEE requirements.

5.2 PROPOSED INTEGRATED PERFORMANCE-BASED SEISMIC DESIGN (IPBSD)

5.2.1 Overview

A novel conceptual seismic design framework that employs EAL as a design metric and requires very little building structure information at the design outset was developed by O'Reilly and Calvi [2019] and forms the basis of the proposed approach. It centres around defining a limiting value of EAL and identifying structural solutions through simplified hand calculations. Several assumptions were made to relate the performance objectives to

a design solution space, which serves as an initial screening before detailing the structural members. SLFs were used to relate ELRs (γ) to EDPs. SLS and ULS were considered to characterise the structure's elastic and ductile behaviour [Shahnazaryan *et al.* 2019], respectively, in line with current code prescriptions.

The proposed framework outlined herein uses MAFC, λ_c , to directly ensure an acceptable level of collapse safety and an EAL limit, $\lambda_{y,\text{limit}}$, to mitigate excessive monetary losses. Both are set by the designer based on the desired building performance. The target MAFC, $\lambda_{c,\text{target}}$, is set and used to limit the actual λ_c described by Equation 5.1.

$$\lambda_c = \int_0^{+\infty} P[C | Sa(T)] dH(Sa(T)) \leq \lambda_{c,\text{target}} \quad (5.1)$$

and the $\lambda_{y,\text{limit}}$ limits the λ_y described by Equation 5.2.

$$\lambda_y = \int_0^{+\infty} E[\gamma] dH \leq \lambda_{y,\text{limit}} \quad (5.2)$$

This integrated consideration of building performance in a risk-consistent manner represents a positive step for future revisions of design codes in line with the goals of modern PBEE.

5.2.2 Step-by-step implementation of the proposed IPBSD framework

A step-by-step guide to the proposed IPBSD framework is outlined herein. It is described with reference to a RC frame, although the framework may be extended to other structural typologies. It comprises four phases:

1. Definition of performance objectives (Figure 5.1);
2. Identification of feasible initial period range (Figure 5.2);
3. Identification of required lateral strength and ductility capacity (Figure 5.3, Figure 5.4);
4. Design and detailing of structural elements (Figure 5.5).

5.2.2.1 *Phase 1: Definition of performance objectives*

In the first phase of IPBSD, the aim is to identify a suitable loss curve to limit λ_y . Performance objectives are characterised through an ELR, γ , and MAFE (λ) of each limit state shown in Figure 5.1. Three limit states utilised are: fully OLS, which represents the onset of damage and monetary loss and is assumed to be $\gamma_{OLS}=1\%$ at a limit state return period of 10 years; SLS, which is where the economic losses will be controlled through the modification of γ_{SLS} ; collapse limit state (CLS), where complete collapse (*i.e.*, $\lambda_{CLS}=\lambda_c$) and economic loss of the building (*i.e.*, $\gamma_{CLS}=100\%$) is expected. With both the OLS and CLS known, a γ_{SLS} and λ_{SLS} are assigned to SLS in Figure 5.1 and the loss curve is identified. O'Reilly and Calvi [2019] have shown that the difference in area between the approximate

and refined loss curve shown in Figure 5.1 could be over 50%, resulting in a large overestimation of EAL. To overcome the overestimation, they suggested a closed form fit for the refined loss curve given in Equation 5.3.

$$\lambda(y) = c_0 \exp[-c_1 \ln y - c_2 \ln^2 y] \quad (5.3)$$

where c_0 , c_1 and c_2 are the fitting coefficients for the three limit state points. The area under the curve (*i.e.* the red shaded area) is λ_y given by Equation 5.4, where a trapezoidal rule may be applied and is checked against $\lambda_{y,\text{limit}}$ defined initially. SLS's characteristics, namely y_{SLS} and λ_{SLS} , are the variables to be adjusted so that λ_y is not exceeding $\lambda_{y,\text{limit}}$. The value of λ_{SLS} should be in line with current code requirements and the value of y_{SLS} be the parameter adjusted to satisfy Equation 5.4.

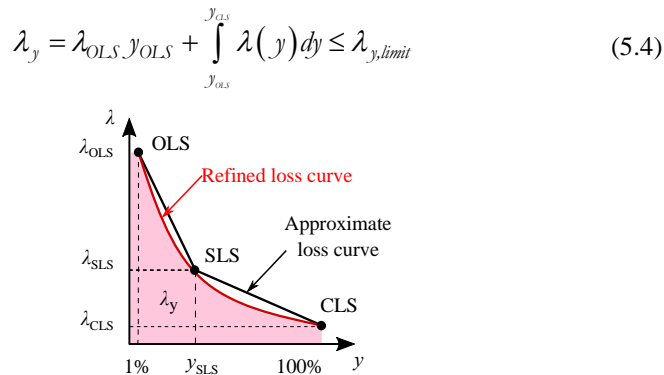


Figure 5.1. Phase 1 of the proposed framework, where the loss curve is constructed and SLS performance objectives established to limit EAL.

5.2.2.2 Phase 2: Identification of a feasible initial period range

Phase 2 of the proposed framework identifies a range of possible initial structural periods $[T_{\text{lower}}, T_{\text{upper}}]$. Using the λ_{SLS} identified in Chapter 5.2.2.1, the design spectrum shown in Figure 5.2(a) can be obtained through an appropriate anchoring of a design spectrum, characterised via PGA, that results in SLS exceedance. A second-order hazard model [Vamvatsikos 2013] is used for the PGA of this spectrum and is given by Equation 5.5.

$$H(s) = k_0 \exp(-k_1 \ln s - k_2 \ln^2 s) \quad (5.5)$$

where k_0 , k_1 , k_2 are the fitting coefficients, and $H(s)$ is the hazard function representing the MAPE of a certain IM, s , equal to PGA in this case, obtained from PSHA. The hazard level corresponding to λ_{SLS} , is determined by solving for H_{SLS} in Equation 5.6 [Vamvatsikos 2013].

$$\lambda_{SLS} = \sqrt{pk_0^{1-p}} H_{SLS}^p \exp\left(0.5pk_1^2 \beta_{SLS}^2\right) \quad (5.6)$$

$$p = \frac{1}{1 + 2k_2 \beta_{SLS}^2}$$

where β_{SLS} is the dispersion anticipated at the SLS, which could be taken as 0.20 and is within the bounds of the recommended values of Appendix F of the recent draft of the revised EC8 [CEN 2018]. Throughout the IPBSD procedure implemented, only RTR variability has been considered for simplicity, although other pertinent sources do exist (e.g., modelling uncertainty [O'Reilly and Sullivan 2018]) but may be easily considered in the process. Furthermore, β_{SLS} in Equation 5.6 may be amplified via SRSS approach to account for these additional sources of uncertainty. Knowing the hazard level, the PGA of SLS is calculated by simply inverting Equation 5.5 and is given by Equation 5.7.

$$PGA = \exp\left[\left(-k_1 + \sqrt{k_1^2 - 4k_2 \ln \frac{H_{SLS}}{k_0}}\right) / (2k_2)\right] \quad (5.7)$$

and the UHS for SLS is obtained (Figure 5.2(a)).

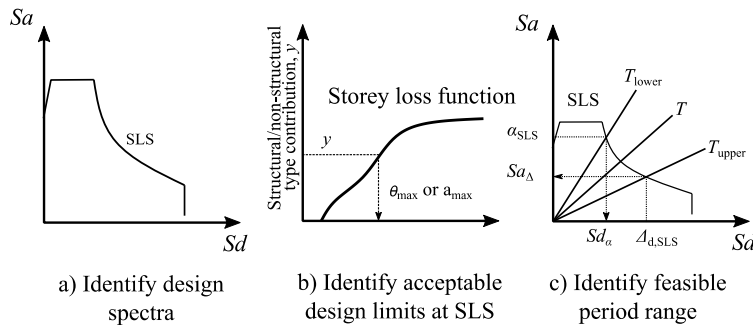


Figure 5.2. Phase 2 of the proposed framework, where design spectrum and acceptable design limits at SLS are identified, leading towards the establishment of the feasible initial period range.

Control in the context of economic losses is established by limiting structural demands at the SLS. This means limiting displacement and acceleration demand on the structure for the design SLS spectrum identified. Using storey loss functions, acceptable structural demand limits are identified, as illustrated in Figure 5.2(b). As further described by O'Reilly and Calvi [2019], relative weights or contributions of different damageable groups to expected loss, Y , at the SLS are required. The ELR at SLS, y_{SLS} , is therefore broken down as in Equation 5.8.

$$\gamma_{SLS} = \gamma_{S,PSD} + \gamma_{NS,PSD} + \gamma_{NS,PFA} \quad (5.8)$$

comprising PSD sensitive structural, $\gamma_{S,PSD}$, and non-structural, $\gamma_{NS,PSD}$, elements, and PFA sensitive non-structural, $\gamma_{NS,PFA}$, loss contributions. These may be computed as a product of target γ_{SLS} and its relative weighting Y by Equation 5.9.

$$\begin{aligned}\gamma_{S,PSD} &= \gamma_{SLS} Y_{S,PSD} \\ \gamma_{NS,PSD} &= \gamma_{SLS} Y_{NS,PSD} \\ \gamma_{NS,PFA} &= \gamma_{SLS} Y_{NS,PFA}\end{aligned}\quad (5.9)$$

By entering the vertical axis in Figure 5.2(b) with the respective value of $\gamma_{S,PSD}$ or $\gamma_{NS,PSD}$, the more critical maximum PSD, $\theta_{max,SLS}$, and the maximum PFA, $a_{max,SLS}$ are obtained. These MDOF demand limits are then converted to SDOF spectral displacement, $\Delta_{d,SLS}$ and spectral acceleration, $a_{d,SLS}$ limits. Similar to the approach adopted in DBD [Priestley *et al.* 2007], the spectral displacement limit is computed by Equation 5.10 and 5.11.

$$\Delta_{d,SLS} = \frac{\sum_{i=1}^n m_i \Delta_i^2}{\sum_{i=1}^n m_i} \quad (5.10)$$

$$\Delta_i = \omega_0 \theta_{max,SLS} H_i \left(\frac{4H_n - H_i}{4H_n - H_1} \right) \quad (5.11)$$

where n is the number of storeys, m_i is the floor mass and Δ_i is the first mode-based displaced shape of the RC frame at storey level i , but other typologies can be considered [Priestley *et al.* 2007], ω_0 is the higher mode reduction factor and H_i is the i -th storey's elevation above the base. Unlike PSD, the maximum PFA along the height, a_{max} , cannot be assumed to be first mode dominated. Here, a simplified assumption is made, where the transformation coefficient is assumed as 0.6, based on the findings of O'Reilly and Calvi [2019] (Equation 5.12). Further refinements have [Silva 2020] and are being currently been investigated for transformation coefficients of different structural typologies.

$$a_{d,SLS} \approx 0.6 a_{max,SLS} \quad (5.12)$$

Based on these design spectral limits, a period range bounded by the lower, T_{lower} , and upper, T_{upper} , limits is identified (Equations 5.13 and 5.14), within which the fundamental period of the structure, T_1 , must be (Figure 5.2(c)). Having a structure whose period falls in this range should ensure that the building is neither too stiff, which would result in

excessive floor acceleration-sensitive losses, nor too flexible, which would give excessive drift-sensitive losses, at the SLS. Meeting these conditions aims to ensure that the EAL limits discussed in Phase 1 are respected.

$$T_{lower} = 2\pi \sqrt{\frac{Sd_\alpha}{\alpha_{SLS}}} \quad (5.13)$$

$$T_{upper} = 2\pi \sqrt{\frac{A_{d,SLS}}{Sa_A}} \quad (5.14)$$

5.2.2.3 Phase 3: Identification of required lateral strength and ductility

Having identified the feasible initial period range to limit economic loss at SLS, it is equally important to control the risk of structural collapse. Unlike the previous iteration of the framework [O'Reilly and Calvi 2019] as discussed in Chapter 3, the direct consideration of ULS is replaced with CLS, and a MAFC is targeted by Equation 5.1. A period between T_{lower} and T_{upper} is selected and the expected backbone behaviour and overstrength q_s are first trialled by the designer. SPO parameters are assumed, such as the spectral acceleration at yield, Sa_y , the fundamental period T_1 , hardening and fracturing ductilities, μ_c and μ_f , hardening ratio to peak, K_h and post-peak softening ratio, K_{pp} , and residual strength, r (Figure 5.3). For the initial estimation of these parameters, several suggestions from the literature may be employed. For example, μ_c may be initially estimated based on the behaviour factors given in current codes; μ_f will depend on the post-peak capping rotation capacity of the RC frame members, which could be based on work by Haselton *et al.* [2016], for example. An r value of around 10-20% of Sa_y and K_{pp} could be within a range of 20-30% to start, but both should be based on pushover analysis or experimental testing when available. All of these parameters may be adjusted based on expert judgement by the designer and since they are structural capacity proportions and should not be too challenging to estimate and quickly refine without any excessive analysis being required.

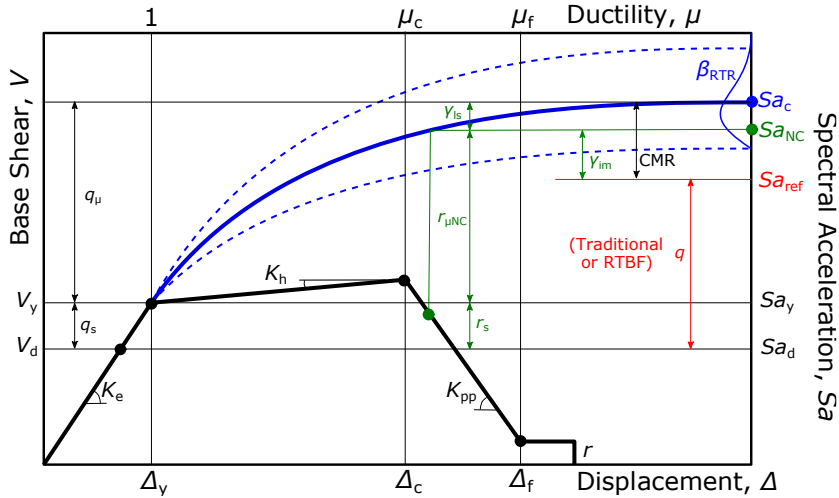


Figure 5.3. Illustration of the SPO backbone response parameters and the various approaches to identify the design value.

The SPO2IDA tool [Vamvatsikos and Cornell 2005] is used to estimate the collapse fragility function of the structure in terms of median collapse capacity, Sa_c , and RTR uncertainty, β_{RTR} , assuming a lognormal distribution. Additionally, β_{RTR} obtained from SPO2IDA may be amplified via SRSS to consider other independent sources of response uncertainty in the collapse capacity estimation. In essence, the SPO2IDA tool offers a quick estimation of the IDA response (*i.e.*, the blue curves in Figure 5.3), which represent the intensities required to exceed displacement-based limit-states of a structure characterised by an SDOF system with a quadrilinear SPO curve (*i.e.* the black backbone curve shown in Figure 5.3). It utilises R- μ -T relationship, developed through extensive dynamic analyses on SDOF oscillators [Vamvatsikos and Cornell 2005] and removes the need of performing multiple dynamic analyses on the trialled backbone behaviour. The identified backbone shape in Figure 5.3 and a trialled lateral strength Sa_y is used to find the ductility-based force-reduction, q_μ and β_{RTR} , using the SPO2IDA tool as:

$$[q_\mu, \beta_{RTR}] = f(Sa_y, T_1, \mu_c, \mu_f, a_p, a_{pp}, r) \quad (5.15)$$

For proper evaluation of collapse capacity, through SRSS combination, modelling (and possibly other types) uncertainty needs to be accounted for (Equation 5.16).

$$\beta_{total} = \sqrt{\beta_{RTR}^2 + \beta_{modelling}^2} \quad (5.16)$$

q_μ is transformed to the spectral acceleration Sa of the actual MDOF system using a transformation factor, Γ , as given by Equations 5.17 and 5.18.

$$Sa_c = Sa_y q_\mu \Gamma \quad (5.17)$$

$$\Gamma = \frac{\sum_{i=1}^n m_i \varphi_i}{\sum_{i=1}^n m_i \varphi_i^2} \quad (5.18)$$

where φ is the fundamental mode shape, which can be taken as the normalised displaced shape (Equation 5.11). The collapse fragility function is then integrated with the hazard curve corresponding to the selected T_1 , $H(Sa(T_1))$, identified from PSHA and λ_c is computed (Figure 5.4(a)) by Equation 5.19. The λ_c computed from the trialled value of Sa_y and the assumed backbone shape is verified against $\lambda_{c,target}$. If the condition is met and the value is sufficiently close to the target, the designer may proceed. Otherwise, the trialled yield properties of the frame and/or ductility should be revised. By varying T_1 and repeating the process, a capacity curve of uniform collapse risk can be plotted in Sa versus Sd , which identifies where the feasible structural solutions are to be found (shaded in red in Figure 5.4(b)). The red dots in Figure 5.4(b) represent several feasible design solutions within the period range and with a strength capacity that satisfies the collapse safety criterion, meaning that any structure with the T_1 in this range and a lateral capacity on the curve should be sufficient.

$$\begin{aligned} \lambda_c &= \sqrt{pk_0^{1-p}} H(Sa_c)^p \exp\left(0.5 p k_1^2 \beta_{total}^2\right) \leq \lambda_{c,target} \\ p &= \frac{1}{1 + 2k_2 \beta_{total}^2} \end{aligned} \quad (5.19)$$

Where, β_{Total} is the combination (SRSS combination) of both aleatory, that is RTR, and epistemic uncertainty (e.g., modelling uncertainty).

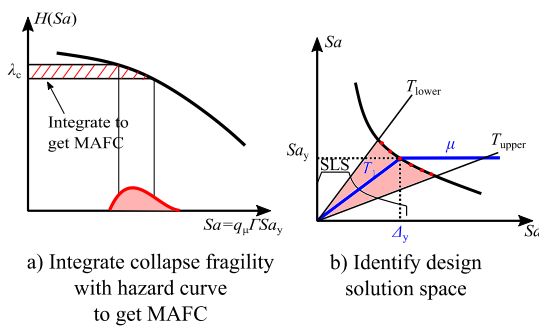


Figure 5.4. Phase 3 of the proposed framework, where the collapse capacity and backbone curve of the solution is identified.

5.2.2.4 Phase 4: Design and detailing of structural elements

The final phase (Figure 5.5) uses the identified required capacity to size the structural elements. Design base shear, V_d , based on the identified Sa_y is given by Equation 5.20, which depends on the first-mode effective mass, M^* (Equation 5.21) and the assumed value of system overstrength, q_s . It is necessary to include a reduction for the anticipated overstrength such that the resulting structure will have an actual yield strength of Sa_y and thus a collapse risk of λ_c , as anticipated by the performance objectives depicted in Figure 5.3.

$$V_d = \frac{Sa_y}{q_s} M^* \Gamma \quad (5.20)$$

$$M^* = \sum_{i=1}^n m_i \varphi_i \quad (5.21)$$

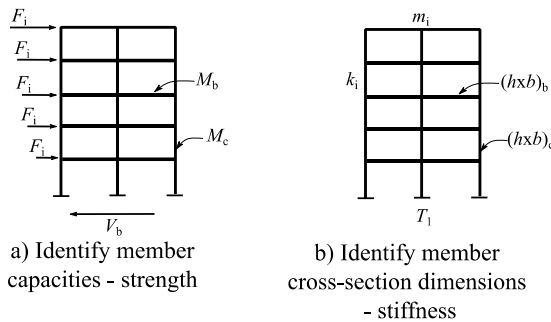


Figure 5.5. Phase 4 of the proposed framework, where the demands on the structural elements are identified and detailing of sections is carried out.

Based on V_d , the lateral distribution of forces may be obtained and is used to identify demands on structural elements, given by Equation 5.22.

$$F_i = V_d \frac{m_i A_i}{\sum_{i=1}^n m_i A_i} \quad (5.22)$$

At this point, any structural member detailing requirement from seismic design codes may be applied to determine the member dimensions and required reinforcement content. Strength hierarchy and local ductility requirements should be accounted for. Of equal importance are higher mode effects and second-order effects (P-Delta). The former one

may be accounted for through a higher mode reduction factor for the possible storey drift amplifications and P-Delta effects may be considered through stability checks similar to EC8 [CEN 2004a], for example. The structural element cross-section and material properties should be selected to remain within a reasonable tolerance of the assumed T_1 selected during the collapse safety verification phase. If this condition is met and the structure's capacity curve matches that of the assumed in Figure 5.3, the identified structural configuration may be adopted. Otherwise, the element dimensions and reinforcement ought to be revised. It is noted, however, that any iterations required in IPBSD are limited to spreadsheet adjustments and extensive analysis verifications are not required.

5.3 CASE STUDY APPLICATION

5.3.1 Definition of case study buildings

To assess the performance of the existing methods compared to the proposed one, several case study applications were carried out. Ten archetypical buildings were examined and are described in Table 5.1. The designs vary in terms of number of storeys, number of bays, storey heights and bay widths, in addition to design targets. Office occupancy was assumed for each and the SLFs provided by Ramirez and Miranda [2009] for this occupancy type were selected.

Table 5.1. Archetypical RC frame structures

Case	$\lambda_{c,target}$	$\lambda_{y,limit}$ [%]	Storeys		Bays			
			Number of storeys	Ground storey/typical storey height [m]	Number of bays	Width [m]		
1	5.0×10^{-4}	0.65	2	3.5/3.0	2	5.0		
2	1.0×10^{-4}					Internal: 2.0 External: 4.5		
3	5.0×10^{-4}		4		3	6.0		
4	1.0×10^{-4}					Internal: 2.0 External: 4.5		
5	5.0×10^{-4}		6					
6	1.0×10^{-4}							
7	5.0×10^{-4}							
8	1.0×10^{-4}	0.45	8					
9	5.0×10^{-4}							
10	1.0×10^{-4}							

The value of λ_y was selected to a rating higher than “A” as classified by Cosenza *et al.* [2018] with values lower than 1%. As pointed out by Cook *et al.* [2019], damage in high-rise structures tends to concentrate on just a few storeys, greatly reducing the loss with respect to the total building value. In contrast, damage in shorter structures tends to be more spread across all storeys. Additionally, Ramirez *et al.* [2012] and Calvi *et al.* [2014] noted a trend whereby increasing building height results in decreasing normalised loss ratios and EAL. From this, one could argue that for taller structures, the λ_y is expected to reduce, hence the reduction of the limiting value for the taller case studies examined here. With regards to the selection of $\lambda_{c,target}$, there is yet to be a widespread consensus on which value should be used in new design. For example, ASCE 7-16 [2016] has an acceptable national risk of 1% in 50 years ($\lambda_c = 2.0 \times 10^{-4}$), while several studies from the literature (e.g. [Duckett 2004; Fajfar and Dolšek 2012; Goulet *et al.* 2007]) note values of around $\lambda_c = 1.0 \times 10^{-5}$ as reasonable. Furthermore, Silva *et al.* [2016] utilised $\lambda_c = 5.0 \times 10^{-5}$ whilst discussing the development of risk-targeted hazard maps for Europe and a review by Dolšek *et al.* [2017] noted typical limits are between $\lambda_c = 10^{-4}$ and 10^{-5} . Using these values from the literature, and also to highlight the possibility of easily tailoring the design performance objectives in the proposed method, two $\lambda_{c,target}$ values of 5.0×10^{-4} and 1.0×10^{-4} were adopted.

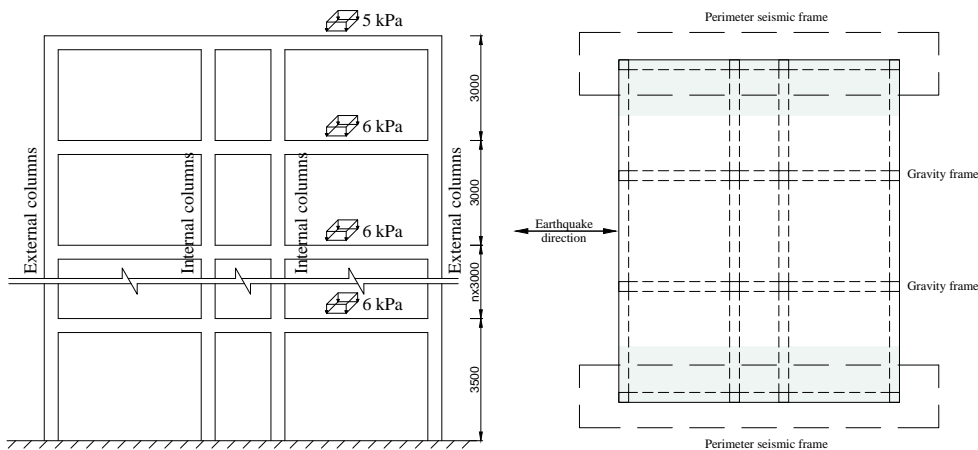


Figure 5.6. Illustration of plan layout and elevation of archetypical RC frames in a discussion (tributary area of gravity loads on seismic frames shaded grey).

Typical plan and elevation illustrations are shown in Figure 5.6. The gravity loads, including imposed and dead loads, were assumed 6kPa and 5kPa at the general floor and roof level, respectively. A stiff clay site according to EC8's site classification [CEN 2004a] located in L'Aquila, Italy was chosen for all design cases. The structural system was a RC moment-resisting frame (MRF). The material properties used in the design and detailing were 25MPa for the concrete compressive strength and 415MPa for the steel yield strength. No plan or elevation irregularities were considered. 2D planar models were used given the symmetric

structures with no irregularities. Alternatively, the framework should be applied in both directions of the structure bearing in mind that some considerations need to be applied for calculation of losses, which are not addressed herein. For simplicity, one direction of seismic action was considered, however the 3D response of the building will be assessed in Chapter 6.

5.3.2 Numerical modelling

For each design method and case study archetype, numerical models of the systems were generated using OpenSees [Mazzoni *et al.* 2006] for subsequent design verification. SPO and NLRHA were performed to assess the seismic performance of each case. The masses were lumped at each floor and the nodes were constrained in the horizontal direction to mimic a rigid diaphragm behaviour (Figure 5.7(a)). Non-linear element behaviour was considered through a concentrated plasticity approach developed by Ibarra *et al.* [2005] (Figure 5.7(b)). P-Delta effects were accounted for through gravity columns, and the columns of the lateral force-resisting system were fixed at the base. Rayleigh damping was implemented with 5% of critical damping assigned to the first and third modes. For the plastic hinge models, element moment-curvature relationships were attained through Response-2000 sectional analysis program [Bentz 2015], which followed the concrete and reinforcement material properties of Eurocode 2 (EC2) [CEN 2004b]. The backbone curve used is described by the parameters: elastic stiffness defined through the elastic slope, $a_{e,\phi}$, yield strength, M_y , yield curvature, ϕ_y , strain-hardening stiffness through hardening slope, $a_{p,\phi}$, capping curvature, ϕ_p , defined through hardening ductility, $\mu_{e,\phi}$, which corresponds to the peak strength, M_p , of the load-deformation curve. The softening branch is defined by the post-capping stiffness defined through softening slope, a_c . Finally, a residual strength, r , of the component is defined, which is preserved once a given deterioration threshold, ϕ_r , is achieved. The fracturing ductility, $\mu_{f,\phi}$, is used to identify a point of fracturing identifying a curvature capacity of the model. Essentially, the backbone curve was fit to the moment-curvature relationship of the element, where μ_e was selected based on the peak behaviour of the element and r was taken as 20% of M_y . The softening slope of the backbone curve was selected, so that the post-capping chord rotation capacity did not exceed 0.10, as per Hazelton *et al.* [2016]; the post-capping curvature capacity, ϕ_{pc} , may be obtained by taking the ratio of this to the anticipated plastic hinge length, L_p , calculated as per Priestley *et al.* [2007], for example.

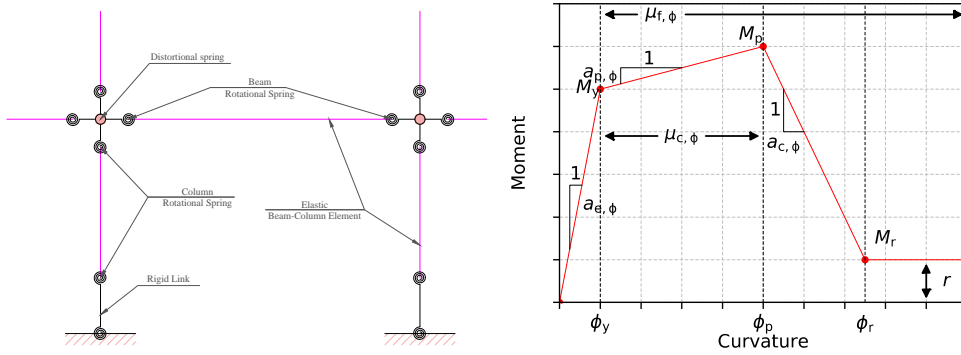


Figure 5.7. Illustration of the numerical modelling approach, where (left) shows the layout of elements and beam-column connection modelling and (right) denotes the hysteretic model adopted for each hinge location.

5.3.3 Site hazard and ground motions

PSHA was performed using OpenQuake [Paganini *et al.* 2014] with the SHARE hazard model [Woessner and Wiemer 2005]. To characterise the structural response with increasing intensity for each design case, a set of 30 ground motion records were selected from the NGA West-2 database [Ancheta *et al.* 2014] with each record's soil type being consistent with that of the site. PSHA disaggregation results at the 2475 years return period and at a period of 0.7s, around which the majority of the case study RC frames' T_1 fell, were used to select the records. Hazard curves obtained from PSHA were used in each design procedure under consideration. For the proposed framework, the initial definition of a target loss curve and identification of a suitable PGA value for the SLS was needed. Furthermore, once the acceptable period range for the structure was identified, $\lambda_{c,target}$ was verified by integrating the collapse fragility with the seismic hazard based on an IM of $Sa(T_1)$ for a range of T_1 values. Žižmond and Dolšek [2019], on the other hand, use a 1st order fit of $Sa(T_1)$ using the return periods of 475 and 10,000 years. The slope of the first-order model in the log-log domain was used to calculate the collapse intensity and the risk-targeted design spectral acceleration. For EC8 and DDDB cases, an elastic design spectrum was used. To be consistent with the seismic hazard used for the other methods, the $Sa(T_1)$ value of the elastic design spectrum defined was scaled to match that obtained from PSHA. This essentially meant that the EC8 design spectrum was anchored to a hazard consistent value of $Sa(T_1)$ rather than PGA on rock, as is typically recommended. The seismic hazard corresponding to a period of 0.7s and 1.0s are presented in Figure 5.8. For the 2nd order hazard, least-squares fitting was used with higher weight given to medium to higher intensities, *i.e.*, larger than $Sa(T)=0.1g$, where the collapse behaviour is more relevant for capturing λ_c , while for PGA intensity, higher weight was given to lower to medium intensities, where λ_y calculation is more relevant.

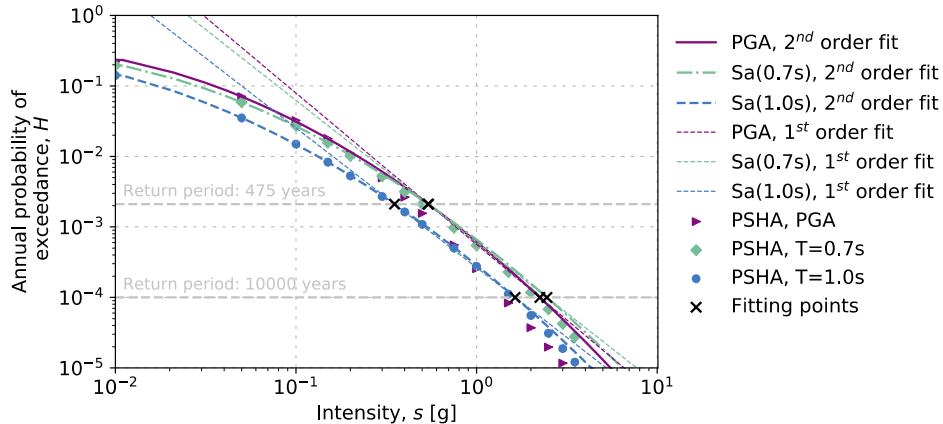


Figure 5.8. Seismic hazard with 1st and 2nd order fits corresponding to a spectral acceleration at a period of 0.7s, 1.0s and PGA.

5.4 DESIGN OF CASE STUDY STRUCTURES

The study aims to examine different methodologies presented in Sections 2.2 and 2.3 for designing structures described in Section 5.3.1. In this chapter, the proposed IPBSD was implemented in addition to FBD as outlined in EC8, RTSA method comprising both direct (D) and indirect (I) approaches by Žižmond and Dolšek [2019]; the RTS approach by Luco *et al.* [2007] and DDBD as per Priestley *et al.* [2007]. The RTBF, CPBD and YFS approaches were not applied mainly for the following reasons. RTBF represents a general approach to update and correct behaviour factors used in design and to the authors' knowledge, none have been formally proposed for RC frame structures in Europe which would have allowed implementation here, although the studies previously discussed in Section 2.3 have indicated how they may be computed in future studies. CPBD was not studied here due to the sheer amount of analysis and iteration required to apply it. It was noted in Section 2.3 that one difficulty of CPBD was that it lacked the simplified tools to practically implement it. In this regard, the proposed IPBSD may be seen as a successor to this method, as the design objectives are similar but much of the heavy analysis work has been substituted with appropriate simplifications and tools for a more expedite design process. Lastly, YFS was also not considered because, if its performance objectives were changed from exceedance rates of multiple drift- and ductility-based conditions to the global collapse condition, the results would closely resemble those from Phase 3 of the proposed IPBSD method.

The objective was to examine contemporary methods of risk-consistent design in addition to code-based formulations. The RTS and DDBD approaches were examined up to the point of establishing a design strength and how it varies with respect to the other methods in the interest of space limitations. The same general approach to design was followed for each structure with the required lateral design strength identified and designed for. The

case study structures were subsequently detailed and sized following the EC8 and EC2 member detailing requirements and a numerical model was built using the approach described in Section 5.3.2, to be evaluated in Section 5.5.

5.4.1 FBD according to EC8

The archetypical RC frames described in Table 5.1 were designed following the EC8 provisions. The design response spectrum provided by EC8 was used and scaled to match the $Sa(T_1)$ value from the PSHA at the no-collapse return period of 475 years. Since EC8 does not utilise λ_c in its design formulation, the values of $\lambda_{c,target}$ specified in Table 5.1 were not considered directly. To distinguish between buildings with differing levels of safety, EC8's importance classes were utilised. Therefore, buildings with $\lambda_{c,target} = 5.0 \times 10^{-4}$ and 1.0×10^{-4} were taken here approximately corresponding to importance classes II and III and the design spectrum was subsequently scaled by 1.0 and 1.2 to account for this, respectively.

The ELF method of analysis was employed to determine the demands on the structural elements and two sets of designs were considered: with and without the consideration of the gravity load combination. This was done to clearly identify the level of safety strictly provided by the ELF method's design resistance. Lateral drift limitations and P-Delta effects were satisfied, and the member reinforcement content and dimensions were selected to be within the recommended local ductility limits for ductility class medium (DCM) frames. Cracked cross-section properties (*i.e.*, 50% of gross) were used to identify the demands and design the structural elements. Adequate strength hierarchy (*i.e.*, capacity design) requirements were also met. The period of the frames was identified via an iterative design procedure, where an initial $T_1 = 0.7\text{s}$ to match the period of the hazard curve was used. If this assumption was not satisfied and element cross-section properties needed revisions, T_1 was updated. The final design values are listed in Table 5.2.

5.4.2 DDBD

The design cases of Table 5.1 were designed using DDBD [Priestley *et al.* 2007] and are presented in Table 5.3. The aim was to have a comparative basis among the design spectral accelerations between different methods of design. Similar to FBD, the values of $\lambda_{c,target}$ specified in Table 5.1 were not directly incorporated and EC8 importance classes were considered instead.

Table 5.2. Summary of the design solutions obtained using FBD according to EC8, where G indicates cases where the gravity load combination was included.

Case	Importance Class	T_1 [s]	Sa_d [g]
1	II	1.1	0.10
1-G	II	1.1	0.16
2	III	1.1	0.11
2-G	III	0.7	0.27
3	II	2.3	0.04
3-G	II	1.3	0.13
4	III	2.3	0.05
4-G	III	1.1	0.15
5	II	1.8	0.06
5-G	II	1.3	0.14
6	III	1.8	0.07
6-G	III	1.3	0.16
7	II	2.3	0.05
7-G	II	1.8	0.08
8	III	2.3	0.05
8-G	III	1.8	0.09
9	II	3.0	0.03
9-G	II	2.5	0.06
10	III	3.0	0.04
10-G	III	2.5	0.07

The same elastic spectrum was utilised and scaled to match the $Sa(T_1)$ of the seismic hazard. ASCE 7-16 [2016], for example, provides drift limit of 4% to 5% depending on the number of storeys, while Gokkaya *et al.* [2016] suggest a more stringent value of 3% at MCE intensity level. Taking into consideration the T_R of 2475 years of MCE and T_R of 475 years used here, the drift limit was assumed to be 2.5%. The Sa_d values in Table 5.3 appeared slightly higher to the ones obtained via the FBD approach in Table 5.2. The design μ , were generally lower than the ones used when designing the EC8 cases. Consequently, this will have compensating effects towards slightly higher Sa_d .

Table 5.3. Summary of the design solutions obtained using DDBD according to Priestley *et al.* [2007]

Case	Importance Class	T_1 [s]	Design μ	Sa_d [g]
1	II	0.7	2.2	0.12
2	III	0.7	2.2	0.17
3	II	0.7	3.6	0.05
4	III	0.7	3.6	0.08
5	II	1.0	2.0	0.06
6	III	1.0	2.0	0.09
7	II	0.7	3.3	0.06
8	III	0.7	3.9	0.07
9	II	0.9	2.4	0.06
10	III	0.9	2.9	0.07

5.4.3 RTSA method

The next approach considered was the RTSA method proposed by Žižmond and Dolšek [2019] and both RTSA-D and RTSA-I formulations were employed. Since the approach is risk-targeted, it is more in line with design objectives (*e.g.*, $\lambda_{c,target}$). Following the method's step-by-step formulation, the risk-targeted design spectral acceleration, Sa_d , was estimated.

Scenarios following the RTSA-D formulation were subdivided into two subcases based on the assumption of the r_s and μ_{NC} to the no-collapse (NC) limit state, which are illustrated in Figure 5.3. Cases A considered $r_s = 1$ and $\mu_{NC} = 3$, whereas cases B considered $r_s = 2$ and $\mu_{NC} = 6$; the latter pair correspond to those used in the design example by Žižmond and Dolšek [2019]. Case A values were selected to be more in line with the structural capacity in the absence of any additional gravity load consideration or significant overstrength. Additionally, an initial choice of T_1 is needed for both formulations. Where this assumed period substantially differed to the numerical model, it was updated, and the design recomputed for all RTSA-D cases but only some RTSA-I cases. These different combinations are listed in Table 5.4.

For both formulations, $\lambda_{c,target}$, was set and the seismic hazard described in Chapter 5.3.3 was used depending on T_1 . The value of design spectral acceleration, Sa_d (Figure 5.3), was determined by setting β_{RTTR} to the suggested value of 0.4 and identifying a median collapse intensity, Sa_c , that satisfied $\lambda_{c,target}$ when integrating in Equation 5.1. An acceptable median spectral acceleration for the non-collapse (NC) limit state, Sa_{NC} , was calculated as the ratio

between Sa_C and the limit-state reduction factor, γ_s , taken from Dolšek *et al.* [2017] as 1.15. Sa_d was determined using the reduction factor, r_{NC} , as illustrated in Figure 5.3, where r_{NC} was determined by Equation 5.23:

$$r_{NC} = \frac{\mu_{NC}}{C_1} r_s \quad (5.23)$$

where C_1 is the inelastic deformation ratio relating the inelastic and elastic deformation at Sa_{NC} . To compute C_1 , an SDOF oscillator model with equivalent period and first mode mass was required and analysed with the aforementioned set of ground motions using IDA, as suggested by Žižmond and Dolšek [2019].

RTSA-I cases use a risk-targeted safety factor, γ_{im} , [Dolšek *et al.* 2017] given by Equation 5.24.

$$\gamma_{im} = \frac{1}{\gamma_s} (T_R \lambda_c)^{-\frac{1}{k}} \exp\left(\frac{k\beta_{RTR}^2}{2}\right) \quad (5.24)$$

where k is the slope of the 1st order hazard function in the log-log domain (Figure 5.8). The risk-targeted reduction factor, q_a , used in this formulation was then computed from Equation 5.25.

$$q_a = \frac{r_{NC}}{\gamma_{im}} \quad (5.25)$$

For the reference seismic design action, Sa_{ref} , a return period of 475 years was assumed, and the $Sa(T_1)$ was divided by q_a to give Sa_d . The design spectrum was then obtained by normalising the EC8 elastic spectrum to Sa_d to implement the RSMA. Both formulations involved an iteration based on the modification of T_1 and cross-sections and re-running of the SDOF model to identify the C_1 ratio.

Contrary to RTSA-I cases, where results were generally consistent, the design solutions obtained for the RTSA-D cases exhibited some atypical values (Table 5.4). This was particularly true for the increase in the assumed values of r_s and μ_{NC} in cases B, which resulted in lower design demands on the structural elements. These high r_s and μ_{NC} values led to a higher value of r_{NC} , as per Equation 5.23, which resulted in much lower Sa_d , as illustrated in Figure 5.3. Conducting elastic analysis on a structural model with this lower design demand led to subsequent iterations of structural element dimension reductions in order to meet the local member ductility requirements. This in turn increased the T_1 of the

structure, as seen for cases 9 and 10 of RTSA-D TB, for example. This highlights the importance not only of strength and ductility in design but also of sufficient stiffness for lateral systems.

Table 5.4. Summary of the RTSA design solutions using the direct and indirect formulations for cases A ($r_s = 1$, $\mu_{NC} = 3$) and B ($r_s = 2$, $\mu_{NC} = 6$), where T indicates period updating.

Case	ID		$\lambda_{c,target}$	T_1 [s]		S_{ad} [g]	
	RTSA-D	RTSA-I		RTSA-D	RTSA-I	RTSA-D	RTSA-I
1	TA	A	5.0×10^{-4}	0.70	0.70	0.36	0.43
	TB	TA		0.90	0.70	0.07	0.43
2	TA	A	1.0×10^{-4}	0.50	0.42	0.91	1.69
	TB	TA		0.74	0.35	0.17	1.13
3	TA	A	5.0×10^{-4}	0.70	0.90	0.39	0.51
	TB	TA		1.57	0.87	0.05	0.38
4	TA	A	1.0×10^{-4}	0.66	0.50	0.72	0.88
	TB	TA		1.10	0.50	0.16	0.85
5	TA	A	5.0×10^{-4}	1.00	1.06	0.30	0.27
	TB	TA		1.70	1.10	0.04	0.24
6	TA	A	1.0×10^{-4}	0.96	0.74	0.52	0.57
	TB	TA		1.04	0.74	0.15	0.91
7	TA	A	5.0×10^{-4}	0.74	1.11	0.48	0.43
	TB	TA		1.92	1.09	0.03	0.25
8	TA	A	1.0×10^{-4}	0.70	0.56	0.80	0.98
	TB	TA		1.66	0.57	0.08	1.20
9	TA	A	5.0×10^{-4}	0.95	1.06	0.34	0.31
	TB	TA		3.50	1.12	0.01	0.27
10	TA	A	1.0×10^{-4}	0.77	0.76	0.81	0.78
	TB	TA		3.46	0.76	0.02	0.78

5.4.4 Proposed IPBSD formulation

The proposed IPBSD framework presented in Section 5.2.2 was implemented and detailed following the EC8 and EC2 provisions. To illustrate, a single design scenario (Case 4) was

selected and is described step-by-step herein. It is recalled that $\lambda_{c,target}$ and $\lambda_{y,limit}$ were 1.0×10^{-4} and 0.65%, respectively.

The first phase of the framework involved the definition of performance objectives following Section 5.2.2.1. The y values of OLS and CLS were fixed to $y_{OLS}=1\%$ and $y_{CLS}=100\%$, respectively, and λ_{OLS} was set as to correspond to a limit state return period of 10 years and $\lambda_{CLS}=\lambda_{c,target}$, respectively. The SLS parameters were then identified by first setting the $y_{SLS}=6\%$, and trialling $\lambda_{SLS}=2.07 \times 10^{-2}$. With these limit state values and resulting loss curve shown in Figure 5.9(a), the λ_y was calculated from the refined loss curve using Equation 5.4 as 0.65%, corresponding to the limiting value. This choice of SLS parameters requires dedicated attention and further refinement through sensitivity studies carried out in Chapter 3.

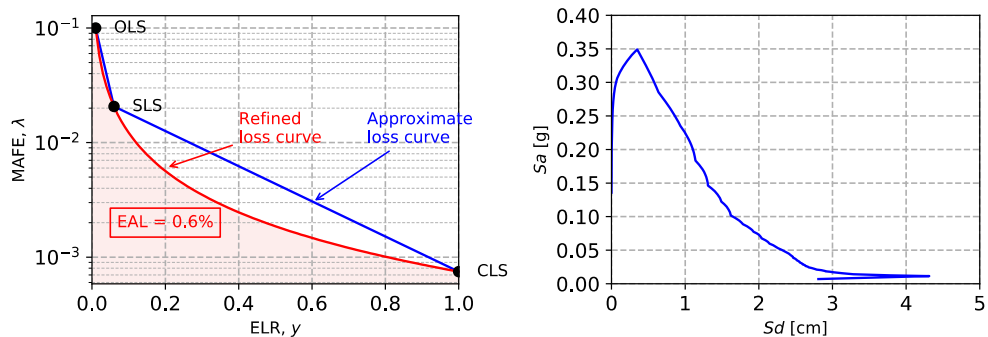


Figure 5.9. (a) Loss curve and (b) design spectrum at SLS of design case 4.

In phase 2, using λ_{SLS} the design spectrum at SLS was identified as per Chapter 5.2.2.2. β_{SLS} was defined as 0.2 and the hazard fitting coefficients were $k_0 = 365 \times 10^{-6}$, $k_1 = 2.043$, $k_2 = 0.155$. The PGA was identified as 0.136g using Equations 5.5 to 5.7, based on which a design spectrum at SLS was identified (Figure 5.9(b)) for the identification of a feasible initial period range. Then, the structural and non-structural loss contributions associated with each EDP were examined and limited based on the y_{SLS} previously identified. The SLFs proposed by Ramirez and Miranda [2009], assuming office occupancy for mid-rise structures were adopted (Figure 5.10). For simplicity, the loss was assumed to be equally distributed along the height of the building and the relative contributions of the different loss groups, Y , were taken from the relative contributions of each SLF shown in Figure 5.10. Given that the summation of each contribution exceeds 100% (Equation 5.26), the ELR associated with the element groups were normalised as shown in Chapter 5.2.2.2.

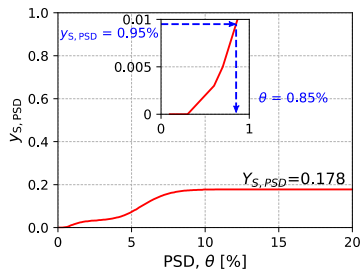
$$Y = Y_{S,PSD} + Y_{NS,PSD} + Y_{NS,PFA} = 0.178 + 0.545 + 0.402 = 1.125$$

$$\gamma_{S,PSD} = Y_{S,PSD} \gamma_{SLS} = \frac{0.178}{1.125} \cdot 6\% = 0.95\%$$

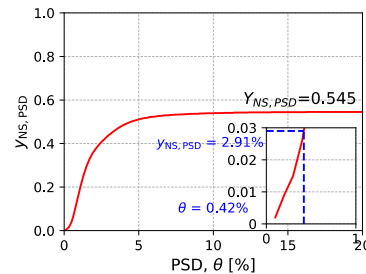
$$\gamma_{NS,PSD} = Y_{NS,PSD} \gamma_{SLS} = \frac{0.545}{1.125} \cdot 6\% = 2.91\% \quad (5.26)$$

$$\gamma_{NF,PFA} = Y_{NF,PFA} \gamma_{SLS} = \frac{0.402}{1.125} \cdot 6\% = 2.14\%$$

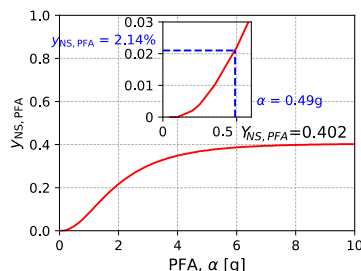
$$\gamma_{SLS} = \gamma_{S,PSD} + \gamma_{NS,PSD} + \gamma_{NS,PFA} = 0.95\% + 2.91\% + 2.14\% = 6.00\%$$



(a) PSD-sensitive structural elements



(b) PSD-sensitive non-structural elements



(c) PFA-sensitive non-structural elements

Figure 5.10. Utilisation of the SLFs adopted from Ramirez and Miranda [2009].

Figure 5.10 presents how limiting EDPs were evaluated. For the PSD-sensitive elements, the most critical one was identified as the non-structural elements with a $\theta_{max} = 0.42\%$

(Figure 5.10(b)). For the PFA-sensitive non-structural elements, a_{max} was calculated as 0.49g (Figure 5.10(c)). Following Section 5.2.2.2, the spectral limits for PSD and PFA were computed as $\Delta_{d,SLS} = 3.2\text{cm}$ and $a_{d,SLS} = 0.29\text{g}$ from Equations 5.10 and 5.12, respectively. Sd_α and Sa_A were retrieved from the SLS spectrum (Figure 5.9(b)) corresponding to the design spectral values and the period range bounds were calculated based on Equation 5.13 and 5.14 as follows:

$$T_{lower} = 2\pi \sqrt{\frac{Sd_\alpha}{\alpha_{SLS}}} = 6.28 \sqrt{\frac{0.61\text{cm}}{0.29 \cdot 981\text{cm/s}^2}} = 0.3\text{s} \quad (5.27)$$

$$T_{upper} = 2\pi \sqrt{\frac{A_{d,SLS}}{Sa_A}} = 6.28 \sqrt{\frac{3.20\text{cm}}{0.014 \cdot 981\text{cm/s}^2}} = 3.0\text{s} \quad (5.28)$$

A $T_1 = 0.9\text{s}$, within the identified period range, was selected as the initial target period of the structure. By ensuring the structure has an initial period in this range, the EAL is expected to be lower than the predefined EAL limit. It is noted that the period range is relatively large and is due to the level of hazard and limiting loss at SLS not being critical with respect to each other. Had a stricter EAL limit been imposed, the spectral limits would have reduced, and the feasible period range would have tightened; likewise, had the seismicity increased and the SLS spectra ‘grown’ outwards, the period range would also have tightened. Further work will explore this in Chapter 6.

The third phase of the formulation involved controlling collapse safety. Several assumptions were needed to utilise the SPO2IDA tool [Vamvatsikos and Cornell 2005] regarding the structural system’s expected SPO behaviour. Following the suggestions outlined in Section 5.2.2.3, the values shown in Figure 5.11 were adopted. For the sake of comparison with other presented formulations, only β_{RTR} was considered for what concerns uncertainty. The collapse fragility was calculated based on the 50th percentile as the median and the β_{RTR} based on the percentile values shown. Following Equations 5.15 to 5.19, the Sa_y was optimised to 0.37g for the case 4 structure, meaning that λ_c equated $\lambda_{c,target}$.

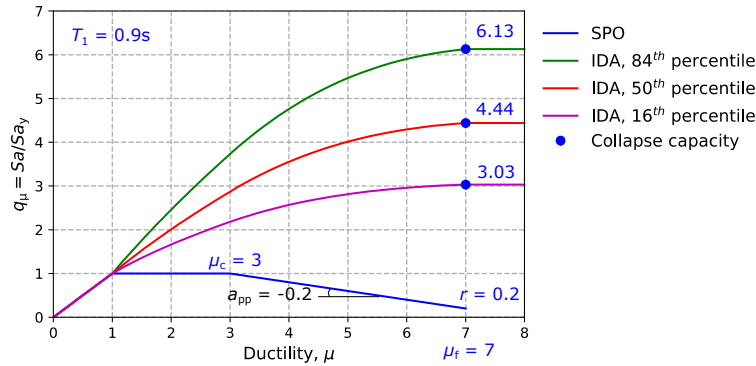


Figure 5.11. SPO and IDA curves attained via the SPO2IDA tool.

Following Section 5.2.2.4, with the identified Sa_y , assuming an initial overstrength q_s of 1.0, the design base shear was calculated with Equation 5.20. The design lateral forces were obtained using Equation 5.22 and the ELF method was performed to compute member design forces. Strength hierarchy, local ductility requirements and P-Delta effects were all accounted for following the EC8 [CEN 2004a] recommendations and structural elements were verified via their moment-curvature relationships using Response-2000 [Bentz 2015] and EC2 [CEN 2004b] material properties. It is important to note, that in the event of the actual SPO of the structure changing, the SPO curve in Figure 5.11 and q_s need to be verified and potentially updated to reflect the actual structural properties. The final design solutions in terms of the T_1 and Sa_d are shown in Table 5.5.

Table 5.5. Summary of the design solutions from the proposed IPBSD.

Case	$\lambda_{c,target}$	T_1 [s]	Sa_d [g]
1	5.0×10^{-4}	0.8	0.24
2	1.0×10^{-4}	0.7	0.54
3	5.0×10^{-4}	1.0	0.18
4	1.0×10^{-4}	0.9	0.47
5	5.0×10^{-4}	1.3	0.09
6	1.0×10^{-4}	0.8	0.48
7	5.0×10^{-4}	1.3	0.09
8	1.0×10^{-4}	1.0	0.38
9	5.0×10^{-4}	1.6	0.08
10	1.0×10^{-4}	1.4	0.27

5.4.5 RTS approach

The approach proposed by Luco *et al.* [2007] for RTS relies heavily on the underlying assumptions regarding the choice of the probability of collapse, X , and $\lambda_{c,target}$ with respect to the reference hazard, H_{ref} (*i.e.*, 1/475 years), as discussed by Gkimprixis *et al.* [2019]. Here, the risk-targeted spectral acceleration, $Sa^{c,X}$, was computed and then reduced by the code behaviour factor, q , corresponding to EC8's DCM, to obtain Sa_d .

Table 5.6 lists the variation of $Sa^{c,X}$ depending on $\lambda_{c,target}$ and the assumption of X . It shows high sensitivity towards the underlying assumptions and is noted to be insensitive to the choice of other structural parameters (*e.g.*, typology, number of storeys). The values are more in line with those attained in the previous section when $X = 1.0 \times 10^{-1}$. This was particularly interesting, since $\lambda_{c,target}$ do not correspond to the recommended values of 2.0×10^{-4} and 1.0×10^{-5} of ASCE 7-16 [2016] and Eurocode 0 (EC0) [CEN 2012], respectively. These observations are possibly due to the indirect assumption of H_{ref} , where Gkimprixis *et al.* [2019] showed a high sensitivity of the H_{ref} to $\lambda_{c,target}$ ratio to values of X , dispersion, β_{RTR} , and seismic hazard slope. In other words, depending on which $\lambda_{c,target}$ and H_{ref} the designer is using, the recommended values should have also been made using those same values. Following the suggestions of Douglas *et al.* [2013], $Sa^{c,X}$ were recomputed and a large difference was noted. The EC0 assumption of λ_c is stricter, hence the much higher Sa_d . The value from ASCE 7-16, where $q = 3/2R = 4.5$, assuming R equal to 3 for ordinary RC moment frames [ASCE 7-16 2016], is of a similar magnitude. If one were to follow the results of RTS, the RC frame designed for 0.07g would most likely not meet the collapse safety condition, as the results presented in Section 5.5.1 will later imply.

Table 5.6. Variation of $Sa^{c,X}$ with X and $\lambda_{c,target}$ for a $\beta = 0.5$ (with the exception of ASCE 7-16, where $\beta = 0.6$), $T_1 = 0.7$ s and $q = 3.9$ (with the exception of ASCE 7-16, where $q = 4.5$).

Assumption	$\lambda_{c,target}$	X	Source for X	$Sa^{c,X}$ [g]	Sa_d [g]
Case study equivalent	5.0×10^{-4}	1.0×10^{-5}	-	0.18	0.05
	1.0×10^{-4}	1.0×10^{-5}		0.40	0.10
	5.0×10^{-4}	1.0×10^{-4}		0.23	0.06
	1.0×10^{-4}	1.0×10^{-4}		0.52	0.13
	5.0×10^{-4}	1.0×10^{-1}		0.78	0.20
	1.0×10^{-4}	1.0×10^{-1}		1.76	0.45
ASCE 7-16	2.0×10^{-4}	1.0×10^{-1}	Luco <i>et al.</i> [2007]	1.21	0.27
EC0	1.0×10^{-5}	1.0×10^{-5}	Douglas <i>et al.</i> [2013]	1.28	0.33

The designs consistent with EC0 and ASCE 7-16 are more reasonable, and much higher than the values of EC8 obtained in Table 5.4 and Table 5.5, due to the stricter $\lambda_{c,target}$. Of importance is the fact that the $\lambda_{c,target}$ corresponding to ASCE 7-16 is more lenient as opposed to EC0, and is of similar level with respect to previously attained values through risk-targeted approaches. However, the lack of design flexibility and disregard towards other characteristics of the building (*i.e.*, number of storeys, typology etc.) should not be neglected.

5.4.6 Summary

For a brief comparison of the case study designs in the previous sections, the Sa_d values obtained from each method are presented in Table 5.7. A disparity is apparent among the risk-targeted and non-targeted approaches. These latter cases tend to be an order of magnitude higher, albeit with shorter periods. A notable exception is the RTS approach (X of 1.0×10^{-5} , β of 0.5, q of 3.9 and T_1 taken as the FBD cases), which is lower than the others and is most likely due to the inconsistencies in assumptions made while applying the method here, as mentioned above. It is noted that the DDBD and RTS design solutions are not examined further in the interest of space limitations. It is envisaged that due to their relative similarity in terms of Sa_d and T_1 with the FBD solutions, that the range of collapse risk values found for these will be generally applicable to each of these methods. Further analysis showed that this was indeed the case. Of note are the low values of Sa_d associated with methods like EC8 and RTS for some cases when compared to other methods. This is a reflection of the corresponding high T_1 values of these cases, where the design lateral demands reduced due to the higher flexibility of these structures. It is important to note that for EC8, for example, the design T_1 was a parameter that was initially estimated and refined without any constraints. This meant that structures could end up very flexible but still respect the seismic design requirements set out, as was the case here. However, it is important to note that design methods such as EC8 would also have other requirements such as wind and snow loads, amongst others, to take into consideration and would likely affect the final stiffness of the building. These were not considered here in order to isolate and examine the specific outcomes of the seismic design approach without any other non-seismic constraints masking the results obtained.

Table 5.7. Comparison of the design spectral acceleration, S_{ad} , obtained for different frameworks.

Cases	$\lambda_{c,target}$	EC8			DDBD		RTS		RTSA-D, TA		RTSA-I, TA		IPBSD	
		T_1 [s]	S_{ad} [g]	$G,$ S_{ad} [g]	T_1 [s]	S_{ad} [g]								
1	5.0×10^{-4}	1.1	0.10	0.16	0.7	0.12	1.1	0.03	0.7	0.36	0.7	0.43	0.8	0.24
2	1.0×10^{-4}	1.1	0.11	0.27	0.7	0.17	1.1	0.06	0.5	0.91	0.4	1.13	0.7	0.54
3	5.0×10^{-4}	2.3	0.04	0.13	0.7	0.05	2.3	0.01	0.7	0.39	0.9	0.38	1.0	0.18
4	1.0×10^{-4}	2.3	0.05	0.15	0.7	0.08	2.3	0.02	0.7	0.72	0.5	0.855	0.9	0.47
5	5.0×10^{-4}	1.8	0.06	0.14	1.0	0.06	1.8	0.02	1.0	0.30	1.1	0.24	1.3	0.09
6	1.0×10^{-4}	1.8	0.07	0.16	1.0	0.09	1.8	0.03	1.0	0.52	0.7	0.91	0.8	0.48
7	5.0×10^{-4}	2.3	0.05	0.08	0.7	0.06	2.3	0.01	0.7	0.48	1.1	0.25	1.3	0.09
8	1.0×10^{-4}	2.3	0.05	0.09	0.7	0.07	2.3	0.02	0.7	0.80	0.6	1.20	1.0	0.38
9	5.0×10^{-4}	3.0	0.03	0.06	0.9	0.06	3.0	0.01	1.0	0.34	1.1	0.27	1.6	0.08
10	1.0×10^{-4}	3.0	0.04	0.07	0.9	0.07	3.0	0.01	0.8	0.81	0.8	0.78	1.4	0.27

5.5 ANALYSIS RESULTS

Each case study design was modelled as described in Section 5.3.2 and IDA was performed to characterise the structural behaviour up to lateral collapse using the ground motions described in Section 5.3.3. With this, the actual λ_c with respect to the $\lambda_{c,target}$ is assessed to evaluate each method in delivering sufficiently safe and uniform risk design solutions. The λ_c values were computed with Equation 5.19 using the hazard described in Section 5.3.3 and are shown in Table 5.8, illustrated in Figure 5.12 and discussed below.

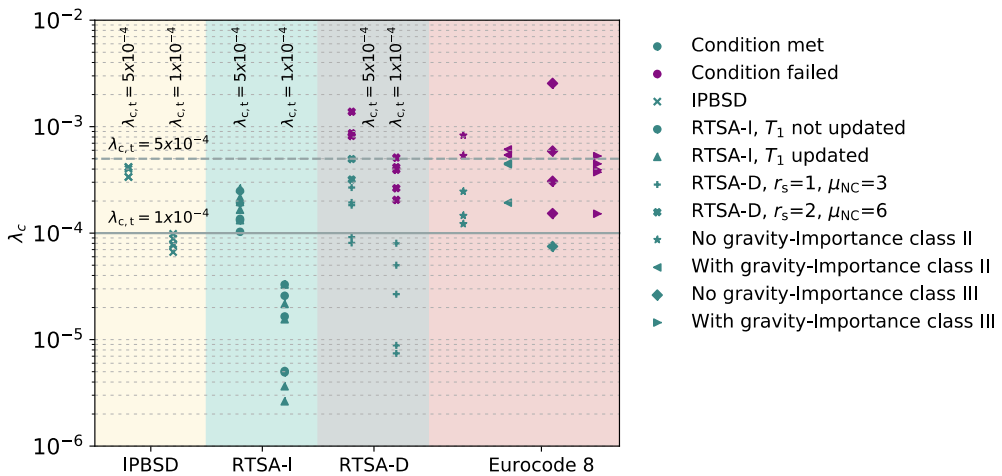


Figure 5.12. Illustration of the λ_c values for each case study structure and design approach considered, where for each group of designs the target value is denoted by the vertical text at the top of the plot.

Table 5.8. Summary of the λ_c for each case study structure and design approach considered.

Cases	$\lambda_{c,target}, x 10^{-4}$	IPBSD, $x 10^{-4}$	EC8, $x 10^{-4}$			RTSA, $x 10^{-4}$			
			Importance class	No G	G	D		I	
						TA	TB	TA	A
1	5.0	4.2	II	8.3	6.1	0.8	13.8	1.3	1.3
2	1.0	0.9	III	25.5	5.3	0.1	4.2	0.1	0.1
3	5.0	4.0	II	1.5	5.4	0.9	3.2	1.7	1.9
4	1.0	0.8	III	3.1	4.5	0.3	2.1	0.1	0.2
5	5.0	4.2	II	5.3	4.4	1.8	8.2	2.1	2.5
6	1.0	0.8	III	5.9	3.9	0.5	3.9	0.2	0.3
7	5.0	3.4	II	2.5	4.5	2.7	8.7	2.0	1.4
8	1.0	1.0	III	1.5	3.7	0.1	2.6	0.2	0.1
9	5.0	3.4	II	1.2	1.9	1.9	5.0	2.6	1.0
10	1.0	0.7	III	0.8	1.5	0.8	5.1	0.3	0.3

5.5.1 FBD according to EC8

All EC8 design solutions showed similar performance in terms of collapse safety with some scatter among the values. Values ranged from 0.8 to 25.5×10^{-4} for the cases without gravity

load considerations and from 1.5 to 6.5×10^{-4} for the cases with gravity load considerations. These are comparable with other values observed in past studies for similar typologies in Italy; Iervolino *et al.* [2018] examined several structural typologies designed using the NTC [2018] and computed λ_c values for RC frames in the order of 10^{-3} and 10^{-4} , which were also similar to the findings for perimeter RC frames of Haselton and Deierlein [2007, chapter 6]. As shown in Figure 5.12, less than 50% of the case study frames met the $\lambda_{c,\text{target}}$. This was not a surprising result given that λ_c did not directly feature as a design input in the FBD method.

The importance class was anticipated to provide an additional degree of collapse safety, although no notable reduction in λ_c was observed. As shown in Table 5.8, λ_c for some of the importance class II cases were lower compared to importance class III cases, which was an unexpected result. This was due to the difference in provided ductility capacity. For a fixed T_1 and higher design spectral acceleration in importance class III cases (Table 5.2), the member reinforcement ratios tended to be higher meaning the member curvature ductility capacities decreased. This translated to an overall lower system ductility, meaning the λ_c of structures with higher importance class tending to be higher. This observation highlights the careful balance between strength, stiffness and ductility in seismic design and illustrates that increasing the strength and stiffness of structural members in the name of improved collapse safety is not always an effective solution.

To better visualise this observation, a general trend may be observed via Figure 5.13. Using Response-2000 [Bentz 2015], moment-curvature relationships were attained and the variation of curvature ductility capacity, μ_ϕ , is plotted with respect to cross-section effective area, A_{eff} , and tensile reinforcement ratio, ϱ . For a fixed value of ϱ , taken as a rough proxy for the lateral resistance of a structure, an increase in A_{eff} is needed to increase μ_ϕ . Additionally, μ_ϕ can be increased by reducing ϱ for a fixed value of A_{eff} . Therefore, by reducing A_{eff} of importance class II frames, one would essentially increase ϱ resulting in decreased μ_ϕ . With the same logic, the resulting λ_c of those frames would be expected to increase.

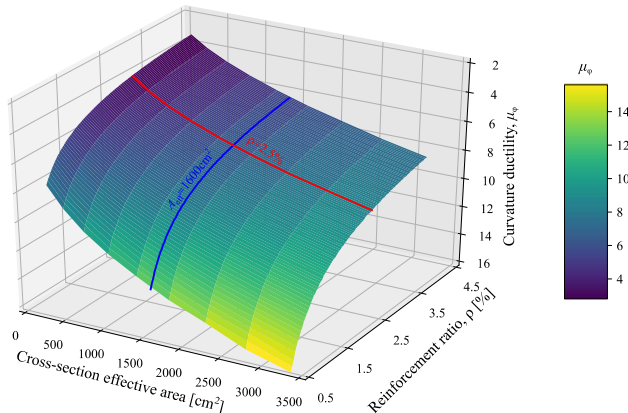


Figure 5.13. Interaction of curvature ductility capacity, μ_ϕ , with respect to cross-section effective area, A_{eff} , and tensile reinforcement ratio, ρ , as per EC2 for square columns with symmetric B500C reinforcement, C25/30 concrete, with μ_ϕ computed as the ratio of curvatures at peak and yield moment.

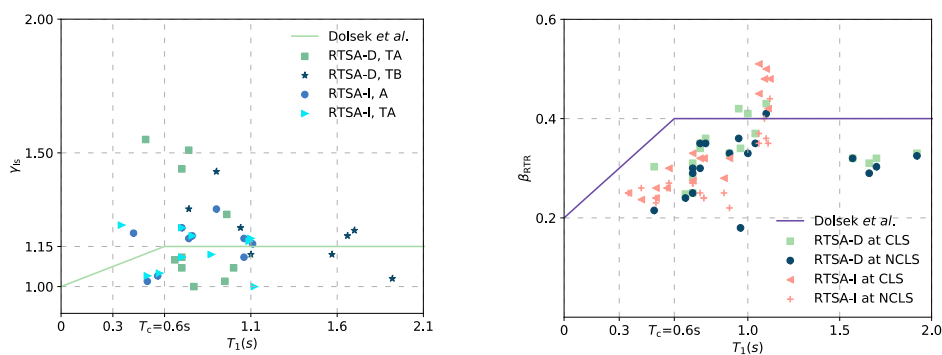
By adding gravity loads, the collapse safety of the frames did not improve significantly. For example, the best performing structure showed a $\lambda_c = 7.5 \times 10^{-5}$, which was meeting the $\lambda_{c,\text{target}}$ of 5.0×10^{-5} , with the addition of gravity loads during design failing to meet the target. The reasons for such a scenario are likely related to similar conclusions made for the consideration of higher importance class, since by increasing the resistance, the performance of the frame is not necessarily improved. Through the inclusion of gravity loads during design, not only did the demands on the elements increase but also the overstrength factors by an average of 35%, which is in a way akin to having a higher importance class. Since there is no direct control to meet $\lambda_{c,\text{target}}$ values, one may argue that the FBD method currently prescribed by EC8 is not suitable for uniform risk solutions. It must be stated that the aim here was not to diminish current code provisions, but rather highlight the absence of risk-targeted procedures which should be the focus of future development.

5.5.2 RTSA method

For the RTSA method, it is noted from Figure 5.12 that both formulations tended to provide the desired collapse safety by meeting $\lambda_{c,\text{target}}$ due to the inherent risk-targeted of the formulation. A fair degree of scatter among results and conservatism is noted for some cases. Structures designed following both formulations generally performed well with the exception of the RTSA-D TB cases. These discrepancies were mainly as a result of the assumptions made for the overstrength and ductility capacity at the no-collapse limit state. Of importance are also the assumptions regarding the conversion factors needed to move from the collapse to no-collapse limit state (*i.e.*, r_s , μ_{NC} and γ_s), where if incorrectly assumed,

disagreement may be anticipated. The design cases presented here were iterated for T_1 only, which for RTSA-I cases seemed to have little impact. Any additional iteration required via SPO analysis or NLRHA to further refine the assumptions of r_s , μ_{NC} and γ_s were not performed, which is important to bear in mind. To this end, the assumed values of r_s , μ_{NC} , γ_s and β_{RTR} were checked against the true behaviour of the frames and how much discrepancy existed.

Figure 5.14(a) compares the observed γ_s values against those proposed by Dolšek *et al.* [2017], where large differences can be observed in some cases but without any consistent trend. This parameter has a notable impact when estimating the actual collapse capacity. Likewise, Figure 5.14(b) compares the dispersions from the model proposed by Dolšek *et al.* [2017] to those observed here. The observed β_{RTR} values follow the proposed model trend to a certain extent but the values tend to stabilise later at around $T_1 = 0.9$ s, as opposed to 0.6s as suggested. Relatively few cases had $\beta_{RTR} > 0.4$, while the majority had slightly lower values. This, in addition to an underestimated γ_s , contributed to a decrease in the observed λ_c of the frames and helps explain the conservative nature of some of the results shown in Figure 5.12. In any case, the assumption of $\beta_{RTR} = 0.4$ is still a reasonable first estimate for most design cases but some instances where validation and possible design iteration would be needed were noted. Additionally, the assumption of equal β_{RTR} for both the CLS and NC limit state (denoted as NCLS in Figure 5.14), which is an inherent assumption of the RTSA methods, does not always appear to be a valid one. They are generally close, but a notable difference could have a significant impact in the definition of collapse capacity fragility (Figure 5.14(b)). This observation just concerns the RTR variability in response but is noted to be only one of many pertinent sources of uncertainty in seismic response.



(a) γ_s of the design cases and the model (b) β_{RTR} of the design cases and the model

Figure 5.14. Comparison of the Dolšek *et al.* model values for (a) γ_s and (b) β_{RTR} as a function of T_1 provided by [Dolšek *et al.* 2017] with the actual values computed from IDA upon designing and detailing.

To evaluate the assumptions of r_s and μ_{NC} used in the RTSA methods, Figure 5.15 plots the values obtained from an SPO analysis of the finalised designs. Observing Figure 5.15(a), the actual values were relatively independent of the initial design assumption and were observed to be between the trialled values of $r_s = 1$ and 2, which is in line with the findings of Haselton and Deierlein [2007, chapter 6], where the overstrength of the perimeter RC frames, defined as the ratio of ultimate base shear to design base shear, was between 1.5 and 1.8, meaning that the overstrength defined herein as the base shear at yield to design base shear should be generally lower. In contrast, the overstrength of space frames had a trend with the number of storeys. It is important to note, that no consideration was given to the hardening slope of the backbone behaviour (*i.e.* elastic-perfectly plastic idealisation was assumed) of the structures of RTSA, which is important for identifying the collapse safety of the structure [Vamvatsikos *et al.* 2009]. Based on the evidence here displayed, the values of overstrength are hard to identify as they depend on parameters like perimeter/space frame, number of storeys and the hardening behaviour of the structure. The under- and overestimation of r_s was seen to have contributed largely to the conservativeness observed for some of the RTSA cases in Figure 5.12. Figure 5.15(b), on the other hand, does not show any trend or consistency in the μ_{NC} values with most conservatively exceeding the design assumption with the exception of D-TB cases. Unlike the parameters evaluated in Figure 5.14, the assumptions of r_s and μ_{NC} may be evaluated and checked using the results of SPO analysis, possibly requiring multiple design iterations.

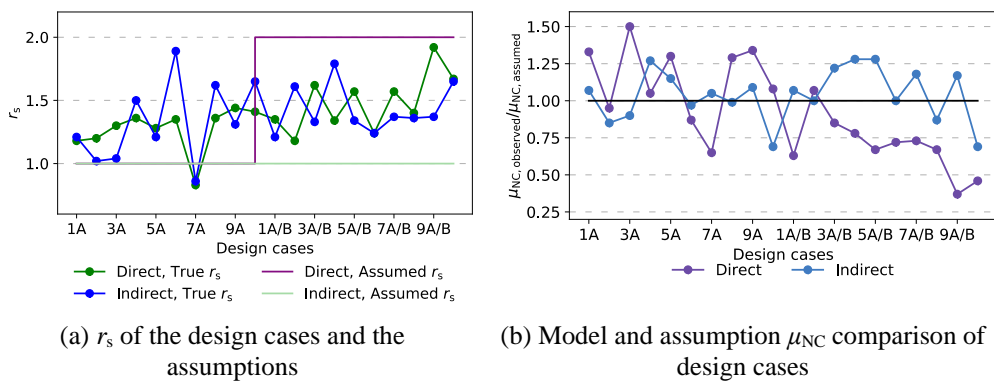
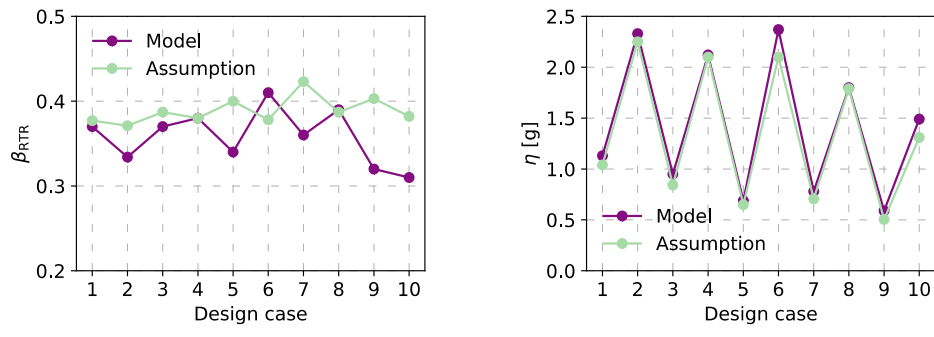


Figure 5.15. Comparison of the assumed values for (a) r_s and (b) μ_{NC} ratios, with the actual values computed from SPO upon designing and detailing, where the notation A refers to D-TA and I-A cases, and A/B refers to I-TA/D-TB cases.

5.5.3 Proposed IPBSD formulation

For what concerns the proposed IPBSD formulation, consistent results were obtained in each case, as shown in Figure 5.12. The actual λ_c computed from IDA met the $\lambda_{c,\text{target}}$ set within a relatively narrow tolerance and without any case of excessive overdesign. This result demonstrated the proposed IPBSD's efficiency in obtaining risk-targeted design

solutions. Furthermore, the median values of collapse capacity observed in IDA matched those identified during design very well and were seen to be independent of any structural characteristics. Figure 5.16 gives the medians, η , and the β_{RTR} of the collapse capacities of the design cases. The β_{RTR} values established from IDA were first compared to the ones assumed via SPO2IDA during the design process. Similar to RTSA in Figure 5.14(b), some conservatism of design assumptions of β_{RTR} may be observed in Figure 5.16(a), but still quite close to actual values and within acceptable bounds; possible iterations could be performed for more refined accuracy. The η used in design were slightly conservative compared to the actual model values (Figure 5.16(b)), possibly due to slight overstrength or ductility in the structures, or due to the approximate nature of the SPO2IDA tool but were nonetheless found to be sufficiently accurate to result in suitable and efficient design solutions.



(a) IDA and Design value comparison of β_{RTR} (b) IDA and Design value comparison of η

Figure 5.16. Comparison of computed and assumed values of (a) β_{RTR} and (b) η at CLS.

The assumed and calculated overstrength values of q_s (Figure 5.3) from SPO analysis are presented in Figure 5.17. As one may notice, the actual values of q_s are not that different from the initial design assumption. For case study frames 5, 7, 9, the design q_s was updated as an additional iteration was required to increase the accuracy of the method. After the initial design of those frames, notable overstrength were inherent due to strong-column weak-beam requirement and local ductility requirement of EC8. To satisfy the demands of ELF, the required longitudinal reinforcement ratio was below the limit value, hence, it was increased to match the demands of the code, thus resulting in relatively high overstrength of the overall structure. For the other frames, where overstrength was relatively negligible, no iteration was performed and was found to have negligible effects on the results. However, as already pointed out in Section 5.5.2, iterations might be necessary for the accurate estimation of q_s , specifically when gravity loads are involved in design, and a certain level of overstrength is expected when any seismic code provisions are utilised.

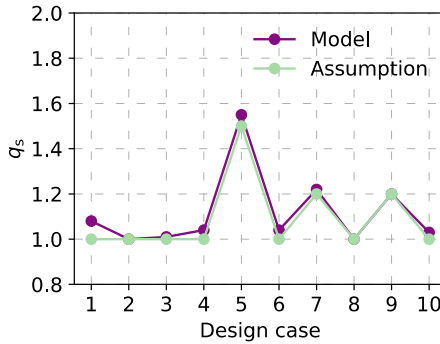


Figure 5.17. Comparison of computed and design values of q_s .

5.5.4 Refined estimate of collapse risk

One of the assumptions of the proposed IPBSD method (and all others evaluated here) was that using $Sa(T_1)$ as an IM and IDA with the ground motions identified in Section 5.3.3 was a suitable strategy for estimating collapse risk. Research in recent years has indicated that this may not be the most robust approach and other IM definitions may be more suitable (e.g., the spectral acceleration at some multiple of T_1 or averaged range around it) and other ground motion selection techniques [Baker 2011] may be more suitable. Eads *et al.* [2015] have shown that spectral acceleration averaged over a period range around T_1 , $\text{Avg}Sa$, is a more efficient IM in collapse risk estimation. Ideally, this IM would be used here but given the simplicity and physical meaning of $Sa(T_1)$ in relation to the design base shear, this simpler option was preferred. Nevertheless, the question remains as to whether using $Sa(T_1)$ as the IM in an IDA with a single set of ground motion records still meets the collapse risk when characterised using more refined, but cumbersome, methods of collapse risk quantification? To shed some light on this, the λ_c of the IPBSD case frames was recomputed to verify that it was in fact slightly conservative when using $\text{Avg}Sa$. For what concerns the use of a single ground motion record set, Eads *et al.* [2015] have shown that λ_c estimates were relatively insensitive to different sets when using $\text{Avg}Sa$. Therefore, if it can be shown that the $\text{Avg}Sa$ -based λ_c values are at least as low as the $Sa(T_1)$ -based ones, the design results may be deemed suitable.

To do this, the IDA results previously established were reprocessed for all structures in terms of $\text{Avg}Sa$, defined within a period range of 0.35s and 3.55s with a 0.10s step for all structures. The distribution of collapse intensities was identified and integrated with the hazard curve associated with $\text{Avg}Sa$ to estimate λ_c . This hazard curve was computed from the same hazard model described in Section 5.3.3. Similar to Eads *et al.* [2015], collapse dispersions using $\text{Avg}Sa$ were lower and the overall λ_c was on the conservative side. Figure 5.18 illustrates the results with reference to original values computed and verified in Section 5.5.3. In short, the more refined $\text{Avg}Sa$ -based λ_c values are indeed lower than the $Sa(T_1)$ -based ones indicating that the designs established using $Sa(T_1)$ are slightly conservative. All

methods evaluated here would be expected to show the same trend, so it is not envisaged to be a drawback to the specific design method proposed per se, but rather a convenience choice for design. It is worth noting that for their implementation of RTBF, Vamvatsikos *et al.* [2020] used *AvgSa* as their IM to address the issue discussed.

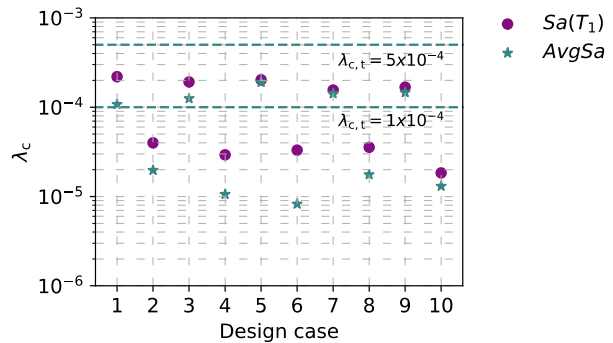


Figure 5.18. Illustration of collapse risks using $Sa(T_1)$ or $AvgSa$ as the IM.

5.6 SUMMARY AND CONCLUSIONS

The ability to design structures following a simplified PBEE-based methodology has been one of the many focusses of the earthquake engineering community. Current design methods, such as those founds in many design codes, deal with design without adequately accounting for the probabilistic nature of both seismic design input and structural response. In the disciplinary discourse of risk-consistent seismic design approaches, there is a tendency to balance the ease of implementation for practitioners with flexibility and accuracy in identifying risk-consistent design solutions.

This chapter proposed the IPBSD framework, allowing the identification of feasible design solutions that limit expected monetary losses and target a given collapse safety. It was described via a step-by-step implementation and tested for several case study RC frame structures. Other existing design code approaches and risk-targeted approaches were tested for the case study structures examined in order to have a broad and thorough comparison of different approaches. Following a full design of each structure's members, numerical models were developed, and NLRHA was performed through an application of IDA. Integrating this IDA response of each structure allowed the actual collapse safety to be quantified and compared with the initial limit targeted in design. The main conclusions of this study are as follows:

- Half of the case study frames following Eurocode 8 met the MAFC condition, which was not surprising given the nature of the non-risk targeted approaches.

Even though two importance classes were considered, no significant degree of increased collapse safety was consistently obtained. In fact, some of the importance class II frames performed better than the III ones since, for a fixed fundamental period, the member reinforcement ratios tended to reduce and led to increased member ductility capacities. This offsets the lower strength to provide a higher collapse capacity via increased ductility. Hence, a careful balance between strength, stiffness and ductility in seismic design is vital and simply increasing the strength and stiffness of structural members in the name of improved collapse safety is not always an effective solution;

- The addition of gravity loads to the design process improved the collapse safety via additional overstrength. However, no consistent trend was observed pointing towards a need for its explicit consideration in design;
- The apparent lack of design flexibility and heavy dependence on the design reference values in current implementations of RTS means that underlying assumptions need subsequent modifications to result in widespread adaptation;
- Design and validation of cases following the RTSA method demonstrated the advantages of risk-targeted approaches, as the majority of cases met the MAFC condition. It was found that assumptions regarding design input parameters had a significant impact when targeting a specific collapse safety. Several design cases initially reported collapse risk values much lower than the design target, which was found to be a result of conservative design input parameters, which could be refined through repeated design iterations;
- Many of the assumptions needed for the RTSA method and the proposed IPBSD method require further quantification studies and experimentation for suitable initial design input parameters and targets; specifically, the anticipated collapse capacity uncertainty β_{RTR} , or on how to quantify the expected ductility capacity and the post-capping strength of structural elements. Some research exists on these issues but much more could be done to consolidate the understanding and render them useful in design practice;
- The proposed IPBSD approach demonstrated consistent results in terms of meeting the collapse safety targets for each of the case study frames. The targets were met with relatively narrow conservatism and without any case of excessive overdesign or requiring multiple design iterations.
- The structures' collapse capacities from IDA (*i.e.* median and dispersion) were slightly conservative, possibly due to supplementary ductility in the structure or the approximate nature of the SPO2IDA tool [Vamvatsikos and Cornell 2005]; however, it was found to be sufficiently accurate to result in suitable and efficient design solutions.

In summary, methods following a risk-targeted approach performed reasonably well, while the cases designed following other traditional approaches, such as Eurocode 8, failed the target collapse safety condition. The beauty of the proposed IPBSD approach is in its flexibility and simplicity, as it combines the advantages of different methods in the

literature, including code-based provisions, to give risk-consistent design solutions. It is envisaged that this approach, following further research and refinements, should form a part of the next-generation seismic design approaches aiming to achieve the goals of PBEE.



6. ON THE SEISMIC LOSS ESTIMATION OF INTEGRATED PERFORMANCE-BASED DESIGNED BUILDINGS

This chapter is based on the following reference:

Shahnazaryan, D., O'Reilly, G. J. and Monteiro, R. [2021] "On the seismic loss estimation of integrated performance-based designed buildings,". *Under review*.

6.1 CHAPTER OVERVIEW

This chapter builds on the developed IPBSD framework of Chapter 5 to explore the impacts of design decisions on the effective targeted limitation of losses. The framework uses collapse risk and economic loss as main design inputs, while the performance objectives remain in line with the goals of PBEE [Vamvatsikos *et al.* 2016]. The proposed framework is extended to 3D buildings with the consideration of damageable component inventory sensitive to the seismic action in both directions. Additionally, a Python-based iterative object-oriented toolbox was developed to aid practitioners carry out a seamless loss-driven risk-targeted design. The framework is briefly recalled through developments to allow its application on buildings and is described for buildings with RC MRF as the main lateral resisting system. Then, the efficiency of the framework in satisfying the pre-established performance objectives (*i.e.*, limitation of economic loss while maintain collapse safety) is investigated through an application to several case-study buildings. A detailed dissection of the main sources of losses within the building is examined to shed further light and provide justification needed to the simplifying assumptions needed to implement such a framework in an efficient manner. Furthermore, the IPBSD framework is compared with the response of buildings designed according to conventional seismic design code, namely EC8 [CEN 2004a].

6.2 INTEGRATED PERFORMANCE-BASED SEISMIC DESIGN (IPBSD)

6.2.1 Performance objectives

As mentioned above, the primary focus of modern seismic design codes is to provide life safety to building occupants by avoiding structural collapse, after which performance during frequent seismic events is checked and verified. Implemented at return periods of 475 and 95 years, these are termed as the *no-collapse* and *damage limitation requirements* in the current version of EC8, with the possibility to account for building importance class.

Similarly, *serviceability* and *ultimate* limit states associated with design return periods of 25 and 500 years, respectively, are defined in New Zealand's NZS1170 [NZS 2016], with the possibility of modifications via importance classes. With slight modifications, a revised design code in the US, ASCE7-16 [2016], sets a fraction of the maximum considered event for the design of the building, determined from a series of risk-targeted hazard maps developed for a target collapse risk of 1% in 50 years.

Those seismic design codes follow a FBD method, which calculates a design base shear force from a reduced elastic spectrum using either the ELF method or RSMA. Priestley [2003] and others pointed out several shortcomings regarding the FBD method, thus advocating a DBD, where deformation demands in the individual elements drive the design process, resulting in the development of the DDBD method [Priestley *et al.* 2007] and other similar methods [Sullivan *et al.* 2003]. While both FBD and DDBD are good approximations for the initial seismic design of structures, neither explicitly quantifies the structural performance in a way that may be considered as fully satisfying the goals and needs of modern PBEE. Essentially, this means that the performance of structures designed using either method will not be considered as risk-consistent (*i.e.*, the annual probability of exceeding a certain performance threshold is not accurately known or consistent among different structures), and metrics such as building collapse risk, expected economic losses or downtime are not included in the design process. Therefore, a more risk-targeted and probabilistic framework is sought here.

IPBSD was proposed as a framework to evaluate building performance and identify structural solutions meeting the target collapse risk and limiting the economic loss. It was expanded from the CSD framework developed by O'Reilly and Calvi [2019], which requires very little structural information at the design onset and has a goal of limiting the EAL of the building. It was further developed by Shahnazaryan and O'Reilly [2021] to explicitly target collapse risk in terms of MAFC along with the limitation of EAL. While they demonstrated the validity of the framework in identifying structural solutions for planar RC MRFs, which met the target MAFC set forth as the performance objective, this chapter aims to extend the IPBSD framework to 3D buildings, while also providing further insight and justification for the assumptions made and demonstrate its validity in meeting both the target MAFC and EAL limits for bidirectional behaviour.

Several assumptions are made to relate the performance objectives to a design solution space, which is now pertinent to both principal directions of the building. The target MAFC, $\lambda_{c,target}$, is used to limit the actual λ_c described by Equation 6.1.

$$\lambda_c = \int_0^{+\infty} P[C | Sa(T)] |dH(Sa(T))| \leq \lambda_{c,target} \quad (6.1)$$

where, $P[C | Sa(T)]$ is the probability of collapse given the IM of spectral acceleration $Sa(T)$ at a period of T , and $H(Sa(T))$ is the site hazard function. An EAL limit, $\lambda_{y,limit}$, is used to control λ_y described by Equation 6.2 such that excessive losses do not manifest over the lifetime of the building.

$$\lambda_y = \int_0^{+\infty} E[y] |dH| \leq \lambda_{y,limit} \quad (6.2)$$

where, $E[y]$ is the loss function.

6.2.2 IPBSD implementation

An overview of the IPBSD framework implementation is briefly outlined with the flowchart depicted in Figure 6.1, whereas a detailed description can be found in Shahnazaryan and O'Reilly [2021]. Particular emphasis is given to the developments and refinements made in this study, supported by parametric studies presented in later sections.

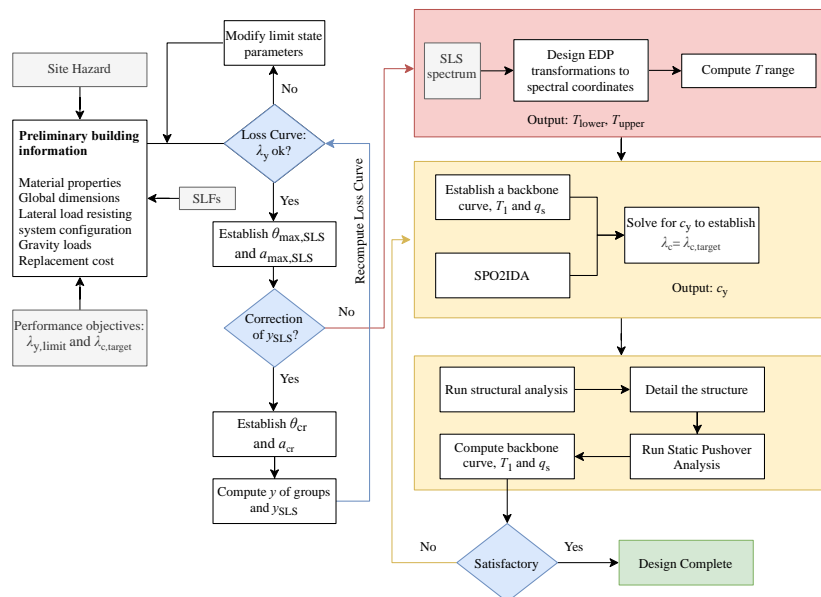


Figure 6.1. Flowchart of the IPBSD framework.

At the beginning of IPBSD, a suitable loss curve is identified to limit λ_y . Performance limit states are characterised through the ELR, y , and MAFE, λ , as shown in Figure 6.2. The loss curve uses three limit states: fully OLS, which defines the onset of damage and monetary loss, assumed to have $y_{OLS}=1\%$ and associated with a return period of 10 years; SLS, where the economic losses are controlled through the modification of y_{SLS} ; and CLS, where complete collapse (*i.e.*, $\lambda_{CLS}=\lambda_c$) and economic loss of the building (*i.e.*, $y_{CLS}=100\%$) are expected. The area under the loss curve is the design EAL, λ_y and the characteristics associated with SLS should be adjusted to make sure that λ_y does not exceed $\lambda_{y,limit}$, ensured by the selection of λ_{SLS} in line with seismic code requirements. In order to ensure that losses are not excessive, a building should be designed to accommodate y_{SLS} , whereby the cost contributions from PSD and PFA-sensitive components are limited, leading to the identification of a range of possible initial (*i.e.*, secant to yield) structural periods [T_{lower}, T_{upper}] for each principal direction of the building. The IPBSD framework is independently applied in each direction sequentially, without disturbing the integrity of results in the perpendicular direction (*e.g.*, design and detailing of corner columns must be the same or static or pushover analysis should be applied to a 3D building model). Before embarking on the computation of a feasible period range, SLFs relating structural demands and economic losses need to be selected or generated, which can be facilitated through a tool recently proposed by Shahnazaryan *et al.* [2021c]. Decisions should be made with regard to subdividing components into different damageable performance groups: structural PSD-sensitive; non-structural PSD-sensitive; and non-structural PFA-sensitive. SLFs should be developed for each storey level and each damageable group. Once the SLFs are generated or selected, relative weights or contributions of different damageable groups to expected loss, Y , at SLS are defined. The ELR at SLS, y_{SLS} , shown in Figure 6.2 is broken down as per Equation 6.3.

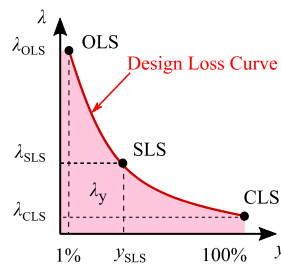


Figure 6.2. Identification of the loss curve and SLS performance objectives to limit the EAL.

$$\mathcal{Y}_{SLS} = \sum_1^j (\mathcal{Y}_{i,S,PSD} + \mathcal{Y}_{i,NS,PSD}) + \sum_0^j \mathcal{Y}_{j,NS,PFA} \quad (6.3)$$

where $\mathcal{Y}_{i,S,PSD}$ is associated with structural PSD-sensitive, $\mathcal{Y}_{i,NS,PSD}$ is associated with non-structural PSD-sensitive, and $\mathcal{Y}_{j,NS,PFA}$ is associated with non-structural PFA-sensitive loss

contributions, i is the number of storeys, j is the number of floors and 0 refers to the ground floor where non-structural PFA-sensitive losses are present. Additionally, each of the PSD contributions comprises damageable components sensitive to the direction of the seismic action (*i.e.*, the principal directions of the building), while, generally, PFA-sensitive components are considered sensitive to both directions and a non-directional factor is applied to account for the increased demands and therefore associated losses on the components. The loss contributions for each building level and, in the case of components with directionality properties, along each direction of the building, may be computed as the product of target y_{SLS} and its relative weighting Y by Equation 6.4. The Y weighting factors depend on the component inventory information and therefore on the SLFs developed.

$$\begin{aligned} y_{S,PSD} &= y_{SLS} Y_{S,PSD} \\ y_{NS,PSD} &= y_{SLS} Y_{NS,PSD} \\ y_{NS,PFA} &= y_{SLS} Y_{NS,PFA} \end{aligned} \quad (6.4)$$

Having computed all possible ELR values at the different storey or floor levels, as well as directions of the building, demand limits in terms of critical maximum PSD, $\theta_{\max,SLS}$, and maximum PFA, $a_{\max,SLS}$, may be computed using the SLFs shown in Figure 6.3 for each direction.

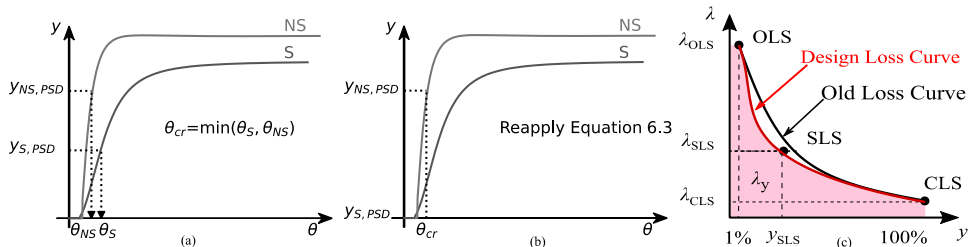


Figure 6.3. Storey loss functions and computation of design limits (S and NS stand for structural and non-structural component groups, respectively). (a) Computation of θ_{cr} and identification of θ for non-structural (NS) and structural (S) components; (b) Reapplication of Equation 6.3 and estimation of $y_{NS,PSD}$ and $y_{S,PSD}$; (c) Computation of design loss curve.

The computation process is applied to each of the principal directions of the building considering damageable groups only sensitive to the direction of interest and all non-directional damageable groups with the application of a non-directional factor. Satisfying these conditions, in both directions, is expected to result in the fulfilment of the EAL limit initially set out. Therefore, two separate design limits are obtained associated with each direction. By entering the vertical axis in Figure 6.3(a) with the values computed via Equation 6.4, the more critical (lower) $\theta_{\max,SLS}$ and $a_{\max,SLS}$ are obtained (the example flow

of the computation is given for PSD sensitive components considering two SLFs). However, this entails the use of the same $\theta_{\max,SLS}$ for both structural and non-structural components (θ_S and θ_{NS} , respectively, in Figure 6.3). In other words, if the critical value of $\theta_{\max,SLS}$ (θ_{cr} in Figure 6.3) was associated with non-structural components (*i.e.*, more vulnerable components), then the assumed value of $\gamma_{S,PSD}$ for the structural elements estimated via Equation 6.4 likely to be overestimated as the associated actual value of $\gamma_{S,PSD}$ will be lower, as shown in Figure 6.3(b). In that example, $\gamma_{S,PSD}$ is near zero thus considerably lower than what was hypothesised earlier in Equation 6.4. Therefore, to avoid the possible underestimation of $\lambda_{y,limit}$, which would be the case following the initial assumptions proposed by O'Reilly and Calvi [2019], a proposed single-step correction through the reapplication of Equation 6.3 with the modified ELRs of damageable groups (*i.e.*, the newly computed significantly lower $\gamma_{S,PSD}$), where applicable, is presented in this work. The correction step is not mandatory to the IPBSD framework but should be applied if more refined or less conservative results are sought. As a result, the new value of γ_{SLS} will be lower, thus resulting in a loss curve that is shifted to the left as shown in Figure 6.3(c), which will also be observed later in Section 6.6 through actual data.

This step proposed here acts as a single-step iteration where the framework, due to the dissimilarity of component fragilities and costs associated with different damageable groups, tries to adjust the assumptions made before the initiation of further computations for the optimization of the solution space towards values desirable by the practitioner. This will provide consistency for loss contribution computation associated with more robust components. Based on the corrected γ_{SLS} , the loss curve is updated as shown in Figure 6.3(c) and a new design EAL, which is lower than the initial value, is identified and compared against the limit $\lambda_{y,limit}$. Alternatively, the practitioner may modify the γ_{SLS} to take advantage of this initial conservatism and refine λ_y to be in the vicinity of $\lambda_{y,limit}$ defined before the onset of the framework. The developments discussed herein will be further detailed and assessed through exploratory analyses in Section 6.6.

Next, the design spectrum at SLS (Figure 6.4(a)) and SLFs (Figure 6.4(b)) are used to compute the demand limits, which, in combination with the design spectrum, may be used to identify the initial period range bounded by the lower, T_{lower} and upper, T_{upper} period limits, as demonstrated in Figure 6.4(c). The building should essentially have secant to yield periods within these ranges in both directions, ensuring that it will be neither too stiff, which would result in excessive floor acceleration-sensitive losses, nor too flexible, which would result in excessive drift-sensitive losses, at SLS. Satisfying these conditions in both directions is expected to result in fulfilment of the EAL limit initially set out, as will be confirmed in the analysis in Section 6.6.

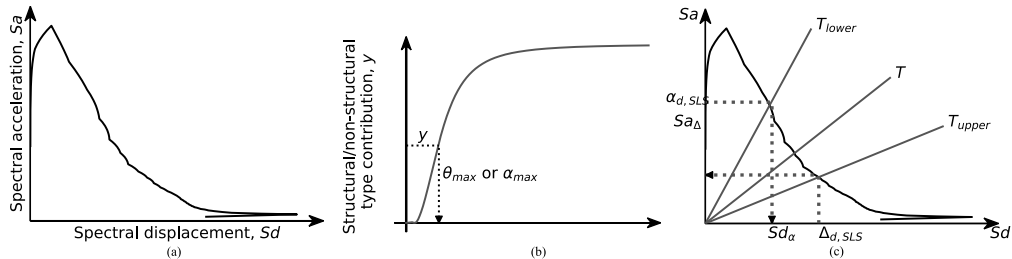


Figure 6.4. Establishment of a feasible initial period range. (a) Design spectrum at SLS, (b) SLF and estimation of design limits, (c) identification of period limits.

With economic loss limited by ensuring that periods along each direction of the building are within the respective period ranges, it is important to control the risk of structural collapse. A period between T_{lower} and T_{upper} is selected and the expected backbone behaviour and overstrength, q_s , are first trialled by the practitioner (Figure 6.5(left)). Here, q_s represents the ratio between the strength at yield, V_y , and design, V_d , and q_u is the ratio between spectral acceleration at collapse, S_{a_c} , and yield, S_{a_y} , while Δ_y , Δ_c and Δ_f represent displacements at yield, capping and fracturing points, respectively. The SPO2IDA tool [Vamvatsikos and Cornell 2005] is used to estimate the collapse fragility function of the building along each direction in terms of median collapse capacity, S_{a_c} , and RTR variability, β_{RTR} , assuming a lognormal distribution. Throughout the IPBSD procedure implemented here, only RTR variability has been considered for simplicity, although other pertinent sources do exist (e.g., modelling uncertainty [O'Reilly and Sullivan 2018]) but may be easily considered in the process. For example, the uncertainty value β_{RTR} obtained from SPO2IDA may be amplified via a SRSS approach to consider other independent sources of response uncertainty in the collapse capacity estimation. Furthermore, the additional uncertainty in the non-collapse response may be considered at SLS. That is, during Phase 2 of the IPBSD description in Shahnazaryan and O'Reilly [2021], the inherent uncertainty at SLS, β_{SLS} , in Equation 5.6 may also be amplified via SRSS to account for these additional sources of uncertainty. Having assumed the SPO shape (backbone curve), the SPO2IDA tool may be used to perform a quick estimation of the IDA response. The output of SPO2IDA will be the collapse fragility function, which is then integrated with the hazard curve corresponding to the selected T_1 , $H(Sa(T_1))$, to compute λ_c (Figure 6.5(right)). The trialled structural capacity of the frame, q_s and/or backbone shape characteristics are revised until λ_c equates to $\lambda_{c,target}$, satisfying Equation 6.1. The process is repeated for each principal direction of the building and the critical (larger) of S_{a_y} is selected as the design yield strength for further design and detailing.

The identified design base shear is then used to compute the lateral distribution of forces and perform static analysis including gravity loads to estimate demands on structural

elements. Seismic design codes may be followed to perform member detailing to determine the required element cross-section dimensions and reinforcement content. Strength hierarchy and local ductility requirements must be accounted for as well. The final structural solutions should have T_1 in both directions within a reasonable tolerance of the assumed value and within the feasible period range identified. If the condition is met, the identified structural configuration may be adopted. Otherwise, the element dimensions and reinforcement content should be revised.

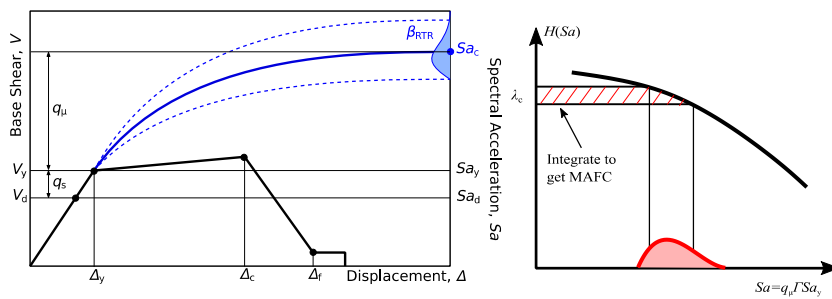


Figure 6.5. (left) Expected backbone behaviour, (right) identification of collapse capacity and computation of λ_c .

6.2.3 Python-based iterative framework

To aid the designer avoid some of the cumbersome tasks involved within the framework, specifically regarding the assumption of the backbone curve shape or computation of design yield strength, an object-oriented Python-based software has been created and is freely available on GitHub [Shahnazaryan *et al.* 2021b]. The software is based on the framework described here and in previous works by the authors. Some of the more difficult aspects involving iterations or calibrations are automated within the software to simplify the tasks for a designer. However, it is noted that the use of this software is not a strict requirement to implement IPBSD but rather a supplementary tool to facilitate and expedite the process for users familiar with the design steps. The open-source and object-oriented nature of the code lets users customise and tailor their code to suit diverse design situations.

Essentially, based on the design Sa_y , lateral force analysis including the gravity loads is carried out for both directions of the building and the structural elements are designed following the recommendations of EC2 [CEN 2004b], and EC8. Based on the maximum demands from both analyses, structural elements are designed using moment-curvature relationships attained following the Response-2000 sectional analysis program [Bentz 2015], which utilises the concrete and reinforcement material properties of EC2. The output will be the hysteretic hinge model properties or the spring properties based on the findings of Haselton *et al.* [2016], depending on the choice of the hinge model types. Hinge

properties are then fed into the module, which, using OpenSees [McKenna *et al.* 2010], creates a 3D numerical model of the building and runs a modal analysis to compute the modal properties of the building. Rayleigh damping was used with 5% of critical damping assigned to the principal modes associated with the directions of the building, although other damping models may be used [Hall 2018] but the impact of this choice was not pursued further. Then, SPO analysis is carried out to calculate the backbone curve in both directions. Based on the findings, a new estimate of the backbone curve shape, as well as secant-to-yield periods, are used to calibrate the input arguments for the SPO2IDA toolbox. These iterations are automated and are repeated until convergence of assumptions is achieved and the final solution is derived. It is again important to note that, due to the modularity of the software, different building code recommendations, as well as different procedures for the detailing of structural elements, may be adapted.

6.3 CASE STUDY APPLICATION

6.3.1 Definition of case study buildings and numerical modelling

Several case study buildings were defined and the IPBSD framework was applied. Similarly, EC8 provisions were applied to design buildings of similar configurations. With the solutions identified, non-linear numerical models were produced, and IDA was performed, followed by loss assessment to assess the validity of different design methods and compare them with the loss-driven risk-targeting framework outlined earlier. Twelve case study buildings consisting of RC MRFs in a *spare* configuration were examined and are described in Table 6.1.

Table 6.1. Case study building configurations.

Case	Seismicity	Configuration			$\lambda_{c,target}$	$\lambda_{y,limit} (\%)$
		N_{st}	N_x	N_y		
1-IPBSD	High	2			2.0×10^{-4}	0.60
2-IPBSD						0.80
3-IPBSD					1.0×10^{-4}	0.60
4-IPBSD					2.0×10^{-4}	0.60
5-IPBSD		4		3	2.0×10^{-4}	0.80
6-IPBSD					1.0×10^{-4}	0.60
7-IPBSD					2.0×10^{-4}	0.60
8-IPBSD		6			2.0×10^{-4}	0.80
9-IPBSD					1.0×10^{-4}	0.60
10-IPBSD					2.0×10^{-4}	0.60
11-IPBSD	Medium	2			2.0×10^{-4}	0.60
12-IPBSD						0.60

The designs vary in terms of the number of storeys, design targets in terms of MAFC and EAL, as well as seismicity region. Two seismic locations in Italy were selected corresponding to soil type C, as defined by EC8, with L'Aquila representing high seismicity and Ancona representing medium seismicity. In Table 6.1, the case number reflects the unique identifier for each case study building, N_{st} is the number of storeys, N_x and N_y are the number of bays in X (first principal direction) and Y (second principal direction). Ground and typical storey heights are 3.5 and 3.0 m, respectively, while the bay widths in both directions are 4.5 m.

The value of $\lambda_{y,\text{limit}}$ was indicatively selected considering designs code-compliant with a rating of "A" or higher, according to the classification proposed by Cosenza *et al.* [2018] thus with values lower than 1%. In addition, Ramirez *et al.* [2012] and Goulet *et al.* [2007] have found values from 0.6% to 1.1% for RC MRF spatial buildings designed according to the design and seismic provisions in force at the time in the US. Keeping this in mind, two different limits of 0.6% and 0.8% were selected to explore the variation of design solutions. Regarding $\lambda_{c,\text{target}}$, various values are reported in the literature and discussed in Shahnazaryan and O'Reilly [2021]. For example, ASCE 7-16 [2016] recommends an acceptable national risk of 1% in 50 years (2.0×10^{-4}), while other studies from the literature suggest values of around 1.0×10^{-5} . Additionally, Dolšek *et al.* [2017] noted typical limits between 10^{-4} and 10^{-5} , while Silva *et al.* [2016] used 5.0×10^{-5} while discussing the development of risk-targeted hazard maps for Europe. Accordingly, a decision was made to select two different values of 2.0×10^{-4} and 1.0×10^{-4} for $\lambda_{c,\text{target}}$, also highlighting the capability of easily tailoring the design performance objectives within the IPBSD framework.

Typical plan and elevation layouts are shown in Figure 6.6. The gravity loads, including imposed and dead loads, were assumed as 8.06 kN/m^2 and 6.56 kN/m^2 at the typical floor and roof level, respectively. Dead loads included an assumption of a RC slab of 150 mm thickness and a factor of 1.35, while imposed loads assumed a Category A for residential buildings with a load of 2 kN/m^2 and a roof load of 1 kN/m^2 with a factor of 1.5 in line with EC2 [CEN 2004b]. The specific weight of the concrete was taken as 25 kN/m^3 . The material properties used in the design and detailing were 25 MPa for the concrete compressive strength and 415 MPa for the steel yield strength. No plan or elevation irregularities were considered.

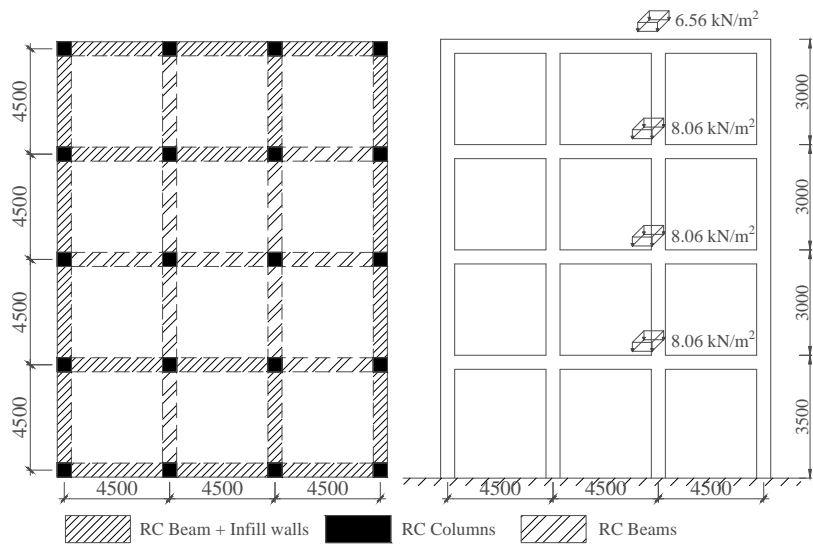


Figure 6.6. Illustration of plan layout and elevation of the case study buildings.

The case study buildings outlined were designed and examined following different methodologies. The IPBSD framework and the EC8's ELF approach was implemented. The goal was to demonstrate the capability of having loss-driven risk-consistent designs following the IPBSD framework when compared to a code-based design formulation. The case study buildings were detailed and sized following the EC8 and EC2 member detailing requirements.

For all case study buildings, 3D numerical models were generated using OpenSees [McKenna *et al.* 2010] to perform SPO and NLRHA. The masses were lumped at each floor and the nodes were constrained in the horizontal direction to mimic a rigid diaphragm behaviour. A concentrated plasticity approach developed by Ibarra *et al.* [2005] was used to consider non-linear behaviour in beams and columns. The plastic hinges at both ends of beams and columns were modelled using a lumped plasticity model with bilinear hysteretic properties available in OpenSees, while the elastic sections of the elements were modelled using an elastic cracked section stiffness object. Concrete compressive strength was assumed 25 MPa while the yield strength of reinforcement was taken as 415 MPa. All columns were fixed at the base. Rayleigh damping was implemented with 5% of critical damping assigned to principal modes associated with each direction of the building. To obtain the hysteretic models, the backbone curve associated with each structural element was fit to the moment-curvature relationship of the element obtained using Response-2000. Additionally, the plastic hinge length required for the hysteretic model was computed following Priestley *et al.* [2007]. P-Delta effects were considered through application of

vertical gravity loads during nonlinear analysis and consideration of the PDelta transformation method available in OpenSees. Beam-column joints were assumed to be rigid, and no shear mechanisms were modelled since the design of the structure followed capacity design criteria hence no shear failures are expected. It is important to note that torsional response of the building was not explored given the main scope of this study. Additionally, attempting to address situations where torsional response is pertinent may not be appropriate. In such cases, the IPBSD may be considered as a method useful for providing a more optimal initial design satisfying more advanced performance goals, but these design solutions would necessitate detailed analysis for their verification.

6.3.2 Site hazard and ground motions

PSHA was performed using OpenQuake [Pagani *et al.* 2014] for the two site locations with the SHARE hazard model [Woessner and Wiemer 2005]. A set of 30 ground motion records (consisting of two horizontal components) were selected from the NGA West-2 database [Ancheta *et al.* 2014] with each record's soil type being consistent with that of the site. The ground motions were selected to be representative of the site without any specific selecting and scaling approach in mind. The magnitude and distance ranges of the chosen records were defined to be in line with the hazard disaggregation of period ranges utilized for the case study buildings. During the analysis, the two components of the ground motion were applied to the building and the geometric mean of principal periods, T^* , was used to identify the IM, $Sa(T^*)$. The hazard curves obtained via PSHA were used within the IPBSD framework and, once the acceptable period range was obtained, $\lambda_{c,target}$ was verified by integrating the collapse fragility with the seismic hazard based on an IM of $Sa(T_1)$ for a range of T_1 values, as per Equation 6.1. The seismic hazard curve corresponding to both sites and a period of $T_1=1.0\text{s}$ is displayed in Figure 6.7.

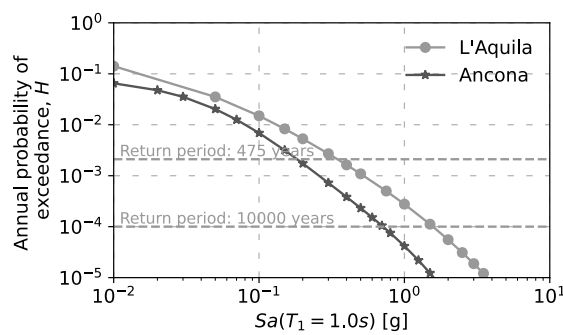


Figure 6.7. Seismic hazard for medium and high seismicity corresponding to a spectral acceleration at a period of $T_1=1.0\text{s}$.

6.3.3 Eurocode 8

The buildings were designed following the EC8 provisions. For consistency, $Sa(T_1)$ of the elastic design spectrum of EC8 was scaled to match the one obtained from PSHA at the no-collapse return period of 475 years. EC8 does not directly consider performance metrics, such as MAFC and EAL, therefore the values provided in Table 5.1 were not considered for the case study applications. As such, only the cases varying in number of storeys and hazard were considered. The ELF method along with gravity loads was used to estimate the demands on structural elements. Structural element dimensions and reinforcement content was selected to satisfy lateral drift limitation and P-Delta effects. Local ductility limits imposed by EC8 for DCM elements were considered. For most elements, minimum local ductility requirements were governing. Cracked cross-section properties (*i.e.*, 50% of gross) were utilised to estimate the demands via the elastic numerical model and design the structural elements. The final design values are listed in Table 6.2. Additionally, buildings were designed as corresponding to importance classes II and III (*i.e.*, scaling of design spectrum by 1.0 and 1.2, respectively) to distinguish between different levels of safety that are anticipated in the IPBSD designs via the MAFC. Independent of the importance class, the periods associated with both directions are the same, which is due to the same cross-section dimensions. The design code does not directly enforce modification of cross-section dimensions to avoid having the minimum local ductility conditions govern the detailing, therefore a decision was made not to modify the designs.

Table 6.2. Summary of design solutions obtained using EC8.

EC8 Case	IPBSD correspondence	Importance class	N_{st}	Seismicity	T_x (s)	T_y (s)	Sa_d (g)
1-EC8	1-IPBSD	II	2	High	0.35	0.35	0.31
2-EC8	4-IPBSD		4		0.69	0.68	0.13
3-EC8	7-IPBSD		6		1.11	1.09	0.07
4-EC8	10-IPBSD		2	Medium	0.44	0.44	0.11
5-EC8	11-IPBSD		4		0.89	0.88	0.05
6-EC8	12-IPBSD		6		1.42	1.39	0.03
7-EC8	1-IPBSD	III	2	High	0.35	0.35	0.28
8-EC8	4-IPBSD		4		0.69	0.68	0.15
9-EC8	7-IPBSD		6		1.11	1.09	0.10
10-EC8	10-IPBSD		2	Medium	0.44	0.44	0.13
11-EC8	11-IPBSD		4		0.89	0.88	0.06
12-EC8	12-IPBSD		6		1.42	1.39	0.04

6.3.4 IPBSD formulation

Similar to the case of the EC8 designs, each case study was also designed following the IPBSD framework to meet the stated performance objectives in terms of target MAFC and EAL limit. To better visualize the framework, a single case study application (Case 1-IPBSD) is followed step-by-step herein. It is recalled that $\lambda_{c,target}$ and $\lambda_{y,limit}$ are 2×10^{-4} and 0.60%, respectively, and the location is of high seismicity (L'Aquila).

Initially, performance objectives were defined; the y values of OLS and CLS were fixed to 1% and 100%, respectively, and λ_{OLS} was set to correspond to a limit state return period of 10 years and $\lambda_{CLS} = \lambda_{c,target}$, as illustrated in Figure 6.2, meaning that only the SLS parameters needed to be defined to respect the limiting EAL, meaning that only the SLS parameters needed to be defined to respect the limiting EAL. The choice of SLS parameters was analyzed through sensitivity studies in Shahnazaryan *et al.* [2019] and was defined initially as $y_{SLS}=14\%$ and $\lambda_{SLS}=1.67 \times 10^{-2}$, which correspond to a loss curve leading to an EAL meeting the EAL limit (*i.e.*, the y_{SLS} was fixed as 14% and λ_{SLS} was iterated until the $\lambda_{y,limit}$ was met). Given these values, the resulting loss curve was identified and λ_y was calculated as the area under the design loss curve as 0.96%, which is exceeding the desired $\lambda_{y,limit}$. However, this slight overestimation was not deemed to be an issue since, as discussed in Section 6.2.2, a single-step correction should be made with regard to the actual contributions of different performance groups to y_{SLS} . Note that the SLFs were normalised using a replacement cost of €589,712.40 corresponding to a 2-storey building and the relative contributions of different performance groups are given in Table 6.3, which, when summed, give $y_{SLS}=14\%$. Costs were computed based on the SLFs corresponding to the critical (lowest) EDP. Subsequent design limits for X and Y directions were obtained as: $\theta_{max,S}$ of 1.54% and 1.56%; $\theta_{max,NS}$ of 0.23% and 0.20% and $a_{max,NS}$ of 0.44g and 0.51g, respectively.

Table 6.3. Performance group contributions to y_{SLS} in % and associated EDPs.

Direction	Storey level	θ_S , (%)	θ_{NS} , (%)	a_{NS} , (g)	$y_{S,PSD}$, (%)	$y_{NS,PSD}$, (%)	$y_{NS,PFA}$, (%)
		Before the corrections					
	Ground floor	-	-	0.44	-	-	0.98
Dir X	1 st storey	1.54	0.23	0.51	0.83	1.57	1.32
	2 nd storey	1.54	0.25	0.51	0.82	1.45	0.99
Dir Y	1 st storey	1.56	0.20	-	1.44	1.65	-
	2 nd storey	1.58	0.22	-	1.45	1.51	-
		After the corrections					
	Ground floor	-	-	0.44	-	-	1.00
Dir X	1 st storey	0.23	0.23	0.51	0.00	1.63	0.82
	2 nd storey	0.25	0.25	0.51	0.00	1.38	0.68
Dir Y	1 st storey	0.20	0.20	-	0.00	1.72	-
	2 nd storey	0.22	0.22	-	0.00	1.43	-

However, since the design will be based on 0.23% and 0.20% in each direction, as it is the critical PSD value between structural and non-structural groups, the values of 1.54% and 1.56% PSD for structural components will not be exceeded at SLS. Similarly, the design for PFA-sensitive components will be based on 0.44g in direction X and 0.51g in direction Y. Therefore, the single-step correction discussed in Section 6.2.2 was made by using 0.23% as the critical PSD for structural component groups as well. To do so, the contributions to costs were recalculated after the corrections based on the EDP value of each level (Table 6.3), which then summed up to $y_{SLS} = 8.66\%$. This value was used as the new y_{SLS} , and the loss curve was updated effectively resulting in an EAL of 0.60%, thus equal to $\lambda_{y,\text{limit}}$. It is interesting to note that the contribution coming from structural components at SLS was effectively zero, which was largely due to the structural members being well-designed and detailed and the SLS loss stemming almost entirely from the non-structural elements.

The feasible period range was identified as between 0.20s and 0.42s for the X direction, and 0.20s and 0.37s for the Y direction. Following the procedure outlined in Section 6.2.2, a final design solution with secant to yield periods of 0.38s in both directions was identified, which is slightly over but within a tolerable difference compared to the upper period limit of 0.37s for the Y direction. By ensuring the structure has an initial period within a tolerable range with respect to the period range identified, the EAL is expected to be lower than the predefined EAL limit, as it does not reach the period limits, at which excessive losses of drift- or acceleration-sensitive non-structural elements would start to become problematic to the performance objectives (Figure 6.4(c)). Next, collapse safety was controlled via a targeted MAFC. Several assumptions were needed before using the SPO2IDA tool [Vamvatsikos and Cornell 2005] regarding the structural system's expected SPO behaviour as illustrated in Figure 6.5(left). However, given the iterative process, all assumptions regarding its shape and secant-to-yield period were established, and the resulting output of SPO2IDA is given in Figure 6.8, where on the vertical axis q_u represents the normalization of spectral acceleration, Sa , concerning Sa_y . Only β_{RTR} was considered for what concerns uncertainty. The collapse fragility was calculated based on the 50th percentile as the median and the β_{RTR} based on the percentile values shown. The Sa_y was optimised to 0.44g for both X and Y directions, respectively, meaning that λ_c equated $\lambda_{c,\text{target}}$.

With the identified Sa_y , assuming an initial q_s of 1.0, the design base shear was calculated. In each direction separately, design lateral forces were obtained using the ELF method together with gravity loads to perform static analysis and compute element design forces. Strength hierarchy, local ductility requirements and P-Delta effects were all accounted for following the EC8 [CEN 2004a] recommendations and structural elements were verified via their moment-curvature relationships using Response-2000 [Bentz 2015] and EC2 [CEN 2004b] material properties.

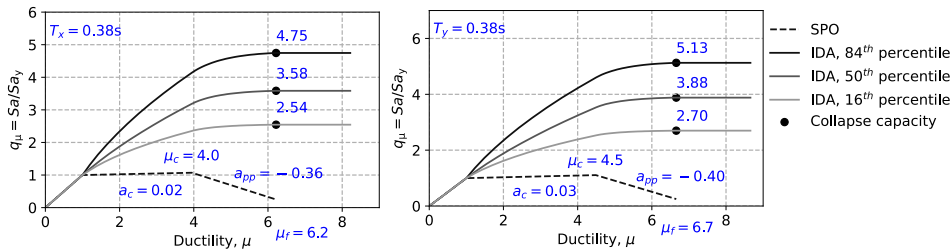


Figure 6.8. SPO and IDA curves obtained via the SPO2IDA tool.

If any of the sections required cross-section dimension modifications, or the secant-to-yield periods were not within the identified period ranges, or the actual SPO shape varied from the assumed shape initially, the process was repeated. In general, it took from two to five iterations to complete one design. To aid the designer with the workload required for iterations, object-oriented Python-based software [Shahnazaryan *et al.* 2021b] has been created, as mentioned in Section 6.2.3. The final design solutions in terms of the T_x , T_y , q_{sx} , q_{sy} , and Sa_d for all case study buildings considered are shown in Table 6.4.

Table 6.4. Summary of design solutions from the IPBSD.

Case	$\lambda_{c,target}$	$\lambda_{y,limit} (\%)$	Seismicity	T_x (s)	T_y (s)	q_{sx}	q_{sy}	Sa_d (g)
1-IPBSD	2.0×10^{-4}	0.60	High	0.38	0.38	1.22	1.17	0.54
2-IPBSD	2.0×10^{-4}	0.80		0.52	0.49	5.25	5.64	0.12
3-IPBSD	1.0×10^{-4}	0.60		0.37	0.36	7.96	8.22	0.13
4-IPBSD	2.0×10^{-4}	0.60		0.66	0.61	1.00	1.00	0.38
5-IPBSD	2.0×10^{-4}	0.80		0.95	0.92	1.55	2.16	0.14
6-IPBSD	1.0×10^{-4}	0.60		0.71	0.64	1.30	1.70	0.32
7-IPBSD	2.0×10^{-4}	0.60		1.25	1.06	2.86	3.80	0.08
8-IPBSD	2.0×10^{-4}	0.80		1.36	1.35	1.00	1.00	0.23
9-IPBSD	1.0×10^{-4}	0.60		1.20	1.15	1.00	1.00	0.39
10-IPBSD	2.0×10^{-4}	0.60	Medium	0.56	0.60	1.00	1.00	0.22
11-IPBSD	2.0×10^{-4}	0.60		1.16	1.20	1.00	1.00	0.10
12-IPBSD	2.0×10^{-4}	0.60		1.41	1.38	1.00	1.00	0.10

For some of the case study buildings, high values of q_s were observed in both directions. This is predominant for the medium seismicity region, as well as for the cases where local ductility requirements of EC8 governed in terms of minimum reinforcement amount. Thus, independent of Sa_d , the elements had the same moment capacity. In other words, if Sa_d reduced, the q_s subsequently increased. This in turn is a result of having very stiff sections, which could be governed by the period range condition of IPBSD. However, in cases where the period range condition was not too strict, one possible way of avoiding the

issue is by decreasing the cross-section dimensions. It is noted that for solutions with high stiffness, masonry infill or RC wall systems it could be more optimal to act against seismic loads, the absence of which for RC MRFs required larger cross-sections for columns and beams, therefore triggering the local ductility and minimum reinforcement requirements of EC8 because of relatively low demands. Ideally, the framework allows practitioners to have solutions of different variations and configurations, thus it is not limited to a unique solution or structural typology. Consideration of other structural typologies is not within the scope of this chapter and will require further research and application.

More conclusions may be drawn from the results displayed in Table 6.4. Looking at a lower value $\lambda_{c,target}$ of Case 3-IPBSD compared to Case 1-IPBSD, S_{ad} is expected to be lower for the latter case but is seen to be notably higher. This could be attributed to the variation of ductilities as well as q_s . In other words, ductilities and q_s in both directions are higher for Case 3-IPBSD, thus the target MAFC may be met with lower S_{ad} . So, while the two performance objectives are verified within two parts of the IPBSD framework, there is still an indirect relationship between the two. This relationship is more apparent when the period range is more stringent. It is a combination of $\lambda_{c,target}$, $\lambda_{y,limit}$, seismic hazard as well as initial secant-to-yield period (controlled by the stiffness of the structure), and the backbone shape that results in an efficient loss-driven risk-targeted design. To test this statement, Case 3-IPBSD was forced to have structural systems in each direction with a T_x and T_y of 0.65s and 0.61s, respectively. As a result, the new S_{ad} was identified as 0.33g as a direct impact of seismic hazard and period. While this is only slightly higher than S_{ad} of Case 1-IPBSD, one should not forget about the SPO shape, which is characterised by a certain ductility value as well. Essentially, choices before and during the IPBSD framework will dictate how the building design solution will shape up, simultaneously without hindering the ability of the IPBSD framework to provide solutions meeting the desired performance objectives.

6.4 STOREY LOSS FUNCTIONS

As mentioned previously, in order to implement the IPBSD framework, SLFs need to be provided. The SLF toolbox proposed in Chapter 4 (Shahnazaryan *et al.* [2021c]) was utilised to generate SLFs for residential occupancy for the entire building. To estimate the replacement cost of the case study buildings, a mean unit cost of €1,213.40 related to RC buildings in L'Aquila was adopted from Di Ludovico *et al.* [2017]. This cost includes the charges related to the design and technical assistance of practitioners but not the VAT (value added tax). Components sensitive to only two EDPs, PSD and PFA, were considered within the component inventory of the case study buildings. Components of the same sensitivity towards one direction of seismic action, same EDP sensitivity and located within the same storey level were grouped into the same performance group, while

non-directional components were grouped into a different performance group following the same reasoning. Cost distributions for the structural and non-structural components, quantities as well as fragility function sources are summarised in Table 6.5 to

Table 6.7. The component inventory was built based on design drawings following an idealized building layout (Figure 6.6) that was adopted as case-study for the purposes of implementation and validation of the IPBSD framework. The tables provide information on the type of component, the demand parameter to which they are sensitive, the units and quantities for each type of component. Components for which a second number between parenthesis is missing are sensitive to the seismic action of both directions. For a detailed component inventory, readers are referred to the additional sample files available on [Shahnazaryan *et al.* 2021b].

Table 6.5. Mean quantities for the damageable PSD-sensitive structural components in the X(Y) direction.

Component	Fragility function source	Consequence function source	Unit	Quantities per storey	
				Ground	Typical
External columns	FEMA P58-3 [2012b]	Cardone [2016]	each	4	4
Internal columns				4(10)	4(10)
Central columns				10	10

Table 6.6. Mean quantities for the damageable PSD-sensitive non-structural components in the X(Y) direction.

Component	Fragility function source	Consequence function source	Unit	Quantities per storey	
				Ground	Typical
Exterior masonry infill				84(168)	72(144)
Internal masonry partitions	Cardone & Perrone [2015]			67.8(59.8)	32.3(24.2)
Internal masonry infill partitions	Sassun <i>et al.</i> [2016]			138.5(80.4)	118.7(68.9)
Non-monolithic precast concrete stair assembly	FEMA P58-3 [2012b]			1	1
Doors	Correlated to collapse of internal masonry partitions	Market research	each	6(6)	6(6)
Windows				2(13)	2(13)
Chairs				18	18
Oven with cooker				2	2
Fridge				2	2
Washing machine				2	2

Table 6.7. Mean quantities for the damageable PFA-sensitive non-structural components.

Component	Fragility function source	Consequence function source	Unit	Quantities per floor		
				Ground	Typical	Roof
Fancoil	FEMA P58-3 [2012b]		each	0	8	8
Ceiling system			m ²	0	274.5	288.0
Lighting			each	0	19	19
Piping – water distribution			250m	0	0.605	0.605
Piping – heating distribution			250m	0	0.638	0.638
Sanitary waste piping			250m	0	0.605	0.605
Bookshelves	Correlated to collapse of piping distribution systems	Market research	each	0	6	6
Wardrobes				0	8	8
Sofas				0	4	4
Tables				0	8	8
Shelves				0	11	11
Beds				0	6	6
Kitchen equipment				0	2	2
Computers				8	8	0
TV				4	4	0
Fire sprinkler water piping	FEMA P58-3 [2012b]		250m	0	0.5184	0.5184
Fire sprinkler drop			each	0	12	12
Distribution panel				1	1	0
Hydraulic elevator				1	0	0
Battery rack				1	0	0
Battery charger				1	0	0
Distribution panel for the elevator				1	0	0

The selection of representative fragility and consequence functions is a complex issue and could be a cause of inaccuracy when conducting loss assessment. However, it is not within the scope of this study to provide reference component inventory and loss assessment results, but rather demonstrate the capabilities of the IPBSD framework given the input arguments in terms of SLFs. Existing fragility and consequence functions [Cardone 2016; Cardone and Perrone 2015; Sassun *et al.* 2016] were adopted for structural and non-structural components in RC structures. The costs associated with structural components are associated with existing structures, whereas the repair actions are assumed to be the

same for newly designed structures and the fragility functions must accommodate for ductile beam-column subassemblies. Fragility and consequence functions of PFA-sensitive components, as well as for stairs, were adopted from FEMA P58 [2012b]. In addition, consequence functions of components from FEMA P58 use a conversion of 0.79 based on the work by Silva *et al.* [2020], which are further multiplied by 0.83 to reflect the conversion of USD to Euro as of January 2021.

For some non-structural components, specific fragility and consequence functions were not available thus some assumptions were made using engineering judgement. For example, PSD-sensitive components with missing fragility information were correlated to the fragility functions assumed for partition walls. Similarly, PFA-sensitive components with missing fragility information were correlated to the fragility functions of piping systems. The logic behind the correlations lies within the assumption that damaged or collapsed partition walls will inadvertently damage the windows or doors located within the walls, while the leakage of piping systems would result in damage to electronics or furniture, as discussed in De Risi *et al.* [2020] for example. The costs associated with those components were adapted from typical values of available market prices in Italy.

Figure 6.9 illustrates sample SLFs for the 2nd level of the case study building's plan layout. Losses of NS components start rising at low values of PSD, which may be attributed to the low capacities of interior and exterior infills. In contrast, structural components' costs start accumulating once a certain threshold of PSD is reached, which is a direct result of the high capacities of well-designed ductile beam-column sub-assemblies. For what concerns the Y of different performance groups utilized in Equation 6.4, as an example, the Y values for a two-storey building were: 12% and 21% for PSD-sensitive structural components in directions 1 and 2, respectively, 22% for PSD-sensitive non-structural components in both directions, and 23% for PFA-sensitive non-structural components.

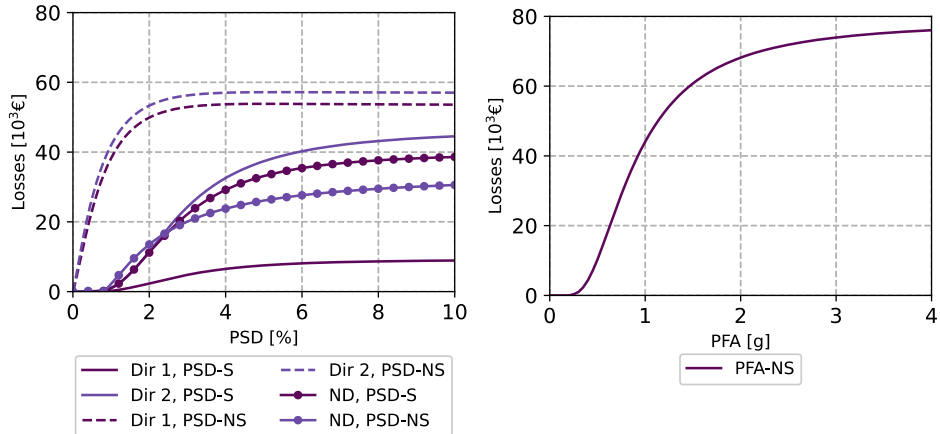


Figure 6.9. SLFs for the case study building's (left) 2nd storey level for PSD-sensitive elements and (right) 2nd floor for the PFA-sensitive elements.

6.5 STRUCTURAL PERFORMANCE AND LOSS ASSESSMENT RESULTS

In order to thoroughly investigate and validate the designs described previously, each case study building was modelled as described in Section 6.3.1 and IDA was performed to characterise the structural behaviour up to lateral collapse using the ground motions described in Section 6.3.2. Based on the IDA outputs, the SLF-based loss assessment was carried out, using the approach proposed by Ramirez and Miranda [2012]. The economic loss conditioned on the ground motion intensity was computed as the summation of the following losses: building collapse; repair costs associated with damageable components of the building; and losses because of demolition of the building due to excessive residual drifts. For the case study applications, the probability of demolition of a building as a function of RPSD was assumed to be lognormally distributed with a median of 0.015 and a logarithmic standard deviation of 0.3 [Ramirez and Miranda 2012]. Even though low residual drifts are expected, in line with common practice, these were included in the assessment, confirming the expected low contribution of demolition to direct losses in newly designed buildings, following the IPBSD framework. The λ_y was computed by integrating the vulnerability curve, expressed in terms of expected direct economic loss as a function of $Sa(T^*)$, with the site hazard curve at a corresponding geometric mean of principal periods, T^* (Equation 6.2). Using these extensive analysis outputs, the actual λ_c and λ_y values were compared to $\lambda_{c,target}$ and $\lambda_{y,limit}$, respectively, to assess each method in delivering sufficiently safe and uniform risk design solutions. The λ_c and λ_y values were computed using the hazard described in Section 6.3.2 and are presented in Table 6.8 and illustrated in Figure 6.10. It could be argued from Figure 6.10 that, in terms of MAFC, the EC8-designed buildings demonstrate good results when compared to the IPBSD cases.

While true, this stems from the fact that most of the EC8 cases, independent of importance class, have been overdesigned due to governing local ductility requirements regarding minimum required reinforcement. Consequently, a similar backbone behaviour has been observed for most of the EC8-designed cases. Additionally, the EC8-designed cases were anticipated to have MAFC and EAL not far off the target and limit values set for the IPBSD cases, since these were set based on the actual attained values from the literature, as described in Section 6.3.1.

Table 6.8. Summary of actual λ_c and λ_y for each case study building and design approach considered.

IPBSD Cases	λ_c	λ_y (%)	EC8 cases	λ_c	λ_y (%)
1-IPBSD	1.1×10^{-4}	0.56	1-EC8	1.5×10^{-4}	1.14
2-IPBSD	1.8×10^{-4}	0.69	2-EC8	2.3×10^{-4}	0.88
3-IPBSD	1.0×10^{-4}	0.66	3-EC8	2.8×10^{-4}	1.01
4-IPBSD	0.6×10^{-4}	0.50	4-EC8	0.5×10^{-4}	0.58
5-IPBSD	2.2×10^{-4}	0.72	5-EC8	0.5×10^{-4}	0.49
6-IPBSD	0.6×10^{-4}	0.51	6-EC8	0.4×10^{-4}	0.44
7-IPBSD	1.4×10^{-4}	0.52	7-EC8	1.4×10^{-4}	0.96
8-IPBSD	1.3×10^{-4}	0.58	8-EC8	2.3×10^{-4}	0.87
9-IPBSD	0.9×10^{-4}	0.58	9-EC8	2.9×10^{-4}	1.02
10-IPBSD	0.4×10^{-4}	0.31	10-EC8	0.5×10^{-4}	0.58
11-IPBSD	0.3×10^{-4}	0.32	11-EC8	0.7×10^{-4}	0.49
12-IPBSD	0.2×10^{-4}	0.27	12-EC8	0.4×10^{-4}	0.44

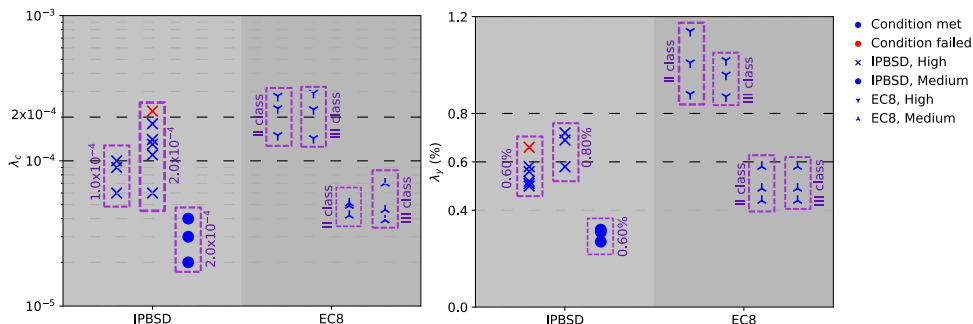


Figure 6.10. Illustration of λ_c and λ_y values for each case study building and design approach considered.

6.5.1 Buildings designed according to EC8

Performance metrics obtained for the case study buildings designed following EC8 recommendations were at a similar level. MAFC values ranged from 1.5×10^{-4} to 3.0×10^{-4} and 0.4 to 0.7×10^{-4} for cases located in high and medium seismicity regions, respectively. Similarly, values of EAL ranged from 0.88 to 1.15% and 0.44 to 0.58% for high and medium

seismicity regions, respectively. Very minor variations were observed in terms of the selected importance class. Hence, there is no indication of improved performance with increased importance class as per EC8. This could be attributed to buildings of the same configurations sharing the same periods as well as having minimum local ductility requirements governing the design. In other words, for the medium seismicity region, the buildings had lower overstrength compared to the high seismicity region, while the dimensions and reinforcement content of sections remained intact. Similarly, no significant variation of EAL values was observed for the buildings located in the medium seismicity region as the variations of S_{ad} given in Table 6.2 were not significant enough. While it is possible to achieve variations of design within the limits allowed by EC8 through the modification of reinforcement content and cross-section dimensions, it is important to note that, due to the absence of direct consideration of MAFC and EAL objectives during design, a practitioner is not forced to modify the design solution. Therefore, the solutions obtained here are some of the possible outcomes following the EC8 recommendations, which highlights the need for the development of risk-targeted procedures.

6.5.2 Buildings designed using IPBSD

6.5.2.1 *Collapse safety assessment*

Regarding the IPBSD framework, consistent results were obtained in terms of satisfying both performance objectives (*i.e.*, EAL limit and MAFC target) for each case study building as shown in Figure 6.10, whereby both primary performance objectives were met. However, it is important to note that performance objectives were not always close to those identified before the design. While demonstrating the efficiency of the IPBSD framework, minor adjustments could be made to narrow the gap between the actual and target or limit values of performance objectives. One of the possible reasons for the variation could be attributed to the use of SPO2IDA, which was not developed accounting for bidirectional effects, but rather a one-dimensional response. The values of λ_c were computed using the seismic hazard at the geometric mean of the periods from two principal modes (X and Y directions) of the building. Figure 6.11 provides the medians, η , and β_{RTR} of the collapse capacities of the design cases. A high variation of β_{RTR} is observed, while the values of η were within tolerable proximity of each other. It is interesting to note that even for the cases where η was lower than the assumption, due to the corresponding value of β_{RTR} being lower, the MAFC condition was still met.

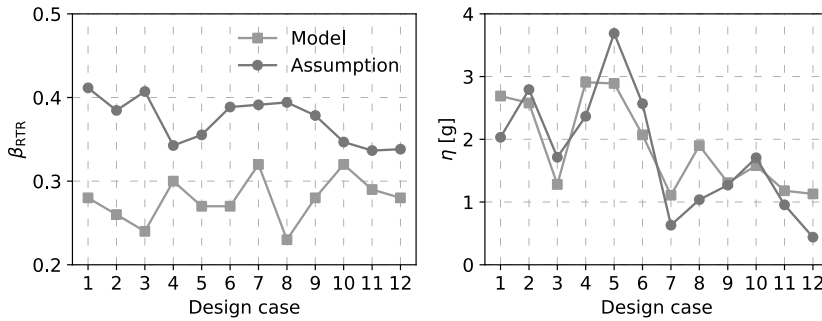


Figure 6.11. Comparison of computed and assumed values of (left) β_{RTR} and (right) η at CLS.

Similarly, Figure 6.12 demonstrates the values of q_s (for both directions, q_{sx} and q_{sy}) during design and the actual values obtained from the non-linear model. Several of the cases where actual q_s was higher than 1, while the assumption was equal to 1. Essentially, minimum local ductility requirements were governing, meaning that the sections were larger than necessary, and the demands were subsequently low. However, there is a necessity to keep those cross-sections to satisfy the period condition. In that case, if the assumed overstrength is increased the yield strength will reduce, meaning that in the next iteration, q_s will be even larger, since the minimum ductility condition will be even more relevant with newly reduced demands. Accordingly, this is a cycle, where no convergence could be achieved therefore it was forced to have $q_s=1$, which is why for many of those cases the MAFC condition is met with a larger than the anticipated gap. In addition, larger variations of λ_c compared to $\lambda_{c,target}$ was observed due to the building failing in either of the directions depending on the ground motion record pair.

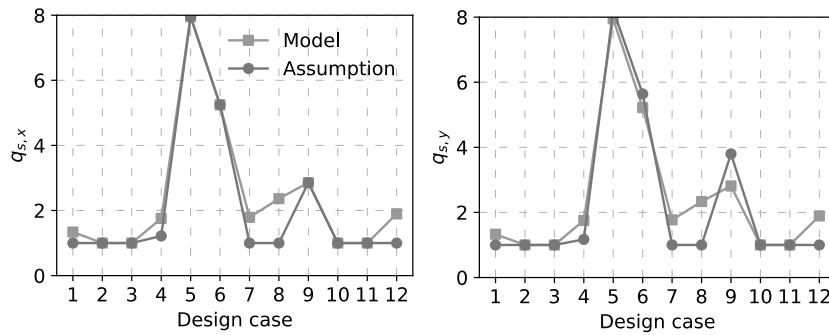


Figure 6.12. Comparison of computed and design values of q_s .

6.5.2.2 Loss assessment

For most of the cases, λ_y were below $\lambda_{y,limit}$ and only for a single case the limit was exceeded and the performance objective was not met. Furthermore, case study buildings of a medium

seismicity region demonstrated consistently very low values of λ_y regardless of the $\lambda_{y,\text{limit}}$. This is primarily due to the lower hazard, which is not likely to cause high losses despite the well-designed and risk-targeted design solutions. At the same time, this is an indication of possible directions to optimise the designs, if a λ_y closer to the limit is desired. For example, the medium seismicity buildings may be revised to have stiffer structural systems or different structural typologies may be sought (*e.g.*, with masonry infills or RC walls as the main lateral load resisting system). To test such a hypothesis, the cases associated with medium seismicity were redesigned and reassessed with stricter performance objectives, *i.e.*, 0.5×10^{-4} and 0.40% for target MAFC and EAL limits, respectively. The results for these new case study buildings are given in Table 6.9, where it can be seen how the computed λ_y and λ_c are closer to the new performance objectives. As mentioned, this was a direct impact of lower seismic hazard and modern design code provisions, as higher values of performance objectives were not likely to be attained with the current structural typology in hand. However, it is important to note that IPBSD was able to ensure that the performance objectives set by the practitioner were met for both scenarios. As expected, stricter performance objectives resulted in higher requirements in terms of collapse capacity. However, the period limits and therefore periods associated with both directions, T_x and T_y , were largely unaffected, which is again attributed to lower seismic hazard, for which the periods are still within the limits. Further restriction of $\lambda_{y,\text{limit}}$ to lower values will likely result in a direct impact for significant variations in periods.

Table 6.9. Summary of case study buildings located in medium seismicity region.

Case	T_x (s)	T_y (s)	q_{sx}	q_{sy}	S_{ad} (g)	η (g)	β_{RTR}	λ_c	λ_y (%)
10-IPBSD-R	0.42	0.43	1.14	1.00	0.51	2.44	0.25	0.2×10^{-4}	0.30
11-IPBSD-R	0.77	0.72	1.00	1.00	0.35	1.96	0.32	0.2×10^{-4}	0.31
12-IPBSD-R	1.31	1.20	1.00	1.00	0.18	1.31	0.29	0.2×10^{-4}	0.27

Figure 6.13(left) demonstrates the variations of period limits in X direction for case 10-IPBSD, and through the subsequent modification of $\lambda_{y,\text{limit}}$ for case 10-IPBSD-R. While T_{lower} was unaffected due to no further constraint towards acceleration sensitive components, T_{upper} has decreased from 0.73s to 0.50s, meaning that a target period of 0.56s is no longer satisfactory. The new building has a period of 0.42s in X direction, as listed in Table 6.9. To further visualise the impact of stricter performance objectives, Figure 6.13(right) plots the change in λ_y , S_{ad} and the geometric mean of principal periods, T^* , for the paired cases. As expected, S_{ad} is larger for cases with stricter performance objectives, while, for the contrary conditions, T^* is reducing. However, while true for cases 10-IPBSD

and 11-IPBSD, λ_y did not decrease for 10-IPBSD-R. The slight reduction of λ_y for two of the cases indicate the improvement of building performance through stricter performance objectives, however, as discussed earlier, the goal was not to improve performance but rather have λ_y closer to $\lambda_{y,\text{limit}}$ for the medium seismicity region.

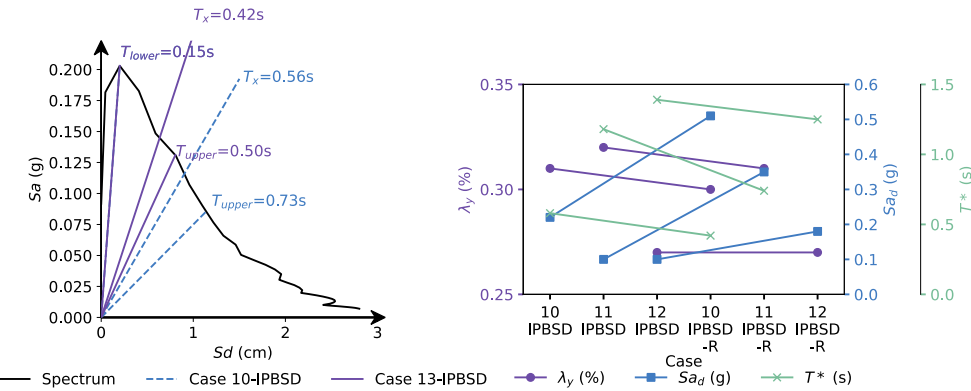


Figure 6.13. (left) Period limits in X direction and (right) Variation of design solutions through the modification of performance objectives, where three distinct lines corresponding to three separate axes are superposed for graphical correspondence.

Table 6.10. Summary of IPBSD results for a single seismic frame.

Solution ID	T_1 (s)	$S_{\Delta SLS}$ (g)	λ_y (%)
1-IPBSD-2D	0.74	0.143	0.79
2-IPBSD-2D	0.69	0.143	0.68
3-IPBSD-2D	0.64	0.169	0.68
4-IPBSD-2D	0.60	0.169	0.60
5-IPBSD-2D	0.54	0.207	0.65
6-IPBSD-2D	0.52	0.207	0.62
7-IPBSD-2D	0.46	0.207	0.49
8-IPBSD-2D	0.42	0.254	0.55
9-IPBSD-2D	0.39	0.254	0.50
10-IPBSD-2D	0.29	0.304	0.41
11-IPBSD-2D	0.35	0.254	0.39
12-IPBSD-2D	0.23	0.356	0.34
13-IPBSD-2D	0.20	0.356	0.32

The design loss curve was then compared to the actual loss curve for case 1-IPBSD in Figure 6.14, denoting quite a good match. For comparative purposes, the actual loss curve was computed without considering demolition and collapse loss contributions. As anticipated, when plotting the area under the actual loss curve with respect to ELR, the

bulk of the contribution to EAL comes at lower ELR values, where the corresponding MAFE is significantly larger. In addition, while easily disregarded, the selection of the OLS point, *i.e.*, its return period, is important, as the contribution of high-frequency seismic events could have a significant contribution to the EAL of the building. Therefore, the return period at the OLS may be further reduced to have a better representation of the actual loss curve during the design stage. In contrast, the contribution to EAL at large ELRs is negligible, even if the loss curve mismatch further highlights the importance of high frequency events for computation of losses.

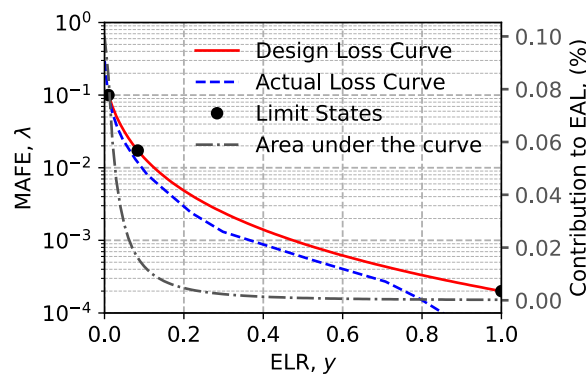


Figure 6.14. Loss curves for case 1-IPBSD.

6.6 DETAILED ANALYSIS OF LOSS ESTIMATES

6.6.1 Secant-to-yield (T_1) period range considerations

To better understand how the assumptions involved within the IPBSD framework affected the actual loss computations and their accuracy, the results were scrutinised to understand the loss contributions of different performance groups at the SLS. Moreover, the variation of EAL was explored by modifying the initial secant-to-yield period, T_1 . Since this method's inception in O'Reilly and Calvi [O'Reilly and Calvi 2019], the effect of T_1 has not yet been thoroughly examined via actual analysis data but rather conceptual considerations and logic. Therefore, the results included in this section provide such evidence. For the analysis, performance objectives were set to 1.0×10^{-4} and 0.8%, for λ_c and λ_y , respectively, however only λ_y will be focused on herein. As mentioned in Section 6.5.2.2, the return period at OLS is a non-trivial point and was reduced to 5 years to better capture the actual loss curve at the design stage, while the return period at SLS was assumed to be 60 years. SLFs were generated for a 3-storey residential RC building with two seismic frames similar to the layout presented in Figure 6.6 but assuming a *perimeter* seismic resisting system which is more suitable for two-dimensional analysis given the symmetry of the layout. Therefore, only one direction was analysed for simplicity to directly visualise the contributions to loss.

IPBSD was applied as originally foreseen to identify the initial secant-to-yield period range within 0.24s and 0.53s, corresponding to a PFA of 0.43g and PSD of 0.22%, respectively. Loss contribution ratios amounted to 0.57 and 0.43 for non-structural PSD-sensitive and PFA-sensitive components, respectively. The ratio for structural components was significantly lower (*i.e.*, <0.01). Also, a decision not to meet the period range condition was made to analyse its impact on loss variations when not met. IDA and loss assessment was performed for each solution as conducted in previous sections. Table 6.10 provides the EAL values for each considered T_1 . As observed, the EAL limit was met for all solutions. Additionally, EAL tends to decrease with decreasing T_1 (Figure 6.15), indicating that the more flexible structures tend to accumulate more losses, which is a reflection of SLF contributions outlined in Section 6.3.4. In contrast, if the acceleration-sensitive components were more to increase in value (with no change in fragility), the decrease in EAL will be less apparent, as the loss contributions of those components would be higher in comparison with displacement-sensitive components.

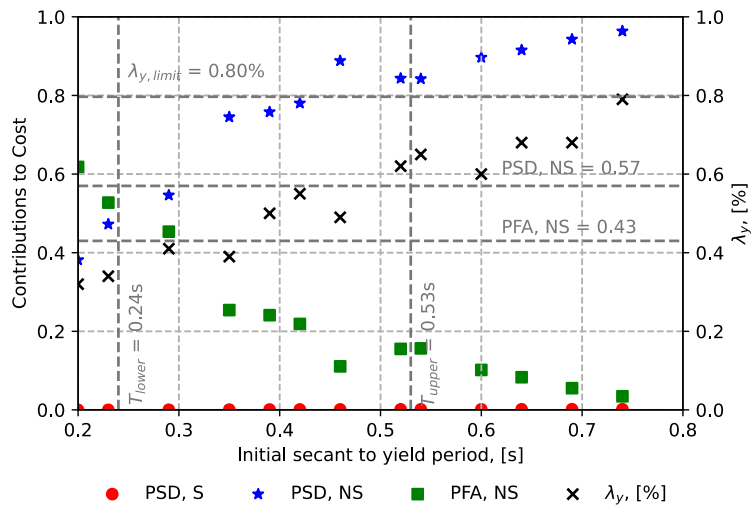


Figure 6.15. Loss contributions of different performance groups to the total repair cost at SLS.

At $S_{\alpha SLS}$ values for each solution provided in Table 6.10, loss contributions were evaluated to see how the assumptions fared. As expected, demolition and collapse loss contributions proved to be negligible at SLS design intensity, which relates to direct economic loss only and not to other factors, such as downtime and indirect losses. Therefore, they were not considered, and the remaining performance group losses were normalised by the total costs (Figure 6.15 and Table 6.11). At lower periods, the significant contribution to total losses comes from PFA-sensitive components, while, with increasing T_1 , the loss contributions associated with PSD-sensitive non-structural (NS) components start increasing. In

contrast, the loss contributions from PSD-sensitive structural (S) components were negligible, which confirmed the considerations made in Figure 6.3. The actual loss contributions did not quite match the assumed ones through the design process, which is primarily due to having the same design EDP along the height of the building, which will be further explored in Section 6.6.2. As expected, with the increase of the initial secant-to-yield period, the loss contributions from PFA-sensitive components decrease, while the contributions due to PSD-sensitive components increase. It is important to note that the period range is not a direct representation of precise loss contributions. For example, the upper period limit is based on the critical PSD, while the lower period limit is based on the critical PFA. This means that, during design, reasonably high values of 0.57 and 0.43 for PSD- and PFA-sensitive component groups, respectively, will be assumed. However, it is not reasonable to expect high loss contributions from PFA-sensitive components at the upper period limit, whereas the opposite is true at the lower period limit. The compromise between both component groups ensures that the losses will not be exceeded within the period range.

Table 6.11. Loss contributions of different performance groups to the total repair cost at SLS.

Solution ID	PSD, S (%)	PSD, NS (%)	PFA, NS (%)
1-IPBSD-2D	0.2	96.3	3.5
2-IPBSD-2D	0.2	94.3	5.5
3-IPBSD-2D	0.2	91.5	8.3
4-IPBSD-2D	0.2	89.6	10.2
5-IPBSD-2D	0.1	84.3	15.6
6-IPBSD-2D	0.1	84.4	15.5
7-IPBSD-2D	0.1	88.8	11.1
8-IPBSD-2D	0.1	78.0	21.9
9-IPBSD-2D	0.1	75.8	24.1
10-IPBSD-2D	0.0	54.7	45.3
11-IPBSD-2D	0.1	74.5	25.4
12-IPBSD-2D	0.0	47.3	52.7
13-IPBSD-2D	0.0	38.2	61.8

From Figure 6.15, one may infer that the computed λ_y is expected to be closer to $\lambda_{y,\text{limit}}$ at the vicinity of T_{lower} , where the component group contributions are in the vicinity of values obtained during design (*i.e.*, 0.57 and 0.43 for PSD- and PFA-sensitive components, respectively). However, while the contributions in terms of ratios are expected, the actual EAL contribution values in terms of percentage are lower than expected. This is a direct impact of the period where there is always a compromise. That is, the limits are set based on discrete values of PFA and PSD during design, while it is highly unlikely to have critical

PSD (associated with T_{upper}) when critical PFA (associated with T_{lower}) was estimated. The goal of the framework is not to optimize for $\lambda_{y,limit}$, but rather ensure that period range is not disrupted, hence, losses associated with component groups of both EDP-sensitivities are not exceeded

6.6.2 Influence of the EDP profiles

To further understand possible improvement paths, the EDP profiles of the solutions were plotted in Figure 6.16. PSD averages around 0.15% for all solutions at the first two storeys and 0.10% at the third storey level, while the value used in IPBSD was 0.22%. In contrast, the PFA profile varies between 0.1 and 0.4g, while during the application of IPBSD, a value of 0.43g was observed at SLS. A possible improvement for this is the utilisation of reduction factors during design to account for possible variations of EDP values at different storeys. However, empirical equations available in the literature [Priestley *et al.* 2007] generally assume a reduction of PSDs along the height, while here, as observed, PSDs at the first and second storeys were nearly equal. As such, a decision was made not to implement PSD reduction factors. On the other hand, this may be of more importance for PFA-sensitive components, as there is a notable discrepancy of values along the height of the building. To aid that, recent simplified methodologies based on a modal superposition approach [Calvi and Sullivan 2014; Welch and Sullivan 2017] may be investigated in the future to estimate floor accelerations more accurately.

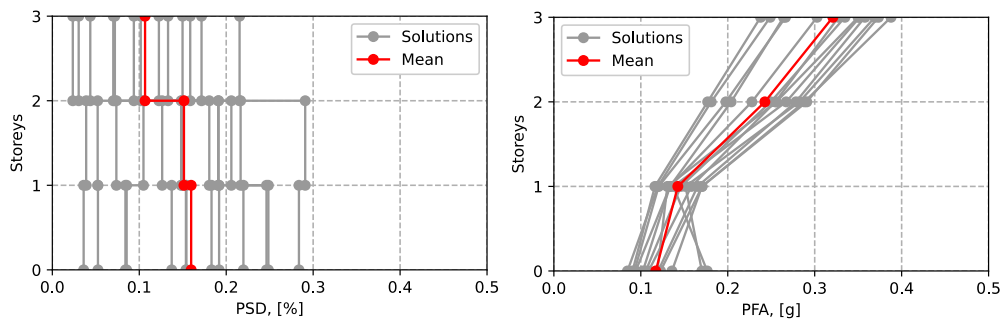


Figure 6.16. PSD and PFA profiles along with the height of the structure at SLS.

Instead of using predefined EDP profiles based on empirical equations available from the literature, the PSD and PFA profiles obtained in Figure 6.16 were used as benchmarks to scale the design EDPs accordingly. The updated EDPs and corresponding y values at SLS are given in Table 6.12. The EDP values at each storey or floor level were scaled based on the mean profiles presented in Figure 6.16 resulting in reduced y values, therefore, the loss curve was subsequently updated and the new EAL limit was set to 0.58%. None of the solutions having a period larger than the upper period limit (Table 6.10) met the new EAL limit, demonstrating the non-conservative, yet optimized, nature of the modification. The

same does not hold for a solution with a period below the lower period bound, which could be attributed to significant reductions of losses associated with PSD-sensitive components, as opposed to an increase in losses associated with PFA-sensitive components.

Table 6.12. Updated EDP profiles and corresponding y values.

Floor/Storey	PSD, NS [%]	PFA, NS (g)	$y_{PSD,NS}$ (%)	$y_{PFA,NS}$ (%)
0	-	0.16	-	0.00
1	0.22	0.19	1.81	0.03
2	0.21	0.33	1.46	0.25
3	0.15	0.43	0.99	0.74

Finally, the loss curves for all the case study frames were plotted together with the design loss curve, identified via the IPBSD framework, in Figure 6.17. As one may note, the larger variations are for high return periods (low MAFFE levels). This indicates a possible improvement when fitting the design loss curve at the outset. However, similar to the findings in Section 6.5.2.2, this option was not adopted, as the variations at high return periods do not significantly affect EAL, which is more sensitive to events associated with low return periods as shown in Figure 6.14. Furthermore, the loss curve before the modifications through the reduction factors has an ELR at SLS that is higher than the one of any of the actual loss curves, which is an indication of lower EALs compared to the design or limit.

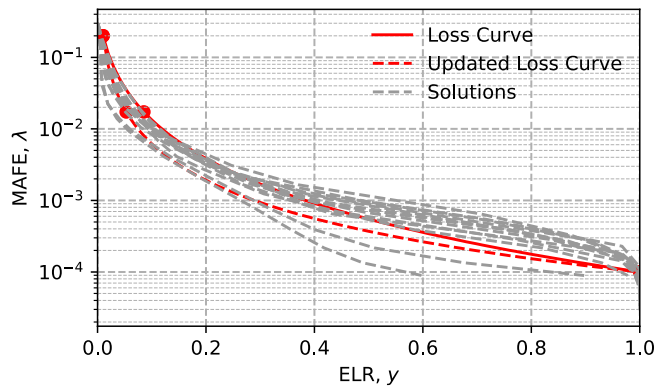


Figure 6.17. Comparison of loss curves for the 2D frames with the initial and updated loss curves.

6.7 SUMMARY AND CONCLUSIONS

This chapter presented and further validated an IPBSD framework, based on the fundamental objectives of PBEE, that aims to design buildings by limiting expected monetary losses while targeting acceptable collapse safety. The IPBSD framework was applied to several case study RC frame buildings, for which the structural elements were designed, and numerical models developed to perform non-linear IDA. The IDA response of each building was then used to assess the collapse safety and perform loss assessment with the ultimate goal of estimating EAL and comparing it with the limit initially set for the IPBSD implementation. Similarly, Eurocode 8 provisions were applied, and an additional set of frames were designed for comparative purposes with respect to the IPBSD framework. The main conclusions of this study are as follows:

- The IPBSD framework, applied in a Python-based object-oriented environment, yielded consistent results in terms of meeting the performance objectives of both MAFC and EAL. It was demonstrated through the application of the framework on multiple case study RC buildings and validated through its bidirectional response and loss assessment. Regardless of the seismic hazard, number of storeys and performance objective levels, the performance of the IPBSD framework was consistently satisfactory;
- Some of the assumptions within the IPBSD framework require further research and parametric studies for more optimised designs that require less computational effort. The anticipated collapse capacity uncertainty, β_{RTR} , proved to be significantly higher than the actual ones obtained through IDA. This is primarily related to its computation being based on three distinct points of the collapse fragility curve during design (in the absence of all points given by a specific tool (*e.g.*, SPO2IDA)) whereas, during the assessment, the whole spectrum of points on the fragility curve is used for a more precise computation;
- All of the Eurocode 8-designed case study buildings demonstrated MAFC values similar to the ones found in the literature. Buildings of importance class III exhibited improved performance in neither collapse safety nor loss reduction in a significant manner when compared to buildings of importance class II. This is primarily due to the chosen configurations and local ductility requirements in terms of minimum element reinforcement that governed the design. Furthermore, this also denotes the wide variety of possible design solutions via Eurocode 8 provisions, when specific criteria to achieve risk and loss-targeted solutions are not foreseen;
- The comparison of the multiple loss curves with the design loss curve indicated the need for refining the first limit state point, *i.e.*, OLS, through the reduction of its return period. This stemmed from larger contributions to EAL at frequent seismic events associated with high return periods and contributions from the structural performance group.

- The effects of the assumptions on the performance of buildings in terms of limiting economic losses were further assessed. It was shown that the assumption of uniform EDP profiles at the design stage is not representative of actual EDP profiles. Consequently, the mean EDP profiles of all buildings were used to generate reduction factors and reapplied at the design stage. The updated loss curve resulted in a reduction of limiting EAL by around 25%. In lieu of generated reduction factors, empirical equations available from the literature may be used to perform the reductions for more optimised and less conservative EAL limit identification.
- A simpler corrective measure for the establishment of ELRs and EAL using the critical EDP (associated with non-structural or structural component groups) was implemented. Compared to the previous versions of the framework, the refined approach of re-computing the EAL is less conservative and not far from the limit EAL initially set out, which represents a notable improvement.

Overall, the IPBSD framework performs well hence is suitable for the next-generation seismic design approaches meeting the goals of PBEE. The flexibility and simplicity of the framework in achieving risk-consistent and loss-driven designs lie within its ability to combine advantages of various methods available in the literature, with the inclusion of code-based provisions. The parametric investigations described here serve to illustrate the applicability of the method and also the aspects for which there is still room for improvement.



7. SUMMARY AND CONCLUSIONS

7.1 SUMMARY

This thesis focused on the design of buildings following a risk-targeting and loss-driven approach. The aim of the work was to establish a framework that follows undemanding mathematical and conceptual approaches while not compromising the complex nature of probabilistic seismic design frameworks. Essentially, a framework was developed to incorporate heavy computations on a code level (*e.g.*, in object-oriented Python) guaranteeing the integrity of probabilistic methods and using tools easily applicable by practitioners on a front-end level. Therefore, the framework pursued within this work had to be affordable by both academic and practising communities.

Within the objectives of this thesis, a new framework, building upon the one outlined in Chapter 3, was developed to allow the attainment of design solutions with limited economic loss and targeted collapse safety. In other words, expected annual loss (EAL) was used as a metric to characterise direct losses deriving from damaged components following a seismic event, whereas mean annual frequency of collapse (MAFC) was used as a proxy for targeting the life safety of the building occupants. The developed framework was termed integrated performance-based seismic design (IPBSD) and uses both metrics to obtain valid design solutions. The proposed IPBSD framework is presented again in Figure 7.1, for convenience. Initially, the seismic hazard of the site location is identified. Next, a suitable loss curve for the limitation of EAL is identified (Figure 7.1a). At this step, the performance objectives are characterised through the expected loss ratio (ELR) and mean annual frequency of exceedance (MAFE) of three performance limit states. Economic losses are generally controlled through the modification of ELR at the serviceability limit state (SLS), whereas operational and collapse limit states (OLS and CLS, respectively) represent the onset of monetary loss and collapse, or total economic loss, of the building, respectively. The design spectrum at SLS is identified (Figure 7.1b), which, together with storey loss functions (SLFs) (Figure 7.1c), is used to identify a suitable period range, within which the building's principal initial secant-to-yield periods must lie to satisfy the initial design objectives (Figure 7.1d). To control the risk of structural collapse, an expected backbone behaviour and overstrength are trialled by the practitioner. The SPO2IDA tool is used to estimate the collapse fragility function of the building along each direction in terms of median collapse capacity and record-to-record variability, assuming a lognormal distribution (Figure 7.1e). The fragility function is then integrated with the hazard curve to compute the MAFC (Figure 7.1f). The goal is to identify capacity, overstrength and

backbone shape of a building to have the calculated MAFC matching the target MAFC. The identified strength is then used to compute the lateral distribution of forces and perform equivalent static analysis with the inclusion of gravity loads to analyse and detail the structural elements of the building resulting in the final structural solution (Figure 7.1g).

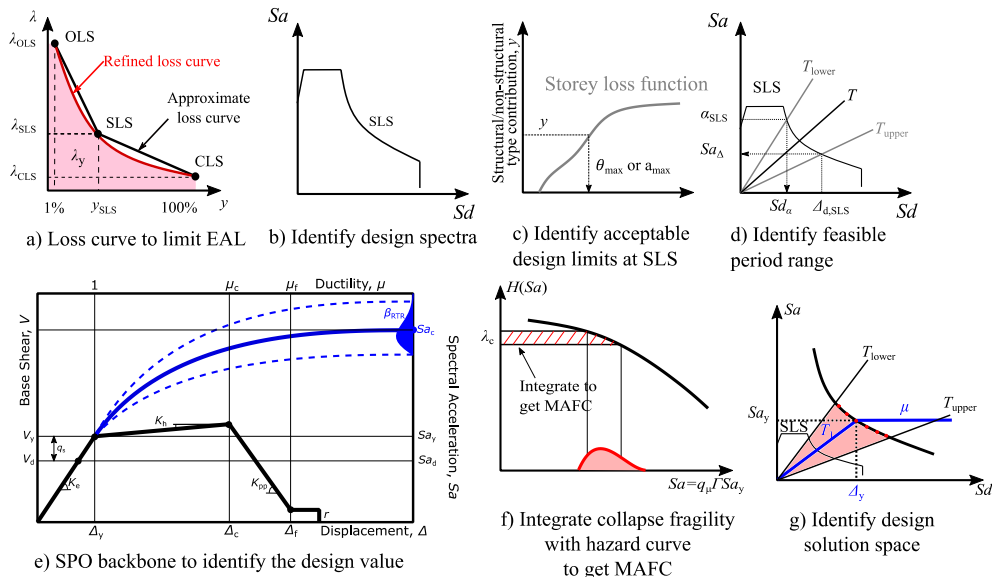


Figure 7.1. Proposed IPBSD framework.

7.2 KEY FINDINGS AND RESEARCH OUTCOMES

7.2.1 Storey loss functions for seismic design and assessment: development of tools and application

Chapter 4 aimed to fill the gap of the lack of practical and customisable tools for easy-to-implement loss estimation by introducing an SLF generation toolbox for seismic design and assessment of buildings. Its implementation was described step by step and validated through the application to a case-study school building. It was also compared with the more rigorous component-based loss assessment described in FEMA P-58 to validate the results obtained. Additionally, the toolbox was applied to a single storey of a building, with the goal of comparing the effects of considering interdependency between damage states of different components on losses. The main conclusions from this chapter are as follows:

- The proposed toolbox is capable of accounting for component correlation and can avoid the problem of double counting of repair costs that is sometimes encountered in practice [Ramirez and Miranda 2009]. The toolbox was applied to a single storey to investigate how the consideration of component dependency and

interaction impacts the observed vulnerability when compared to the independency assumption. An increase in vulnerability was observed when considering dependent components. Additionally, the significance of the impact is dependent on the fragility function of components, where the increase in overlap between the fragility functions of causation and dependent component results in higher impact on the modification of the vulnerability. Essentially, greater the overlap, the higher is the probability of being in higher damage state, hence the expected loss will be higher;

- SLFs were developed for an entire case-study school building in Italy accounting for the response in both directions and a subsequent loss assessment was carried out. Results were compared to a more rigorous component-based loss assessment approach with a good match in EAL between the two approaches;
- This close matching of the SLF-based loss estimates to the detailed FEMA P-58 component-based loss assessment was also observed in the distribution of the losses among performance groups per intensity and engineering demand parameter (EDP). The classification of components into different performance groups and EDP allows further disaggregation of losses to identify the main contributors to the economic losses. This comparison highlighted the validity of the developed tool and its accurate applicability for the intended scopes initially outlined;
- In addition to the typical objective of performing loss assessment on existing buildings, SLFs could also act as an important tool for new designs within novel risk-based design approaches. Simplified relationships between expected losses and structural demands (*i.e.*, storey loss functions) were integrated and used when designing new structures to limit potentially excessive monetary losses due to building damage.

7.2.2 Integrating expected loss and collapse risk in performance-based seismic design of structures

Chapter 5 proposed the integrated performance-based seismic design (IPBSD) framework, allowing the identification of feasible design solutions that limit expected monetary losses and target a given collapse safety. It was described via a step-by-step implementation and tested for several case study reinforced concrete (RC) frame structures. Case study buildings were designed following IPBSD and risk-targeted seismic action (RTSA) frameworks, Eurocode 8 provisions and a direct displacement-based design approach. Following a full design of the members of each structure, numerical models were developed, and non-linear response history analysis was performed through incremental dynamic analysis (IDA) to compute the actual collapse safety, then compared with the initial design targeted. The main conclusions of this chapter are as follows:

- Half of the case study frames following Eurocode 8 met the MAFC condition, which was not surprising since MAFC was not used as criterion to design the case

study frames. Even though two importance classes were considered, no notable difference in collapse safety was consistently obtained. In fact, some of the importance class II frames performed better than the III ones given that, for a fixed fundamental period, the member reinforcement ratios tended to reduce and lead to increased member ductility capacities. This offsets the lower strength to provide a higher collapse capacity via increased ductility. Hence, a careful balance between strength, stiffness and ductility in seismic design is vital and simply increasing the strength and stiffness of structural members to achieve improved collapse safety is not always an effective solution;

- The addition of gravity loads in the design process improved the collapse safety via additional overstrength. However, no consistent trend was observed pointing towards a need for its explicit consideration in design;
- The apparent lack of design flexibility and heavy dependence on the design reference values in current implementations of risk-targeted spectra (RTS) means that some of the underlying assumptions need subsequent modifications to result in widespread adaptation;
- Design and validation of cases following the RTSA method demonstrated the advantages of risk-targeted approaches, as the majority of cases met the MAFC condition. It was found that assumptions regarding design input parameters had a significant impact when targeting a specific collapse safety level. Several design cases initially reported collapse risk values much lower than the design target, hence a result of conservative design input parameters, which could be refined through repeated design iterations;
- The proposed IPBSD approach demonstrated consistent results in terms of meeting the collapse safety targets for each case study frame. The targets were met with relatively narrow conservatism and without any case of excessive overdesign or requiring multiple design iterations;
- The structures' collapse capacities from IDA (*i.e.*, median and dispersion) were slightly conservative, possibly due to ductility reserves in the structure or the approximate nature of the SPO2IDA tool; however, it was found to be sufficiently accurate to result in suitable and efficient design solutions.

To summarise, methods following a risk-targeted approach performed well, while the cases designed following other traditional approaches, such as Eurocode 8, failed the target collapse safety condition and also showed no uniformity in the safety across different structural solutions. The main strength of the proposed IPBSD approach is in its flexibility and simplicity, as it combines the advantages of different methods in the literature, including code-based provisions, to give risk-consistent design solutions for different structures. It is envisaged that this approach, following further research and refinements, should form a part of the next-generation seismic design approaches aiming to achieve the goals of performance-based earthquake engineering (PBEE).

7.2.3 On the seismic loss estimation of integrated performance-based designed buildings

Chapter 6 presented and further validated the IPBSD framework. The IPBSD framework was applied to several case study RC frame buildings, for which the structural elements were designed and analysed via IDA. The results were then used to assess the collapse safety and perform loss assessment with the ultimate goal of estimating EAL and comparing it with the limit initially set for the IPBSD implementation. Similarly, Eurocode 8 provisions were applied to the case study buildings, and an additional set of frames were designed for comparative purposes with respect to the IPBSD framework. The main conclusions of this chapter are as follows:

- The IPBSD framework, applied in a Python-based object-oriented environment, yielded consistent results in terms of meeting the performance objectives of both MAFC and EAL. It was demonstrated through the application of the framework on several case study RC buildings and validated through its bidirectional response and loss assessment. Regardless of the seismic hazard, number of storeys and performance objective levels, the performance of the IPBSD framework was consistently good;
- The comparison of the multiple loss curves with the design loss curve indicated the need for refining the first limit state point, *i.e.*, operational limit state, through the reduction of its return period. This stemmed from larger contributions to EAL at frequent seismic events associated with lower return periods and contributions from the structural performance group;
- The effects of the assumptions on the performance of buildings in terms of limiting economic losses were further assessed. It was shown that the assumption of uniform EDP profiles at the design stage is not representative of actual EDP profiles. Consequently, the mean EDP profiles of all buildings were used to generate reduction factors and reapplied at the design stage. The updated loss curve resulted in a reduction of limiting EAL by around 25%. In lieu of generated reduction factors, empirical equations available from the literature may be used to account for this and perform reductions for more optimised and less conservative EAL limit identification.

Overall, the IPBSD framework performs well, hence it is deemed suitable for the next-generation seismic design approaches meeting the goals of PBEE. The flexibility and simplicity of the framework in achieving risk-consistent and loss-driven designs lie within its ability to combine advantages of various methods available in the literature, with the inclusion of code-based provisions. The parametric investigations described here served to illustrate the applicability of the method and the aspects for which there is still room for improvement.

7.3 LIMITATIONS AND FUTURE DEVELOPMENTS

While the developments outlined in this work have shown an ease of the application of the proposed IPBSD framework, some future extensions may be made. In particular, to what pertains the SLF generation toolbox, consideration of interactions between components physically located at different storeys of a building or associated with different performance groups may be included. A tool for quick processing and browsing of component data may also be foreseen to allow the user to add or remove components and visualise all existing components. Additionally, the toolbox currently operates with only two types of distributions (*i.e.*, normal, and lognormal). Future extensions could foresee the possibility of including other, such as truncated distributions or multi-modal distributions, that would add flexibility to the toolbox. These possible additional features would be easy to implement, considering the object-oriented programming used to develop the SLF generation toolbox structured through modular class definitions in Python.

To what pertains to the RTSA and the IPBSD methods, many assumptions require further quantification studies and experimentation for suitable initial design input parameters and targets; specifically, the anticipated collapse capacity uncertainty β_{RTR} , or on how to quantify the expected ductility capacity and the post-capping strength of structural elements. Some research exists on these issues but much more could be done to consolidate the understanding and render them useful in design practice.

The IPBSD framework could be further updated to consider different structural typologies apart from the systems consisting of RC moment-resisting frames. Other typologies might include the consideration of RC walls, steel structural systems, as well as base-isolated buildings, which could be further validated through case study applications for the refinement of the framework. Some of the assumptions within the IPBSD framework require further research and parametric studies for more optimised designs that require less computational effort. The anticipated collapse capacity uncertainty, β_{RTR} , proved to be significantly higher than the actual ones obtained through IDA. This is primarily related to its computation being based on three distinct points of the collapse fragility curve during design (in the absence of all points given by a specific tool (*e.g.*, SPO2IDA)) whereas, during the assessment, the whole spectrum of points on the fragility curve is used for a more precise computation. Additionally, within this thesis, Eurocode 8 was the primary seismic design code utilised for design and detailing of structural elements, however, this final stage, in particular within the object-oriented tool implemented via Python, could be adjusted to consider different seismic design codes.

REFERENCES

- Ancheta, T. D., Darragh, R. B., Stewart, J. P., Seyhan, E., Silva, W. J., Chiou, B. S. J., Wooddell, K. E., Graves, R. W., Kottke, A. R., Boore, D. M., Kishida, T., and Donahue, J. L. [2014] “NGA-West2 database,” *Earthquake Spectra*, Vol. 30, No.3, pp. 989–1005.
- ASCE 7-16. [2016] *Minimum Design Loads for Buildings and Other Structures*, Reston, VA, USA.
- Aschheim, M., and Black, E. F. [2000] “Yield point spectra for seismic design and rehabilitation,” *Earthquake Spectra*, Vol. 16, No.2, pp. 317–335.
- Aslani, H., and Miranda, E. [2005] “Fragility assessment of slab-column connections in existing non-ductile reinforced concrete buildings,” *Earthquake Spectra*, Vol. 31, No.1, pp. 159–177.
- ATC. [2009] “Quantification of building seismic performance factors,” *Fema P695*, No.June, p. 421.
- Baker, J. W. [2011] “Conditional mean spectrum: Tool for ground-motion selection,” *Journal of Structural Engineering*, Vol. 137, No.3, pp. 322–331.
- Balboni B. [2007] *2007 RS Means Square Foot Costs*, Kingston, MA.
- Bentz, E. [2015] “Appendix A : Program Manuals from Sectional Analysis of Reinforced Concrete Members By : Graduate Department of Civil Engineering University of Toronto.”
- Bucher, T., and Helmond, A. [2017] “The Affordances of Social Media Platforms,” *The*

- SAGE Handbook of Social Media*, No.June 2017, pp. 233–253.
- Calvi, G. M., Rodrigues, D., and Silva, V. [2018] “Introducing new design spectra derived from Italian recorded ground motions 1972 to 2017,” *Earthquake Engineering & Structural Dynamics*, Vol. 47, No.13, pp. 2644–2660.
- Calvi, G. M., Sullivan, T. J., and Welch, D. P. [2014] “A Seismic Performance Classification Framework to Provide Increased Seismic Resilience,” *Geotechnical, Geological and Earthquake Engineering*.
- Calvi, P. M., and Sullivan, T. J. [2014] “Estimating floor spectra in multiple degree of freedom systems,” *Earthquake and Structures*, Vol. 7, No.1, pp. 17–38.
- Cardone, D. [2016] “Fragility curves and loss functions for RC structural components with smooth rebars,” *Earthquake and Structures*, Vol. 10, No.5, pp. 1181–1212.
- Cardone, D., and Perrone, G. [2015] “Developing fragility curves and loss functions for masonry infill walls,” *Earthquake and Structures*, Vol. 9, No.1, pp. 257–279.
- CEN. [2004a] *Eurocode 8: Design of Structures for Earthquake Resistance - Part 1: General Rules, Seismic Actions and Rules for Buildings (EN 1998-1:2004)*, Brussels, Belgium.
- CEN. [2004b] *EC EN 1992-1-1 Eurocode 2: Design of concrete structures - Part 1-1: General rules and rules for buildings*. Brussels, European Committee for Standardization (CEN), Brussels, Belgium.
- CEN. [2012] *EN 1990:2002 + A1 Eurocode-basis of structural design*, European Committee for Standardization (CEN), Brussels, Belgium.
- CEN. [2018] *Design of Structures for Earthquake Resistance (Draft) - Part 1: General Rules, Seismic Actions and Rules for Buildings (EN 1998-1:2018)*, Brussels.
- Chiozzi, A., and Miranda, E. [2017] “Fragility functions for masonry infill walls with in-plane loading,” *Earthquake Engineering and Structural Dynamics*, Vol. 46, No.15, pp. 2831–2850.
- Cook, D., Liel, A. B., Luco, N., Almeter, E., and Haselton, C. [2019] “Implications of seismic design values for economic losses,” *13th International Conference on Applications of Statistics and Probability in Civil Engineering, ICASP 2019*, No.January 2019.
- Cornell, C. A. [1996] “Calculating building seismic performance reliability: a basis for multi-level design norms,” *11th World Conference on Earthquake Engineering*, p. 8.

- Cornell, C. A., Jalayer, F., Hamburger, R. O., and Foutch, D. A. [2002] "Management Agency Steel Moment Frame Guidelines," *Journal of Structural Engineering*, Vol. 128, No. April 2002, pp. 526–533.
- Cornell, C. A., and Krawinkler, H. [2000] "Progress and Challenges in Seismic Performance Assessment," *PEER Center News*, Vol. 3, No.2, pp. 1–2.
- Cosenza, E., Del Vecchio, C., Di Ludovico, M., Dolce, M., Moroni, C., Prota, A., and Renzi, E. [2018] *The Italian guidelines for seismic risk classification of constructions: technical principles and validation*, *Bulletin of Earthquake Engineering*, Springer Netherlands.
- Dolšek, M., Lazar Sinković, N., and Žižmond, J. [2017] "IM-based and EDP-based decision models for the verification of the seismic collapse safety of buildings," *Earthquake Engineering and Structural Dynamics*, Vol. 46, No.15, pp. 2665–2682.
- Douglas, J., Ulrich, T., and Negulescu, C. [2013] "Risk-targeted seismic design maps for mainland France," *Natural Hazards*, Vol. 65, No.3, pp. 1999–2013.
- Duckett, W. [2004] "Risk Analysis and the Acceptable Probability of Failure," No.July, pp. 1–5.
- Eads, L., Miranda, E., and Lignos, D. G. [2015] "Average spectral acceleration as an intensity measure for collapse risk assessment," *Earthquake Engineering & Structural Dynamics*, Vol. 44, No.12, pp. 2057–2073.
- Emergency, F., and Agency, M. [2000] "Prestandard and commentary for the seismic rehabilitation of buildings," No.November.
- Fajfar, P. [2018] *Analysis in seismic provisions for buildings: past, present and future: The fifth Prof. Nicholas Ambraseys lecture*, *Bulletin of Earthquake Engineering*, Springer Netherlands.
- Fajfar, P., and Dolšek, M. [2012] "A practice - oriented estimation of the failure probability of building structures," No.July 2011, pp. 531–547.
- FEMA. [2009] "NEHRP Recommended Seismic Provisions," *Fema P-750*, p. 406.
- FEMA. [2012a] *FEMA P-58-1: Seismic Performance Assessment of Buildings: Volume 1 - Methodology*, Washington, DC.
- FEMA. [2012b] *FEMA P58-3. Seismic Performance Assessment of Buildings Volume 3 - Performance Assessment Calculation Tool (PACT)*, Washington, D.C.
- Del Gaudio, C., De Risi, M. T., Ricci, P., and Verderame, G. M. [2019] "Empirical drift-

- fragility functions and loss estimation for infills in reinforced concrete frames under seismic loading,” *Bulletin of Earthquake Engineering*, Vol. 17, No.3, pp. 1285–1330.
- Gibson, J. J. [1979] “The Theory of Affordances,” *The Ecological Approach to Visual Perception*, pp. 127–137.
- Gkimprixis, A., Tubaldi, E., and Douglas, J. [2019] “Comparison of methods to develop risk-targeted seismic design maps,” *Bulletin of Earthquake Engineering*, Springer Netherlands, Vol. 17, No.7, pp. 3727–3752.
- Gokkaya, B. U., Baker, J. W., and Deierlein, G. G. [2016] “Quantifying the impacts of modeling uncertainties on the seismic drift demands and collapse risk of buildings with implications on seismic design checks,” *Earthquake Engineering & Structural Dynamics*, Vol. 45, No.10, pp. 1661–1683.
- Goulet, C. A., Haselton, C. B., Mitrani-reiser, J., Beck, J. L., Deierlein, G. G., Porter, K. A., and Stewart, J. P. [2007] “Evaluation of the seismic performance of a code-conforming reinforced-concrete frame building — from seismic hazard to collapse safety and economic losses,” No.June, pp. 1973–1997.
- Günay, S., and Mosalam, K. M. [2013] “PEER performance-based earthquake engineering methodology, revisited,” *Journal of Earthquake Engineering*, Vol. 17, No.6, pp. 829–858.
- Hall, J. F. [2018] “Performance of viscous damping in inelastic seismic analysis of moment-frame buildings,” *Earthquake Engineering and Structural Dynamics*, Vol. 47, No.14, pp. 2756–2776.
- Haselton, C. B., and Deierlein G.G. [2007] “Assessing seismic collapse safety of modern reinforced concrete moment frame buildings,” Stanford University.
- Haselton, C. B., Liel, A. B., Taylor-Lange, S. C., and Deierlein, G. G. [2016] “Calibration of model to simulate response of reinforced concrete beam-columns to collapse,” *ACI Structural Journal*, Vol. 113, No.6, pp. 1141–1152.
- Ibarra, L. F., Medina, R. A., and Krawinkler, H. [2005] “Hysteretic models that incorporate strength and stiffness deterioration,” *Earthquake Engineering & Structural Dynamics*, Vol. 34, No.12, pp. 1489–1511.
- Iervolino, I., Spillatura, A., and Bazzurro, P. [2018] “Seismic Reliability of Code-Conforming Italian Buildings,” *Journal of Earthquake Engineering*, Taylor & Francis, Vol. 22, No.sup2, pp. 5–27.
- Kennedy, R. C., and Short, S. A. [1994] *Basis for seismic provisions of DOE-STD-1020*,

Livermore, California.

- Krawinkler, H., Zareian, F., Medina, R. A., and Ibarra, L. F. [2006] "Decision support for conceptual performance-based design," *Earthquake Engineering and Structural Dynamics*, Vol. 35, No.1, pp. 115–133.
- Luco, N., Ellingwood, B. R., Hamburger, R. O., Hooper, J. D., Kimball, J. K., and Kircher, C. A. [2007] "Risk-Targeted versus Current Seismic Design Maps for the Conterminous United States," *Structural Engineering Association of California 2007 Convention Proceedings*, pp. 1–13.
- Di Ludovico, M., Prota, A., Moroni, C., Manfredi, G., and Dolce, M. [2017] "Reconstruction process of damaged residential buildings outside historical centres after the L'Aquila earthquake: part I—"light damage" reconstruction," *Bulletin of Earthquake Engineering*, Springer Netherlands, Vol. 15, No.2, pp. 667–692.
- Mazzoni, S., Mckenna, F., Scott, M. H., and Fenves, G. L. [2006] "OpenSees Command Language Manual."
- McKenna, F., Scott, M. H., and Fenves, G. L. [2010] "Nonlinear Finite-Element Analysis Software Architecture Using Object Composition," *Journal of Computing in Civil Engineering*, Vol. 24, No.1, pp. 95–107.
- NTC. [2018] *Norme Tecniche Per Le Costruzioni*, Rome, Italy.
- NZS. [2016] *NZS 1170.5 Supp 1:2004 - Structural Design Actions Part 5: Earthquake Actions - New Zealand - Commentary*, Wellington, New Zealand.
- NZS 1170.5:2004. [2004] *Structural design actions part 5: Earthquake actions*, Wellington, New Zealand.
- O'Reilly, G. J., and Calvi, G. M. [2019] "Conceptual seismic design in performance-based earthquake engineering," *Earthquake Engineering & Structural Dynamics*, Vol. 48, No.4, pp. 389–411.
- O'Reilly, G. J., and Calvi, G. M. [2020] "Quantifying seismic risk in structures via simplified demand–intensity models," *Bulletin of Earthquake Engineering*, Vol. 18, No.5, pp. 2003–2022.
- O'Reilly, G. J., Perrone, D., Fox, M., Monteiro, R., and Filatrault, A. [2018] "Seismic assessment and loss estimation of existing school buildings in Italy," *Engineering Structures*, Elsevier, Vol. 168, No. February, pp. 142–162.

- O'Reilly, G. J., Perrone, D., Fox, M., Monteiro, R., Filiatrault, A., Lanese, I., and Pavese, A. [2019] "System Identification and Seismic Assessment Modeling Implications for Italian School Buildings," *Journal of Performance of Constructed Facilities*, Vol. 33, No.1, p. 04018089.
- O'Reilly, G. J., and Sullivan, T. J. [2018] "Quantification of modelling uncertainty in existing Italian RC frames," *Earthquake Engineering and Structural Dynamics*, Vol. 47, No.4, pp. 1054–1074.
- O'Reilly, G. J., Sullivan, T. J., and Filiatrault, A. [2017] "Implications of a More Refined Damage Estimation Approach in the Assessment of RC Frames," *16th World Conference on Earthquake Engineering*, No.February.
- Ottонelli, D., Cattari, S., and Lagomarsino, S. [2020] "Displacement-Based Simplified Seismic Loss Assessment of Masonry Buildings," *Journal of Earthquake Engineering*, Taylor & Francis, Vol. 24, No.sup1, pp. 23–59.
- Pagani, M., Monelli, D., Weatherill, G., Danciu, L., Crowley, H., Henshaw, P., Butler, L., Nastasi, M., Panzeri, L., Simonato, M., and Vigano, D. [2014] "OpenQuake Engine : An Open Hazard (and Risk) Software for the Global Earthquake Model," No.September.
- Papadopoulos, A. N., Vamvatsikos, D., and Kazantzi, A. [2019] "Development and application of FEMA P-58 compatible story loss functions," *Earthquake Spectra*, Vol. 35, No.1, pp. 39–60.
- Perrone, G., Cardone, D., O'Reilly, G. J., and Sullivan, T. J. [2019] "Developing a Direct Approach for Estimating Expected Annual Losses of Italian Buildings," *Journal of Earthquake Engineering*, Taylor & Francis, Vol. 00, No.00, pp. 1–32.
- Porter, K. A. [2003] "An Overview of PEER's Performance-Based Earthquake Engineering Methodology," *9th International Conference on Applications of Statistics and Probability in Civil Engineering*, Vol. 273, No.1995, pp. 973–980.
- Priestley, M. J. N. [2003] *Myths and Fallacies in Earthquake Engineering , Revisited, The Ninth Mallet - Milne Lecture*, IUSS Press, Pavia, Italy.
- Priestley, M. J. N., Calvi, G. M., and Kowalsky, M. J. [2007] *Displacement Based Seismic Design of Structures*, IUSS Press, Pavia, Italy.
- Ramirez, C. M., Liel, A. B., Mitrani-Reiser, J., Haselton, C. B., Spear, A. D., Steiner, J., Deierlein, G. G., and Miranda, E. [2012] "Expected earthquake damage and repair costs in reinforced concrete frame buildings," *Earthquake Engineering & Structural Dynamics*, Vol. 41, No.11, pp. 1455–1475.

- Ramirez, C. M., and Miranda, E. [2009] "Building specific loss estimation methods & tools for simplified performance-based earthquake engineering," *Blume Center Report*, No.171.
- Ramirez, C. M., and Miranda, E. [2012] "Significance of residual drifts in building earthquake loss estimation," *Earthquake Engineering and Structural Dynamics*.
- De Risi, M. T., Del Gaudio, C., and Verderame, G. M. [2020] *A component-level methodology to evaluate the seismic repair costs of infills and services for Italian RC buildings*, *Bulletin of Earthquake Engineering*, Springer Netherlands.
- Ruiz-García, J., and Negrete, M. [2009] "Drift-based fragility assessment of confined masonry walls in seismic zones," *Engineering Structures*, Vol. 31, No.1, pp. 170–181.
- Sassun, K., Sullivan, T. J., Morandi, P., and Cardone, D. [2016] "Characterising the in-plane seismic performance of infill masonry," *Bulletin of the New Zealand Society for Earthquake Engineering*, Vol. 49, No.1, pp. 98–115.
- SEAOC. [1995] *Vision 2000: Performance-based seismic engineering of buildings*, Sacramento, California.
- Shahnazaryan, D., and O'Reilly, G. J. [2021] "Integrating expected loss and collapse risk in performance-based seismic design of structures," *Bulletin of Earthquake Engineering*, Vol. 19, No.2, pp. 987–1025.
- Shahnazaryan, D., O'Reilly, G. J., and Monteiro, R. [2019] "Using direct economic losses and collapse risk for seismic design of RC buildings," *COMPDYN Proceedings*, pp. 4968–4983.
- Shahnazaryan, D., O'Reilly, G. J., and Monteiro, R. [2021a] "Storey Loss Function Generator."
- Shahnazaryan, D., O'Reilly, G. J., and Monteiro, R. [2021b] "IPBSD."
- Shahnazaryan, D., O'Reilly, G. J., and Monteiro, R. [2021c] "Story loss functions for seismic design and assessment: Development of tools and application," *Earthquake Spectra*, p. 875529302110235.
- Silva, A. [2020] "Implications of Earthquake-Induced Loss Control in Seismic Design Provisions," *PhD Thesis: IUSS Pavia, Italy*, No.June.
- Silva, A., Castro, J. M., and Monteiro, R. [2020] "A rational approach to the conversion of FEMA P-58 seismic repair costs to Europe," *Earthquake Spectra*, Vol. 36, No.3, pp.

- 1607–1618.
- Silva, V., Crowley, H., and Bazzurro, P. [2016] “Exploring risk-targeted hazard maps for Europe,” *Earthquake Spectra*, Vol. 32, No.2, pp. 1165–1186.
- Sinković, N. L., Brozović, M., and Dolšek, M. [2016] “Risk-based seismic design for collapse safety,” *Earthquake Engineering & Structural Dynamics*, Vol. 45, No.9, pp. 1451–1471.
- Sullivan, T. J. [2016] “Use of Limit State Loss versus Intensity Models for Simplified Estimation of Expected Annual Loss,” *Journal of Earthquake Engineering*, Vol. 20, No.6, pp. 954–974.
- Sullivan, T. J., Calvi, G. M., Priestley, M. J. N., and Kowalsky, M. J. [2003] “The limitations and performances of different displacement based design methods,” *Journal of Earthquake Engineering*, Vol. 7, No. August 2014, pp. 201–241.
- Vamvatsikos, D. [2013] “Derivation of new SAC/FEMA performance evaluation solutions with second-order hazard approximation,” *Earthquake Engineering & Structural Dynamics*, Vol. 42, No.8, pp. 1171–1188.
- Vamvatsikos, D. [2017] “Performance-Based Seismic Design In Real Life : The Good, The Bad And The Ugly,” *Anidis*, No.2, pp. 17–24.
- Vamvatsikos, D., Akkar, S. D., and Miranda, E. [2009] “Strength Reduction Factors for the Dynamic Instability of Oscillators With Non-Trivial Backbones,” No.June, pp. 22–24.
- Vamvatsikos, D., and Aschheim, M. A. [2016] “Performance-based seismic design via yield frequency spectra,” *Earthquake Engineering & Structural Dynamics*, Vol. 45, No.11, pp. 1759–1778.
- Vamvatsikos, D., Bakalis, K., Kohrangi, M., Pyrza, S., Castiglioni, C. A., Kanyilmaz, A., Morelli, F., Stratan, A., D’Aniello, M., Calado, L., Proença, J. M., Degee, H., Hoffmeister, B., Pinkawa, M., Thanopoulos, P., and Vayas, I. [2020] “A risk-consistent approach to determine EN1998 behaviour factors for lateral load resisting systems,” *Soil Dynamics and Earthquake Engineering*, Vol. 131, No.November 2019.
- Vamvatsikos, D., and Cornell, C. A. [2005] “Direct Estimation of Seismic Demand and Capacity of Multidegree-of-Freedom Systems through Incremental Dynamic Analysis of Single Degree of Freedom Approximation,” *Journal of Structural Engineering*, Vol. 131, No.4, pp. 589–599.

- Vamvatsikos, D., and Cornell, C. A. [2006] "Direct estimation of the seismic demand and capacity of oscillators with multi-linear static pushovers through IDA," *Earthquake Engineering & Structural Dynamics*, Vol. 35, No.9, pp. 1097–1117.
- Vamvatsikos, D., Kazantzi, A. K., and Aschheim, M. A. [2016] "Performance-based seismic design: Avant-garde and code-compatible approaches," *ASCE-ASME Journal of Risk and Uncertainty in Engineering Systems, Part A: Civil Engineering*, Vol. 2, No.2.
- Del Vecchio, C., Eeri, M., Di Ludovico, M., and Prota, A. [2020] "Repair costs of reinforced concrete building components: From actual data analysis to calibrated consequence functions," *Earthquake Spectra*, Vol. 36, No.1, pp. 353–377.
- Welch, D. P., and Sullivan, T. J. [2017] "Illustrating a new possibility for the estimation of floor spectra in nonlinear multi-degree of freedom systems," *Proceedings of the 16th world conference on earthquake engineering (16WCEE), Santiago, Chile*.
- Woessner, J., and Wiemer, S. [2005] "Assessing the quality of earthquake catalogues: Estimating the magnitude of completeness and its uncertainty," *Bulletin of the Seismological Society of America*, Vol. 95, No.2, pp. 684–698.
- Zareian, F., and Krawinkler, H. [2012] "Conceptual performance-based seismic design using building-level and story-level decision support system," *Earthquake Engineering & Structural Dynamics*, Vol. 41, No.11, pp. 1439–1453.
- Žižmond, J., and Dolšek, M. [2019] "Formulation of risk - targeted seismic action for the force - based seismic design of structures," No.January, pp. 1–23.